AEROSPACE REPORT NO.
TOR-2022-00016

Best Practices for Generating Space Environment Specifications with Modern Tools

December 31, 2021

Timothy B. Guild[1], Scott C. Davis[1], Alex J. Boyd[1], T. Paul O'Brien[1], Joseph F. Fennell[2], Joseph E. Mazur[2], Douglas G. Brinkman[1], Glenn E. Peterson[3], and Alan B. Jenkin[3]
[1]Space Sciences Department, Space Science Applications Laboratory
[2]Space Science Applications Laboratory, Physical Sciences Laboratories
[3]Astrodynamics Department, Systems Analysis and Simulation Division

Prepared for:

National Reconnaissance Office
14575 Lee Rd.
Chantilly, VA 20151-1715

Contract No. FA8802-19-C-0001

Authorized by: National Systems Group

Acknowledgments

This report was solicited over many years by Mike Vanik at The Aerospace Corporation. Thanks to his persistence, patience, and, ultimately, sponsorship, it was finally written for the benefit of satellite programs. Many of the topics contained herein are paraphrased from earlier reports, conversations, and thoughtful discussions with many of the authors' colleagues from The Aerospace Corporation, AFRL, NASA, and industry—too many to acknowledge here. Suffice to say it is valuable and rewarding to work within a vibrant satellite engineering community devoted to improving the tools and methods used to appropriately design space vehicles. Section 4.5 was inspired by conversations with Jeff George of LANL. We specifically thank Mike Xapsos, formerly of NASA, for providing the ESP confidence levels included in Appendix A, Joe Wehlburg and Scott Schnee of Aerospace for supporting the writing, and Kristopher Heick of Aerospace for alerting us to the Airbus atomic oxygen tool, ATOMOX.

Abstract

At the beginning of a satellite acquisition, the organization responsible for satellite design must estimate the space environment the satellite will experience throughout its mission lifetime, usually captured in a document referred to as the program environmental specification. The goal of an environment specification is to *completely* specify the severity of the space environment the mission must operate in, subject to the *appropriate* conservatism commensurate with the risk tolerance of the mission, for the extent of the mission lifetime. Many tools exist that can assist in the generation of a complete, appropriate environment specification, but these tools are continually developed on faster timescales than satellites are designed and built.

The purpose of this document is to describe the current generation of tools and methods and provide several worked examples to produce a preliminary space environmental specification for the acquisition of a satellite system. This document is intended to be used as an introduction to the subject by survivability engineers new to space vehicle engineering, or an introduction to the latest tools for long-time experts who are unfamiliar with these new capabilities. Sections contained herein are devoted to describing tools, including AE9/AP9-IRENE, the CREME tools, solar energetic particle models, low-energy plasma definitions, micrometeoroids, orbital debris, and the atomic oxygen environment of the upper atmosphere.

These tools are then used to provide worked examples of appropriate environment specifications for whole-mission-accumulated quantities and for whole-mission worst-case quantities. Mission-accumulated environments include trapped electron fluences, proton fluences (trapped and solar), galactic cosmic rays, atomic oxygen ram fluence, micrometeoroid and orbital debris environments and mitigation, and low-energy plasma fluence for surface degradation. Worst-case quantities computed include worst-case electron flux for internal charging mitigation, worst-case proton flux and linear energy transfer flux for single-event effects design, and worst-case low-energy electron fluxes for surface charging design. We also discuss specification-related topics such as model updates, uniform documentation, and radiation design margin, and finally look toward future model and tool development.

We hope this document will serve the satellite engineering community as a useful starting point for the generation of complete and appropriate environment specifications.

Contents

Figures

Tables

1. Introduction

1.1 Background

At the beginning of a satellite acquisition, the organization responsible for satellite design must estimate the space environment the satellite will experience throughout its mission lifetime. Design choices are then made to ensure the satellite will successfully perform its mission throughout the duration of its mission life and in the expected worst-case environments the satellite is likely to experience. The environment that the satellite must operate in is encoded in a document referred to as the program environmental specification. The goal of an environment specification is to *completely* specify the severity of the space environment the mission must operate in, subject to the *appropriate* conservatism commensurate with the risk tolerance of the mission, for the extent of the mission lifetime.

Many tools exist that can help an organization generate a complete, appropriate environment specification. These tools each represent incremental advances in our knowledge of the severity of the climatology of the space environment, translated into quantities useable in satellite design. Though many web-based services facilitate synthesizing these many tools into one framework (for example, Space Environment Information System (SPENVIS) (https://www.spenvis.oma.be/) [81] and Cosmic Ray Effects on Micro-Electronics (CREME) (https://creme.isde.vanderbilt.edu/) [13]), the underlying models are often still individually updated or replaced. Updates are often driven by new observations of the space environment, new orbits chosen, updated estimates of extremes, increased statistical fidelity desired by the satellite engineering community, or a new space technology advancement that is unintentionally sensitive to a unique aspect of the space environment.

1.2 Goal of This document

This document aims to describe the current generation of tools and methods and provide several worked examples to produce a complete, appropriate, preliminary space environmental specification for the acquisition of a satellite system. We relate the aspects of the space environment, and tools describing it, to the satellite hazard design engineers' need to mitigate for a successful mission. When applicable, we describe ongoing research into the next-generation specification capabilities and estimate a schedule when these tools described herein will be superseded by improvements. This document is intended to be used as an introduction to the subject by survivability engineers new to space vehicle engineering organizations or an introduction and tutorial of the latest tools for long-time experts who are unfamiliar with their new capabilities. We hope this document will serve the satellite engineering community as a useful starting point in the process of deriving their organizations' environment specifications.

1.3 Guiding Principles

There are several guiding principles we have found to be useful in reaching a complete, appropriate environment specification. Following these principles should facilitate the environment specification being reviewed by others, revising the environment specification when new knowledge is available, and having a consistent and traceable environmental risk posture.

- The environment specification should specify the environment outside the spacecraft. Consequences (e.g., tables of dose versus depth) of that environment inside the spacecraft may be provided for reference to facilitate requirements analysis.

- The environment specification should identify the environment and models in enough detail that a skilled practitioner can exactly reproduce the specification and a reviewer can effectively audit it. More detail is given in section 4.1.

- Tables should provide the essential numbers an engineer would need for at least a conservative simplified requirements analysis (e.g., dose depth curves, linear-energy-transfer [LET] spectra behind 100 mils, etc.). Tables may be requirements or for reference. Figures of the tabular data are encouraged but should never be requirements.

- The environment specification should not implicitly or explicitly restrict the design. For instance, the document should give the engineer the freedom to perform a more detailed analysis, as needed, to demonstrate the requirements are met.

- When combining separate models with confidence levels, the convenient, reasonable, and conservative approximation of adding the 95 percent confidence levels of quantities computed by two or more different models should be used and this sum cited as the 95 percent confidence level of the combined quantity. If those environments are of a worst-case nature and never seen simultaneously, the envelope of those 95 percent confidence level quantities should be taken.

- The quantity of radiation design margin (RDM) is poorly suited to the rigorous generation of environment specifications, and its use should be discontinued in the future. The reason why and alternatives are discussed in section 4.5.

1.4 From Environments to Satellite Hazards

Many spacecraft hazards caused by the environment originate from the impact of distinct particle populations. These populations share a common range of energies, temporal dynamics, or location within the magnetosphere, and are often described by individual geophysical models that describe their characteristics. These geophysical models serve as a convenient list of sections to build our environment specification from and organize the format of this report. Satellites, however, can sample many of these individual particle populations every orbit or episodically throughout their mission. Further, sometimes different geophysical environments can lead to the same satellite hazard (e.g., trapped protons and solar proton events both cause total ionizing dose). Because there is not a one-to-one mapping between environment and satellite hazard, we provide a mapping from environment (rows) to hazard (columns) in Table 1. Note that sometimes a single environment can cause multiple hazards, and other times a single type of hazard can be caused by multiple environments. Appropriately mitigating these hazards involves combining them in statistically rigorous ways.

Table 1. Mapping from Environments (First Column) to Satellite Hazards (First Row) Covered in this Report

	Environment	Section	Ionizing Dose	Non-Ionizing Dose (Displacement Damage)	Single-Event Effects (SEEs)	Internal Charging	Surface Charging	Surface Material Degradation	Particulate Impacts
Whole-mission aggregated fluence	Trapped proton fluence	3.1.2.1	X	X	X				
	Solar proton fluence	3.1.2.2	X	X	X				
	Solar heavy ions	2.3.1			X				
	Galactic cosmic rays	3.1.3			X				
	Trapped electrons	3.1.1	X						
	Plasma fluence	3.1.6						X	
	Atomic oxygen fluence	3.1.4						X	

	Environment	Section	Ionizing Dose	Non-Ionizing Dose (Displacement Damage)	Single-Event Effects (SEEs)	Internal Charging	Surface Charging	Surface Material Degradation	Particulate Impacts
	Micro-meteroid/ orbital debris	3.1.5							X
Whole-mission worst-case fluxes	Trapped protons	3.2.3.1			X				
	Solar protons	0	X	X	X				
	Solar heavy ions	3.2.4			X				
	Trapped electrons	3.2.2				X			
	Low-energy plasma	3.2.5					X		

The remainder of this document is divided into three main sections. Section 2 is devoted to describing the recommended geophysical models of the space environment for all populations, including appropriate model choices for generating environment specifications. Section 3 describes the currently available software tools that are used to query these geophysical models, describes the methods used to run or combine them into specifications, and carries through worked examples of environment generation. Section 4 includes other special considerations not addressed in earlier sections, and section 5 summarizes current ongoing work that will supersede the currently recommended models or tools at some point in the next few years.

2. Geophysical Models

2.1 AE9/AP9-IRENE

2.1.1 Overview

The de facto standard tool for generating trapped radiation and plasma environments (except surface charging) is the AE9/AP9-IRENE set of models [28][38][64]. IRENE stands for International Radiation Environment Near Earth and will, in time, become the sole name of the model. These models incorporate many different on-orbit datasets, and include mean, perturbed mean, static percentile, and Monte Carlo scenario environments, enabling a user to generate average environments with error bars or confidence levels for cumulative effects, and worst cases with confidence levels for effects from transient environments. AE9/AP9-IRENE addresses energetic electrons and protons, as well as plasma electrons, protons, helium, and oxygen. It can be used to compute environments for total ionizing and non-ionizing dose, proton SEEs, and internal charging. It does not address surface charging, and it does not currently include solar or galactic cosmic ray protons and heavy ions.

AE9/AP9-IRENE is under ongoing development, so it is released with a version number, such as the latest version, 1.5. Minor versions are indicated with additional digits in the version number, such as v1.55, which indicates feature updates or bug patches but not significant changes to the fluxes and fluences produced by the tool. AE9/AP9-IRENE is released both as a standalone Microsoft Windows application and as a source code and library that can be integrated into other third-party applications, such as SPENVIS [81] and Outil de Modelisation de l'Environnement Radiatif Externe (OMERE) (http://trad.fr/en/space/omere-software).

AE9/AP9 is built of several submodels, each of which covers a different particle domain, such as plasma electrons or high-altitude radiation belt electrons. Over time, more such submodels, or modules, will be added to AE9/AP9-IRENE, and the model will simply be known as IRENE. The radiation belt submodels are AE9 (electrons) and AP9 (protons), and the plasma submodels are collectively known as the Space Plasma Models (SPM).

AE9/AP9 is so named to provide continuity with the long-running trapped radiation models from prior decades, NASA's AE8/AP8 models. From 1964 to 1991, a continuous research program routinely updated trapped electron and proton radiation models, culminating with AP8 [75] and AE8 [89]. No updates were developed after 1991. While the AE9/AP9 models are logical follow-ons to the earlier versions, the AE9/AP9 models have been developed from scratch with the needs of modern satellite designers in mind. More details can be found at https://www.vdl.afrl.af.mil/programs/ae9ap9/.

2.1.2 Uncertainties in the Model

AE9/AP9-IRENE provides uncertainties through a Monte Carlo methodology. Running the model multiple times with different random seeds generates unique mission flux profiles. Computing statistics of a quantity of interest over those Monte Carlo scenarios provides the uncertainty. More details can be found at the AE9/AP9-IRENE architecture (https://www.vdl.afrl.af.mil/programs/ae9ap9/architecture.php) and Modes (https://www.vdl.afrl.af.mil/programs/ae9ap9/modes.php) pages. All the submodels provide mean and perturbed mean environments. The mean environment is static, and it represents the best estimate of the average radiation and plasma environment. Each perturbed mean scenario is also static and represents one realistic possibility for what the true mean environment could be, given what we know about the model's uncertainties due to sensor and dataset limitations. The radiation belt models (AE9/AP9) also provide Monte Carlo scenarios, which are dynamic, and include space weather variations. If one averages a Monte

Carlo scenario with a given scenario identifier (1 to 999) long enough, one will obtain the same results as a perturbed mean scenario with the same scenario identifier. Static percentile environments are also available but are used for model diagnostic purposes, not for engineering. Static percentiles should not be confused with confidence levels, which are produced by analyzing many Monte Carlo or perturbed mean scenarios.

AE9/AP9-IRENE is a "consensus" model. It takes estimates of the radiation environment from many different sensors and at different times and attempts to synthesize the particle fluxes. Not all datasets agree with each other, sometimes for good reasons (e.g., taken at different phase of solar cycle), and we retain many of those disagreements in the model as perturbed mean estimates (see section 2.1.4). Because of this, other datasets can differ from the model mean or model statistics. This does not make the model or new conflicting dataset wrong, just another voter in a consensus model. With more unique datasets included in the AE9/AP9-IRENE model architecture, the model output will approach the true distribution of the environment with a shrinking uncertainty.

2.1.3 Mean Environment

The simplest way to run AE9/AP9-IRENE is in static mean mode, which is the current best estimate of the average radiation and plasma environment. Flying a satellite through a mean mode for a representative number of orbits and then scaling up to mission length is an efficient way to estimate the cumulative fluence on the satellite's orbit. A representative number of orbits is itself orbit-dependent but must adequately sample all the radiation belt features the orbit traverses. However, for mission design, it is often necessary to account for model uncertainty and even for space weather dynamics. It is important to note that the prior models AE8/AP8 included only a *median* flux environment.

2.1.4 Perturbed Mean

For cumulative exposures and missions lasting many years, the space weather dynamics average out and only model uncertainty must be accounted for. In such cases, the correct approach is to run many perturbed mean scenarios for a representative number of orbits (a few days or a week) and then scale up the fluence to full mission duration. The spread of the results over perturbed mean scenarios capture the AE9/AP9-IRENE model uncertainty, or uncertainty in the mean. Using many such scenarios, we can compute confidence levels. For surveys of many orbit options, a minimum of 40 scenarios should be used for each option. For definitive orbit specification development (i.e., once the mission orbit has been chosen), at least 200 scenarios should be run.

2.1.5 Monte Carlo

For shorter missions (less than one year) and for computing worst-case effects from space weather transient environments, the model provides Monte Carlo scenarios. Note that Monte Carlo scenarios are only available for the radiation energies (AE9/AP9), not for plasma energies (SPM). Monte Carlo scenarios must be run for the full mission duration, and then the worst-case transient (e.g., a 1-minute average proton flux or a 24-hour average electron flux) must be computed for each scenario. Confidence levels can then be computed over the many scenarios. As above, for surveys of many orbit options, a minimum of 40 scenarios is needed, while for definitive specification development, a minimum of 200 scenarios is needed.

2.1.6 Orbital Time Sampling

AE9/AP9-IRENE calculation time can become cumbersome, so it is important to not over-sample the orbit. However, spatial structure in the radiation and plasma environment requires minimum sampling

along the orbit as well. Therefore, recommended time sampling depends on the satellite location or orbit type. For geostationary orbits, a time step of 1 hour is acceptable because this unique orbit is confined to a very narrow part of the outer radiation belt. For low Earth orbits (apogee less than 2,000 km altitude), a time step of 10 seconds is needed. For other orbits, we provide the following recommendation, in terms of the geocentric radial distance R relative to an Earth radius (R_E ~ 6378 km):

- For $R \leq 1.3\ R_E$, sample every 10 seconds
- For $1.3 < R \leq 2\ R_E$, sample every minute
- For $2 < R \leq 4\ R_E$, sample every 5 minutes
- For $R > 4\ R_E$, sample every 15 minutes

For elliptical orbits, the most recent versions of AE9/AP9 (after v1.35) accept variable time steps, so it is possible to use different time sampling in different parts of the orbit.

2.2 CREME Tools

2.2.1 Overview

CREME is a suite of programs intended to represent the ionizing radiation environment in near-Earth orbits and evaluate the effects of that radiation on electronic systems in spacecraft. CREME includes models to specify the ion radiation environment from trapped particles as well as solar particle events (SPEs). After modulating these radiation environments either through orbit selection, shielding, or a particular duration exposure to a worst-case environment, other tools can determine the LET spectrum of the specified environment, determine SEE upset rates, and calculate the expected dose due to certain particles. It is important to note that although the CREME suite of tools is a convenient end-to-end solution to produce upset rates from external environments, each of the component models *is not the most-recommended* geophysical model to describe the environment. CREME includes more limited trapped proton (AP8), solar proton [85], and galactic cosmic rays (GCRs) [56] models than are available or recommended currently (AP9, ESP-PSYCHIC, and BON2020, respectively). We can overcome these limitations through manual intervention within the standalone CREME tools.

CREME started at Naval Research Laboratory (NRL) with the original CREME86 code [1] and was later updated to CREME96 [85] with improved models and transport codes. This code was ported to the web at NRL but was later re-hosted at Vanderbilt University. The current version of CREME is very similar to the version used at NRL but also introduced the ability to use CREME-Monte Carlo (CREME-MC). CREME-MC uses the CREME96 models but changes the transport code and upset models to use a GEANT4-based model (MRED) to better simulate particle transport and charge deposit. However, this model requires a better understanding of the part structure as a model of the part structure needs to be built instead of using a simpler sensitive volume model.

As of this writing, the CREME tool suite is located online at https://creme.isde.vanderbilt.edu/ and contains extensive documentation as well as an easy interface to run the suite. However, as a web-based tool, there are several drawbacks. First, an internet connection is required. Secondly, as a public website, the user must be careful to only provide publicly releasable information on the orbit or part under consideration. Also, because the CREME website is a series of sequential programs that need input from a web form, it is not possible at this time to develop a series of scripts to run many orbits at a time. Finally, because the tools are linked to web forms, it is difficult to use the output of other models in the CREME website, for example using AP9 instead of AP8.

Alternatively, by contacting the developers on the website above, it is possible to get the original CREME DOS-based executable programs and run the CREME tools in an environment that does not need any internet connection. In this format, CREME is not a single program but a series of programs that run on the output files from previous programs. However, because the programs are run at the command line, it is easier to convert the output files of other models to work with the CREME tool.

As this standalone version of CREME is nothing more than a series of DOS executables, it is easy to generate scripts to run many variations of the tool to explore the effect of certain parameters. Unfortunately, this version is no longer in active development, so there will be no improvements with improved models or bug fixes. As of this writing, the longer-term solution will be to use the SIRE2 tool [3], which is based on the CREME tool set but includes more models, is able to handle non-orbital trajectories, and is not web-based.

It is important to note that the GCR model used in the CREME tool suite is often called CREME or CREME96. This can lead to confusion if someone is using the CREME96 GCR or solar energetic particle (SEP) models, but is using other tools for the trapped environment, particle transport, or upset rate modeling.

2.2.2 Trapped Proton Models in CREME

The CREME tool uses AP8 as the basis for the trapped proton model. It is important to note that the CREME tool does not model electrons, which limits the utility of CREME to mostly SEE calculations. The tool provides only two options relating to the phase of the solar cycle: the median solar maximum proton flux (AP8MAX) or the median solar cycle minimum proton flux (AP8MIN). The intensity of the inner radiation belt is inversely correlated with the solar cycle; therefore, AP8MIN represents a slightly more severe proton environment. AP8MIN is therefore the option typically chosen for conservatism, even though it still represents the median proton flux only.

Because the CREME tool is a series of modules that use the output from previous modules, it is possible to use other trapped proton models in the tool when using the standalone version. A good example is that the TRP module of CREME will generate the trapped proton flux using AP8. The output of TRP will often go to the FLUX module, which is used to generate the particle flux, including geomagnetic transfer and GCR contribution. However, we could convert the format of AP9 to look the same as the output of TRP and then include AP9 results into the CREME suite. A similar method could be used to apply different geomagnetic models or solar protons, but it is more difficult to attempt to use different GCR or solar ion models.

2.2.3 GCR Models in CREME

GCRs are particles accelerated to extremely high energies (~GeV) outside the solar system. They comprise all naturally occurring elements of the periodic table according to their relative abundances in the universe. As they pass from interstellar space into the heliosphere, they can be scattered by the intensity and turbulence in the heliospheric magnetic field, resulting from solar activity propagating into the solar system. This causes the low energy (< 1 GeV) GCR intensity to vary inversely with solar activity, with larger (smaller) GCR fluxes occurring near Earth at solar minimum (maximum). Because GCRs are so energetic, they cannot be appreciably shielded from satellite components, but their effects (SEE) must be estimated and mitigated in other ways, such as by using radiation-hardened parts, redundancy, or error detection and correction (EDAC) schemes.

CREME contains a GCR model derived from the semi-empirical method of Nymmik et al. [56]. This model parameterizes the GCR flux near Earth as a product of two functions: one describing the local

interstellar spectra and the other describing the heliospheric modulation of that spectrum. The model was slightly updated in 2009 and remains the currently available GCR model in CREME described in section 3.1.3. However, several improved models have been developed more recently that have been tested against new and improved GCR observations in the recent solar cycles. Mrigakshi et al. [51] evaluated four models regarding how well they describe the species and energies most associated with astronaut radiation risks and found BON2010 outperformed the CREME96 and CREME2009 GCR models. Further, the most recent BON model [79] upgraded the prior BON models with new data from AMS-02 and PAMELA and improved calibration and uncertainty quantification, resulting in a much-improved description of the GCR flux for satellite design considerations.

The disparity between the recommended GCR model and the one available in end-to-end simulation tools like CREME highlight the need to update these tools. Although we can circumvent this shortcoming by running new models and formatting the results into the format required by the CREME96 standalone tools, we recommend the developers of CREME consider implementing BON2020 in their tool suite.

2.2.4 SEP Models in CREME

The CREME suite of tools also includes severe solar energetic particle environments for worst-case estimates of single-event effects. These SEP environments are also, confusingly, referred to as CREME solar particle environments. The particle fluxes available to specify the worst-case SEPs are all derived from observations of IMP-8 during the October 1989 solar particle events and discussed in Tylka et al., 1997 [87]. CREME users can choose the "worst week," which is the average of observations over 180 hours from October 19–27, 1989; the "worst day," which is the average of observations over 18 hours during the shock event of October 20, 1989; or "peak 5-minute flux," which is the largest measured point. Note that only protons were measured at a cadence of 5 minutes on IMP-8, and the fluxes of heavy ions were scaled from the abundance ratios throughout a longer interval of the October 1989 events. Tylka et al, 1997 [87] concluded that these environments were representative of higher than a 99 percent confidence level at GEO. Continued observations of solar particles in the intervening three decades, which have not exceeded these October 1989 environments, dictate that they are more representative of 99.9% or higher confidence levels at the time of this writing. Dyer et al., 2004 [21] compared the SEP observations of the Halloween storms of October–November 2003 with CREME thresholds and concluded that over a week-long interval, these Halloween events slightly exceeded the CREME worst-week threshold in protons but not heavy ions, more conducive to causing single-event effects.

2.2.5 Geomagnetic Shielding

Earth's magnetic field organizes the dynamics of charged particles in space. It serves to trap protons and electrons in the Van Allen radiation belts around Earth and can also prevent access of external solar and galactic particles to certain regions of the magnetosphere. Access is based on the incident particle's rigidity, which is proportional to its momentum and inversely proportional to its charge state. The higher rigidity a particle has, the more access it has to regions within Earth's magnetosphere. A magnetic surface or boundary inside of which a particle of a given rigidity is excluded by its Lorentz force is referred to as it's "cutoff." As solar protons and galactic cosmic rays exhibit a spectrum of energies and species, determining the regions of space accessible to certain portions of those spectra typically is performed by tracing many particle trajectories and binning them into grids, such as in [78]. In general, locations over the poles and at high altitudes (e.g., GEO) are exposed to the complete interplanetary particle population, and more equatorial locations or lower altitudes (e.g., MEO, low-latitude LEO) can take greatest advantage of geomagnetic shielding to attenuate the solar and galactic cosmic ray flux. CREME computes the attenuation of particles through the geomagnetic field via use of the geomagnetic transmission function (GTF) routine after defining the environments and orbits.

High-altitude currents flowing in the magnetospheric system during geomagnetic storms can have a second-order effect on the location of geomagnetic cutoffs. The primary current system, which dynamically affects the location of the cutoffs with space weather, is the ring current, a population of ions circling Earth westward, generating a field that partially cancels the main field of Earth's dynamo. This has the effect of temporarily decreasing the magnetic latitude of the cutoffs for the duration of the geomagnetic storm (approximately a few days), exposing a slightly larger area over the poles to the external solar or galactic cosmic ray environment. Neal et al. 2013 [53] found a 4-degree latitude suppression for a moderate (Kp=6) geomagnetic storm. Solar particle events and geomagnetic storms often happen together, and orbits that are usually geomagnetically shielded (such as the International Space Station (ISS)) can be suddenly exposed to a severe solar particle environment as the geomagnetic cutoff moves equatorward. CREME parameterizes this additional exposure through the specification of two states of the magnetosphere: quiet or stormy. The geomagnetic field is usually quiet, with no large-scale current systems eroding the magnetic shielding of Earth. Alternatively, a stormy condition arises during a severe geomagnetic storm, which moves the cutoff equatorward. For any orbit, a stormy condition decreases the geomagnetic shielding offered and represents a more conservative setting for solar particles and galactic cosmic rays. Details of the choice and severity of these options are given in Tylka et al., 1997 [85].

Satellite designers can include the benefit of this geomagnetic shielding in their mission design if the satellite orbit resides partially inside the geomagnetic cutoff. Both whole-mission aggregated environmental quantities and whole-mission worst-case quantities can be decreased by considering the geomagnetic shielding. For instance, the residence time a polar LEO vehicle spends outside a cutoff is roughly one third of its orbit, decreasing (by two thirds) the accumulated dose or displacement damage from unattenuated solar particle environments estimated over its mission life. This rough factor depends on particle energy, LET, and orbital altitude. Also, flying a part susceptible to SEE from high LET (high Z, low rigidity) GCR particles in low-inclination LEO orbit can take advantage of the geomagnetic field significantly attenuating the GCR flux the part is exposed to. This might allow the provisional use of the susceptible part in a low-inclination LEO orbit only.

Details of how to run CREME and implement these calculations are given in the CREME documentation on the website.

2.2.6 Single-Event Upset Calculations

While the CREME tool is very useful to generate the expected particle spectrum for an orbit, one of the tool's strengths is the ability to seamlessly use the generated environments to calculate the SEE upset rates in a component due to that particle spectrum. The modules used in CREME to do these calculations are PUP and HUP. PUP is used to calculate the upset rate coming from proton secondary interactions, while HUP is used to calculate upset rates coming from direct ionization effects. Often HUP is called "heavy ion upsets" while PUP is called "proton upsets" because for many parts, the proton LET is so low that they do not add to the direct ionization effects. However, some modern technologies require such a small amount of critical charge to upset a device that proton direct ionization is possible and should be considered with HUP.

While the tool does provide an option to calculate ionizing dose, the lack of the inclusion of any electron model can provide incorrect and misleading results in many orbits. So, in general, CREME should not be used for any dose calculations. Dose calculations can be performed for both trapped electron and proton populations by AE9/AP9-IRENE, Shieldose-2, FASTRAD, NOVICE, and other tools listed in section 4.6.

2.2.6.1 HUP and PUP

A core driver behind the different ways in which PUP and HUP operate is related to the directionality of the incoming particles. For example, the directionality of the incoming protons has a limited effect on the direction of recoil atoms generated from secondary interactions. Therefore, the PUP model treats any incoming proton, from any angle, the same. PUP takes, as input, the proton upset cross-section curve derived from accelerator testing. There is no actual physics modeling in PUP, it just treats the part sensitivity as a measurement of how many upsets the part will get based on a certain number of protons at a certain energy. Because of this simplicity, PUP generally has very few parameters to work with. It is important to note that if there is some directionality for proton secondary effects due to part geometry (for instance, if protons at a certain angle will provide more or less upsets than at other angles), then the core PUP assumptions will be violated, and a different model will be needed. This is likely only possible for devices that show an extreme directional dependence in heavy ion testing with ions that have a low LET or a very short range. Because there is little evidence of such effects in most electronics, there exists no commonly used directional proton secondary effects model. A more detailed discussion of this topic is found in section 5.3

The primary input for PUP is the cross-section curve as a function of proton energy, derived from device testing in a proton beam at an accelerator facility. Ideally, there should be several measurements made at various energies to look for the energy threshold at which the cross section will increase drastically with energy. An example of this is shown in Figure 1. Often the proton cross-section curves are estimated by using a Bendel curve (one or two parameters), a Weibull curve, or a step function for conservatism. However, as testing with different proton energies is often more uncommon than with heavy ions, there are often not enough data points to support a specific type of curve. If possible, it may be beneficial to use several curves that fit the data to determine the overall effect and pick the curve that best represents the mission risk profile.

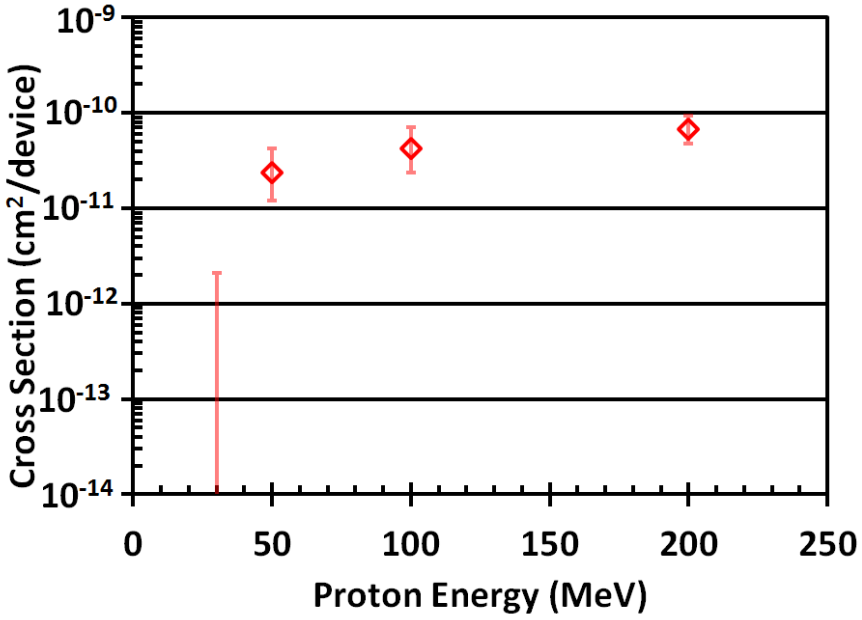

Figure 1. Examples of proton cross section showing the decrease in cross section with decreasing energy until a null measurement is made.

HUP operates differently due to the different physics involved. For HUP, the upsets are caused by the direct ionization from the incident particles. The amount of ionization is linked to the LET of the particle

as well as the length of the particle track. The amount of charge needed to upset a certain sensitive volume is referred to as the critical charge. Because the charge deposited by a particle is related to the LET and track length, HUP needs to model every possible particle track path through a sensitive volume of a certain size. In this case, the model cannot be purely empirical because devices are not tested with an omnidirectional flux as they would experience in space. Instead, HUP can translate the results from a beam test with a known LET and one path length corresponds to a large selection of path lengths and LETs.

2.2.6.2 Other Considerations When Using HUP and PUP

The tools discussed in this section were developed to serve a broad community of engineers with a variety of expertise. However, the SEE rate estimation problem is so complex that there remain a number of ways in which these tools can give misleading results, and a high level of expertise can be required to appreciate the nuances. Here we discuss some of the issues all practitioners should bear in mind when computing and interpreting upset rates generated with these tools.

The topology of the sensitive volume and path length can lead to a wide variety of LETs, which can cause the same upset. For example, if we assume the sensitive volume is a very thin cylinder, then for an incident particle from a direction perpendicular to the cylinder axis, the path length through the volume is small, requiring a high LET to generate enough critical charge for an upset. However, an incident particle from a direction that is parallel to the cylinder's axis will have a large path length through the volume, so a much smaller LET could generate enough critical charge for an upset. This difference in path length can cause a sensitive volume of a certain size to show a surprising sensitivity to low LET particles, such as protons, because the particles have a large path length and will deposit a significant amount of charge. This is very important when running the HUP model and determining if there is an unreasonable increase in the upset rate because of a large sensitive volume. The CREME user can define the sensitive volume size, number of sensitive volumes, the existence of a funnel, and could also modify the input LET spectrum by removing certain particle species (such as protons) or by eliminating low-energy particles (CREME usually includes all particles with greater than 0.1 MeV/nucleon). HUP does not have a transport model, so if you have a particle with a high LET but very low energy, HUP will not simulate this particle losing energy in the sensitive volume and perhaps stopping. Instead, HUP will assume the particle has the same energy and LET as it traverses the entire sensitive volume. This may cause certain low-energy (and high LET) particles to travel further though a sensitive volume than is possible and increase the upset rate.

For some types of upsets, such as SRAM SEUs, the number of sensitive volumes is large and well known, so it may not be possible to get a large enough sensitive volume for protons to deposit enough critical charge. Unfortunately, these types of cells are often the most SEE sensitive devices, so even with the small sensitive volume, direct ionization effects could be significant. For other types of upsets, the actual number of sensitive volumes may not be known (e.g., SEFI or SEL). For a device with many such sites, the cross section can be quite large, but treating this cross section as a single sensitive volume is unrealistic, while making the sensitive volume too small is unphysical. Unfortunately, in these cases, one often must use engineering judgment or a rule of thumb to proceed. For example, it is generally a good idea, if possible, to keep the sensitive volume size smaller than about 1e-4 cm^2 if there is no other information about a part. This volume corresponds to a square of 0.1 mm by 0.1 mm and represents quite a large area for modern technology. For the smallest technology nodes (approximately 7 nm), the sensitive volume may be closer to 1 micron by 1 micron based on the size of the charge cloud and how well the charge will diffuse into the actual transistor. In general, the most conservative measure is to keep the number of sensitive volumes low and accept that longer track lengths are possible.

One possible method that can be used to avoid unrealistic charge deposit by protons is to remove protons from the HUP LET spectrum. In this case, the LET spectrum only includes heavy ions from Z=2 to 92. While the upset from a long pathlength still exists, the proton flux for some orbits can be significantly higher than the heavy ion flux. By removing the proton flux, one can effectively turn off the proton direct ionization while keeping it for heavy ions. Note that this will not affect PUP, since PUP does not use the LET spectrum but uses the actual proton flux. A similar method would be to increase the energy threshold, so that very low-energy particles, which would normally stop in the sensitive volume, are ignored. By default, HUP has a lower energy limit of 0.1 MeV/nucleon, but for large cross sections, it may be useful to increase that energy limit to around 1 to 10 MeV/nucleon. Ideally, one should perform the HUP calculation using multiple methods to understand which method provides the most conservative reduction.

2.2.6.3 Other Tools

It should be noted that while CREME is the major and recommended tool used to calculate upset rates, other methodologies and tools have been explored as well. In general, these tools tend to either involve more complicated device modeling and physics or are simpler upper bound or translational models. Overall, CREME should be used for calculations unless there is a strong reason to use these other tools. Some of these tools require less information, but as a result will have higher uncertainty, which could lead to incorrect calculations or calculations with too much margin. Other tools can provide a more accurate calculation but may require information that is very difficult to get about the part structure.

Examples of simpler models include Edmond's upper bounds model [22] or Petersen's Figure of Merit (FOM) model [66]. Edmond's model is based on attempting to remove a degree of freedom regarding the thickness of the sensitive volume by sampling many shapes to find an upper bound when the shape is not well known. Petersen's FOM model is based on attempting to translate a known upset rate calculation from a part in one orbit to another part in a different orbit. This model is based on scaling the environment by a scalar factor while also including a scaling factor based on how a part's radiation response is different from the known part. This model has fewer parameters and is less accurate because the actual part radiation response is not calculated in the orbit in question but assumes a simple scaling shift. The main purpose of using this model is because the calculation is very quick and can be done easily in spreadsheets, but at the expense of accuracy.

On the other end, a more complicated model like CREME-MC will calculate the energy deposited in a sensitive volume, defined by the user, using a more realistic energy deposition model that includes energy loss of the particle as well as nuclear scattering effects. These models can have multiple sensitive volumes with different efficiencies to represent changes in diffusion or other changes to charge collection. These Monte Carlo-based models often require a more in-depth understanding of the parts in question and can take longer to run.

Finally, the SIRE2 toolkit, which is intended to be an update to the CREME toolkit, is currently in development. The SIRE2 toolkit is a standalone program that will have the ability to perform similar functions as CREME but also work with orbits and trajectories, have more models built into the code, and the ability to be scripted to run over many parameters. This tool could be a clear upgrade of CREME and possibly the new industry standard tool. A description of SIRE2 is included in section 5.2.1.

2.3 SEP Environment Models

SEPs consist mostly of protons, with lesser contributions from helium and heavier ions. These energetic particles have energies from a few MeV/amu to GeV/amu. Their specific origin remains a subject of ongoing study, but there are known to be two main causes: eruptions at the sun and acceleration at

interplanetary shocks, both associated with coronal mass ejections (CMEs). Some of these CMEs are associated with solar flares (increases in x-ray intensity at the eruption site), so the SEPs have historically often been called solar flare particles. We discourage this outdated terminology because SEPs are only sometimes associated with flares. Because of their origin, SEPs may arrive at Earth very quickly, within minutes of the eruption at the highest energies or within days for those particles accelerated in situ by a CME shock. SEP intensities in the near-Earth environment often remain elevated for several days as the CME transits the solar system. Between SEPs, the proton and heavy ion environment is considered quiescent, consisting only of galactic cosmic rays.

For satellite design, there are three environment models to consider relating to SEPs: SEP fluence, SEP peak flux, and geomagnetic cutoff. SEP fluence is used to compute the average recoverable failure/upset rate and the likelihood of unrecoverable failures. The SEP peak flux is used to compute the peak recoverable failure/upset rates that are then used to estimate outage durations and frequencies and to scale error detection and correction (EDAC) systems. Geomagnetic cutoff refers to the fact that Earth's magnetic field shields some regions of space from ionized particles depending on their energy and ionization charge state.

The workhorse models for SEP fluence over the past decade or more have been JPL91 [26][25] and ESP/PSYCHIC [91][92]. New models promising updated data and new capabilities are SAPPHIRE/ VESPER [36][6] and MSSREM [70]. For SEP flux, the most widely used model is a reconstruction of the October 1989 SEP included in CREME96 [85]. The new SAPPHIRE/VESPER models also provide SEP flux and add Monte Carlo time series capabilities.

summarizes the most widely used SEP models and their properties.

For geomagnetic cutoffs, most satellite designs have relied on the cutoff model built into CREME96, but at Aerospace, we have used [44] for solar protons (see section 3.1.2.3). ESA's new MSM model [42] is a promising new development in cutoff modeling because it includes an updated magnetic field and, like the older Shea and Smart [78] model, it includes geomagnetic activity dependence.

Table 2. Notable Solar Energetic Particle Models and Their Properties

Model	Fluence	Peak Flux	Time Series	Reference
JPL91	H^+			*Feynman* et al., 1993 [26]; 2002 [25]
CREME96		H^+,Ions		*Tylka* et al., 1997 [86]
ESP-PSYCHIC	H^+,Ions			*Xapsos* et al., 2000 [91]; 2007[92]
MSSREM	(future)	H^+,Ions		*Robinson* et al., 2020 [70]
SAPPHIRE	H^+,Ions	H^+,Ions		*Jiggens* et al., 2018 [35]
VESPER	H^+	H^+	H^+	*Aminalragia-Giamini* et al., 2018 [6]

2.3.1 Mission Fluence

Mission fluence refers to the time-integrated particle flux and is used to compute both the average rate of recoverable failures or upsets and the likelihood of unrecoverable failures. The fluence is usually expressed separately as integral proton flux versus energy and integral heavy ion flux versus LET, where the integral refers to number of particles above an energy or LET threshold and LET is linear energy transfer, expressed in MeV/(mg/cm^2). A more detailed heavy ion specification may break out the fluence by species, providing an integral flux versus energy for each major heavy ion species; this is the more

fundamental environment specification outside the spacecraft, but it is often cumbersome to include and there are few convenient engineering tools prepared to use its details. In lieu of these details, an additional integral LET spectrum is often provided behind 100 mils Al shielding, usually in spherical geometry.

There are two legacy practices for generating SEP specifications that should be discontinued. The first is the use of JPL91. This model is long out of date and was superseded by ESP-PSYCHIC in the mid-2000s. Another common practice, which is discouraged for lack of statistical rigor, is to assemble a mission fluence by adding together a conservative number of CREME96 worst days. While specifications generated with these legacy approaches are not invalid, the current recommended practice for new programs is to use ESP for proton fluence and PSYCHIC for heavy ion fluence.

Once generated, fluences are adjusted for orbital residence time in different parts of Earth's magnetic field based on geomagnetic cutoffs. For example, if the vehicle spends only 30 percent of its time in a location where 30 MeV protons can have access to the spacecraft, then the free-space 30 MeV proton fluence produced by the SEP model is multiplied by 30 percent. Because cutoffs are stronger at lower energies and higher charge states, the cutoff attenuation must be applied to *differential* particle flux before computing integral energy flux or LET flux.

In the future, as outlined in O'Brien et al. [63], we expect a transition to the SAPPHIRE/VESPER models for generating proton and heavy ion fluences. These models include more up-to-date input data than ESP-PSYCHIC, and they will be integrated directly into the AE9/AP9-IRENE geophysical models. Another promising option on the horizon is MSSREM, which slightly lags SAPPHIRE/VESPER in terms of capability, but which is a direct upgrade of ESP-PSYCHIC.

2.3.2 Peak Flux

Unlike mission fluence, peak flux is not a well-defined concept. It is intended to address the worst case for design of single event effects countermeasures or accommodations. So, for example, an error detection and correction system might be able to handle a certain rate of upsets, and whenever the flux exceeds that rate, the system will be offline. If the system is designed to operate through a flux beyond the peak flux, it will never be offline. However, more often, system specifications require a certain level of system availability (e.g., more than 99 percent) or a certain number of ground interventions (less than 1 per month). In these cases, it is not always clear what peak flux to supply in the specification documents to facilitate requirements verification.

The convention for decades has been to specify a worst five-minute SEP flux using the October 1989 SEP event, as expressed in the CREME96 software, and supplement this with the worst day and worst week averages from that same event. However, not only are these not necessarily the worst cases, there is no current estimate of the probability of occurrence associated with these severe environments. In 1997, Tylka et al. [87] estimated these environments to be around the 99+ percent confidence level. More recently, Jiggens et al. [36] estimated that the CREME96 peak 5-minute flux is comparable to a 1-in-100-year SPE at energies greater than 30 MeV, but this is dependent on data processing methodologies specific to the tails of the observed distributions. So, it is generally difficult to use such specifications to determine how often a ground intervention would be necessary or to compute an availability.

Nonetheless, for practical reasons, the CREME96 worst cases remain the current standard for peak flux specifications. The five-minute worst case is not attenuated by the geomagnetic cutoffs, as most orbits spend at least some time fully exposed to the SEP environment, even polar low Earth orbits. The worst day and worst week, however, should be attenuated in the same way as the mission fluence (i.e., using residence time to compute average attenuation factors). As with mission fluence, the peak flux is usually

provided in terms of integral proton flux versus energy and integral heavy ion flux versus LET, in free space and behind 100 mils Al shielding.

In O'Brien et al. [63], we described a more probabilistic approach to peak flux specification that would replace the CREME96 paradigm. It would be based on three worst-case specifications, tied to impact severities defined in MIL-STD-882E (System Safety) [88]. Table 3 summarizes the three worst-case design levels. Each one is nominally applied to a one-minute average environment, although the solar particle environment does not vary significantly on timescales shorter than about five minutes. Generating specifications like those in Table 3, such as a 95 percent confidence level monthly exceedance, requires SEP models that represent not only events, but their duration, peak flux, and the waiting times between events. SAPPHIRE/VESPER are beginning to provide these capabilities to the community.

Table 3. Severity Categories, after MIL-STD-882E.

Description	Severity Category	Result	Exceedance Level
Catastrophic	1	Permanent damage. Requires redundant capability (B-side or additional channels) to recover.	Less than once per mission at 95% confidence
Critical	2	Non-damaging but requires ground intervention. Hours to days of down time.	Less than monthly at 95% confidence
Marginal	3	Bus-level intervention, e.g., watchdog reset autonomy. Minutes to hours of being out-of-spec or unavailable.	Less than monthly at 50% confidence
Negligible	4	Soft upsets, manageable by payload autonomy. Seconds to minutes of out-of-spec or recycle time.	Less than monthly at 50% confidence

An even more sophisticated approach will also be available when Monte Carlo time series become available: it will be possible to run whole-mission scenarios, compute the single event effect rates at every time step, assess effects, time offline, etc., and repeat for many scenarios. It will then be possible to compute the likelihood distribution of outage durations for a given choice of design. These highly sophisticated calculations will not always be necessary, but they will provide an opportunity to remove excess margin where the relatively simplified approach of worst-case specifications in Table 3 proves too conservative.

2.3.3 Solar Particle Cutoffs

As noted above, the current practice for geomagnetic cutoffs is to apply a cutoff model that does not account for geomagnetic activity. This is even true for models such as MSM that include geomagnetic activity dependence. However, moving forward, especially with Monte Carlo time series, it will be possible to include geomagnetic activity effects, which allow lower energy and higher charge state particles to penetrate closer to Earth. Such models include MSM [42] and Smart and Shea [78].

2.4 Low-Energy Plasma

The low-energy plasma exposure of relevance to satellite design originates in a region of warm plasma (~keV energies) in the tail of the magnetosphere called the plasma sheet. During magnetic activity, this plasma is convected from the nightside of the magnetosphere Earthward, either slowly or impulsively. This plasma source fills the inner magnetosphere with ions and electrons of 1 to 100 keV energies, which comprise a population known as the ring current. Its plasma intensity is highly time variable and local-

time dependent. These populations generally wax and wane in intensity over long timescales [18] and exhibit fast injections of hot (tens of keV) plasma known as substorm injections. These injections are sometimes narrow in local time and flood geosynchronous orbit with hot electrons, which subsequently drift eastward. Long-term exposure to plasma fluxes can lead to surface material degradation from surface dose and is described in section 2.4.1. The severe, impulsive injections of plasma from substorms lead to surface charging of external ungrounded or dielectric materials and is described in section 2.4.2.

2.4.1 Mission-Length Plasma Fluence

Long-term exposure to the plasma fluence in Earth orbits contributes to material degradation on spacecraft surfaces. These hazards include the accumulation of ~Grad levels of surface dose on materials such as thermal-control surfaces, tapes, and optical coatings on lenses, mirrors, and solar array cover glass. Laboratory testing has demonstrated that certain materials such as paints lose their mechanical integrity and darken, and certain type of cover glass darken under simultaneous exposure to plasma proton electron flux and UV exposure [48].

In the past, mission-length estimates of the plasma exposure were estimated from statistics of long-term measurements of individual plasma sensors such as POLAR/CAMMICE-MICS [73] and LANL/MPA [85]. These estimates were based on limited duration of environment measurements or a single orbit and are now superseded by plasma fluence estimates from the Space Plasma Models (SPME and SPMH) modules within AE9/AP9-IRENE. SPME covers plasma electrons from 1 to 40 keV, and SPMH covers protons (H for hydrogen nuclei) from 1 to 200 keV. Both modules include data comprising both Roeder et al., 2005 [73] and Thomsen et al., 2007 [85] plasma estimates in addition to other datasets from NASA. Moreover, the SPM models will likely continue to be updated with the latest plasma measurements made, improving the statistics in the future.

The SPM modules take advantage of the AE9/AP9-IRENE machinery to generate long-term plasma fluence estimates for orbits with a few differences. SPM does not include Monte Carlo dynamics simply because there have not been enough plasma measurements at the same time to determine the required covariances across energies and pitch angles to drive realistic “space weather” dynamics for the plasma environment. SPM only includes uncertainties of the mean environment through choosing the perturbed mean runs. More detailed instructions for running the SPME/SPMH models to generate mission-length plasma fluence spectra are provided in section 3.1.6.

Note: The SPME/SPMH models do not provide specifications appropriate for surface charging calculations. These plasma models are long-term aggregated environmental models only. For spacecraft charging environments see the next Section.

2.4.2 Worst-Case Surface Charging Environment

There are no generally accepted models that generate the worst-case plasma environment that leads to surface charging. Accordingly, the charging community specifies worst-case environments derived from observations of single intervals that led to severe charging potentials or ESD measurements observed on historical spacecraft. Although the space weather event originating these worst-case surface charging environments is the same, high-altitude vehicles sample different parts of that environment than do low-altitude polar orbiting spacecraft. Therefore, we divide our description into two relevant sections below.

2.4.2.1 High-Altitude Orbits

Ungrounded or dielectric surface materials on the exterior of MEO, GPS, GEO, HEO, and similar altitude orbits that pass through Earth’s plasma sheet will charge up to multi-kilovolt levels and can experience

electrostatic discharges. The plasma environment that causes satellite surface charging is highly episodic and can charge surfaces in less than a few seconds. It is also highly spatially structured both in distance from Earth and azimuthally in longitude relative to local midnight. At present there is not a global or even a limited plasma model that can represent the dynamic variations that occur during satellite surface charging conditions. Thus, we currently use a single spectrum, extreme electron environment, that was observed during an intense satellite charging episode [72]. This environment and the associated ion environment are in the MIL-STD-1809 [19]. The MIL-STD-1809 charging spectrum was measured by the SCATHA satellite [84][46] during an intense surface charging event [39][72]. Figure 2 shows this electron environment in blue with additional spectra from higher-energy measurements related to internal charging. All curves are plotted in integral-in-energy electron flux (left y-axis) and directed beam current (right y-axis) versus electron energy (x-axis). Also shown are the internal charging specification of Fennell et al., 2000 [23] in black and spectra of various measured intervals of the LANL-SOPA electron sensors, which roughly match the high-energy end of the surface charging specification near 100 keV.

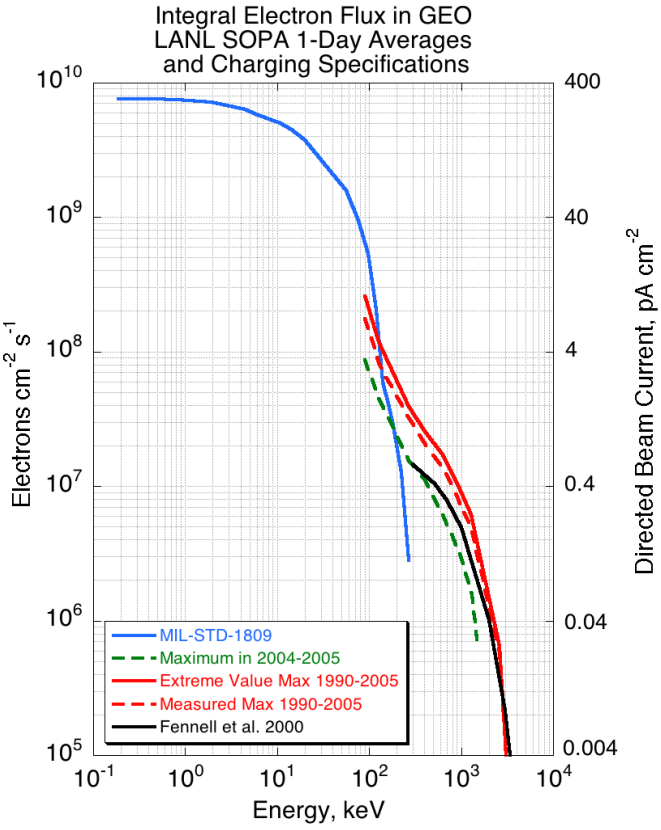

Figure 2. Combination of MIL-STD-1809 GEO surface charging plasma electron specification (blue) and high-energy electron "tails" that can contribute to internal charging.

To generate the worst-case surface charging spectrum in Figure 2, we turn to the methodology of MIL-STD-1809 [19]. Figure 3 shows the electron and proton distribution functions as a function of energy, which are double-Maxwellian fits of the form:

$$f(v) = n_1 \left(\frac{m}{2\pi k T_1}\right)^{\frac{3}{2}} exp\left(\frac{-mv^2}{2kT_1}\right) + n_2 \left(\frac{m}{2\pi k T_2}\right)^{\frac{3}{2}} exp\left(\frac{-mv^2}{2kT_2}\right)$$

Where kT_i is in keV, n_i is number density, v is the particle velocity, m the particle mass (m_e=9.11e-28 grams, m_p=1.67e-24 grams), and $\frac{mv^2}{2}$ is the particle's kinetic energy in keV. The fit parameters for **Error! Reference source not found.** are given in Table 4.

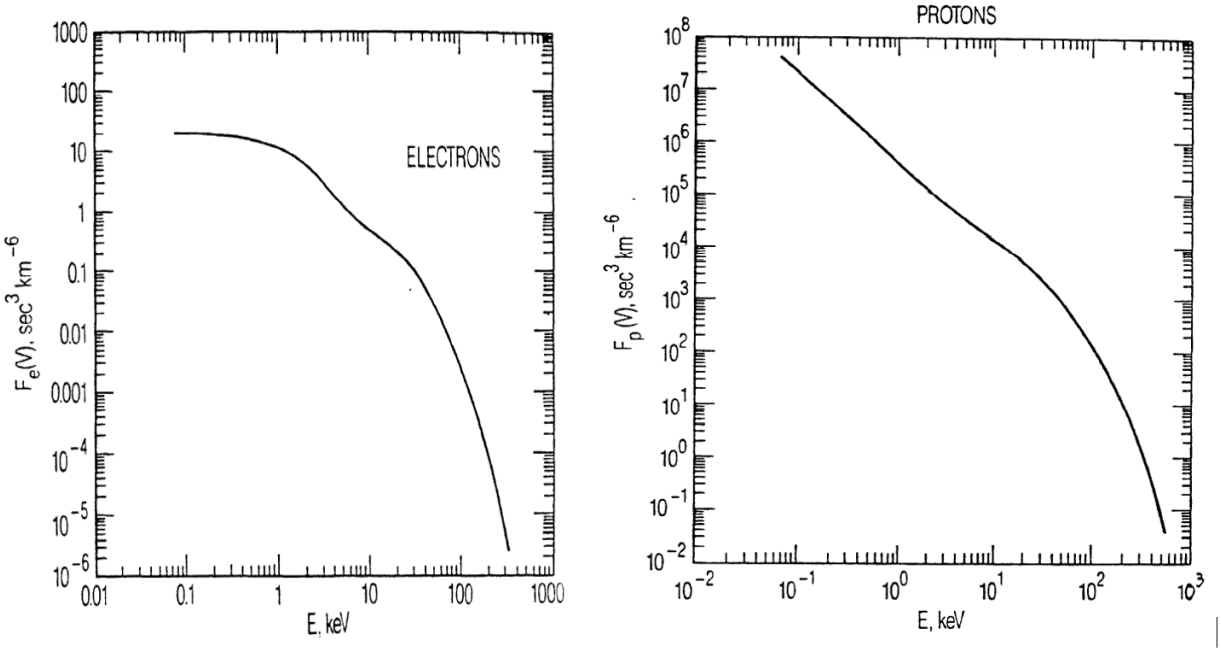

Figure 3. Surface charging distribution functions from MIL-STD-1809 for electrons (left) and protons (right).

Table 4. Double Maxwellian Fit Parameters from MIL-STD-1809

	$n_1(cm^{-3})$	$n_2(cm^{-3})$	$kT_1(keV)$	$kT_2(keV)$
Electrons	2.67	0.625	3.1	25.1
Protons	0.6	1.2	0.2	28

The distribution functions in Figure 3 are used with surface charging modeling tools, such as NASCAP-2K [52], to assess whether high electric fields form on the exterior of a satellite. If the differential electric fields approach breakdown levels (approximately 10^5 kV/cm) in an area of the simulated satellite, that would indicate it has a risk of ESD occurring in that area. Changing the layout of the surface materials or changing the materials themselves may be required. Once done, the changes should be validated by rerunning the simulation with the modifications included until tolerable electric fields are achieved. A more detailed methodology is described in section 3.2.5

NASCAP-2K may be obtained by organizations in support of the U.S. government by requesting it from the following website: https://software.nasa.gov/software/MFS-32056-1.

In addition to NASCAP-2K, the European satellite design community has developed a similar modeling tool called Spacecraft Plasma Interaction System (SPIS), https://www.spis.org/software/spis/. A simpler tool that was developed for rapid assessment of charging likelihood of a surface material is EQUIPOT, available within the SPENVIS suite of tools. Finally, detailed design guidance related to surface and internal charging can be found in NASA-HDBK-4002A [53], https://standards.nasa.gov/standard/nasa/nasa-hdbk-4002.

2.4.2.2 Low-Altitude Polar Orbits (Less Than 2000 km LEO)

Polar orbiting satellites in low- to medium-altitude orbits (300–2000 km—generally, LEO to High LEO orbits) with medium to high inclinations (60°–90°) can experience surface charging in the auroral electron environment. The orientation of surfaces and structures on satellites in these orbits present different aspects relative to the satellite-sun line and the satellite velocity vector. Satellites in LEO or passing through low altitudes have velocities higher than the velocities of the ambient ions. As a result, they generate a ram and wake condition about the satellite. The wake is a region of very low ion density created by the satellite "snow plowing" through the slower background ion environment. The electrons have essentially free access into wake regions because of their high velocity relative to that of the ions. This is unique to LEO orbits, and wakes generally do not occur for satellites in high-altitude orbits. Surfaces on satellites in LEO and High LEO orbits can, at times, be both in Earth or satellite shadow and in the satellite wake at the same time, which enhances the chances of surface charging even if the background ion density is high outside the wake. The satellite self-shadowing intervals are in addition to Earth shadowing, which occurs seasonally. It is recommended that all exterior surfaces be conducting and grounded if surface charging and associated ESD are to be reduced for high inclination LEO and High LEO satellites. Otherwise, the satellite system should be designed to tolerate the worst-case surface ESD that could occur, and the design tested to prove that it works.

The newest NASCAP-2K includes the capability to analyze satellite surface charging for LEO and High LEO vehicles in both low- and high-latitude orbits [55][14]. It requires a plasma spectrum as input for the calculations. The surface charging electron environment for LEO to High LEO altitude vehicles that is often currently used is shown in Figure 4 [24]. This environment is basically an accelerated geosynchronous altitude electron environment from MIL-STD-1809 [19]. It is accelerated by 20 kV to account for the fact that in the near-Earth auroral regions, the environment originally comes from high-altitude equatorial regions near geosynchronous altitude and beyond during magnetically active times. It is accelerated Earthward by auroral processes that can include magnetic-field-aligned electric potential drops of kV to tens of kV. The 20 kV acceleration used with the MIL-STD-1809 high-altitude charging environment results in a spectrum that matches a DMSP spectrum from a significant charging case at 800 km altitude [24]. DMSP is known to experience significant surface charging [7][32] relatively often and was used as a representative LEO polar orbiting satellite when forming the LEO to High LEO charging spectrum. Table 2 shows the values extracted from the fits to the data in Figure 4 (dashed gray curves).

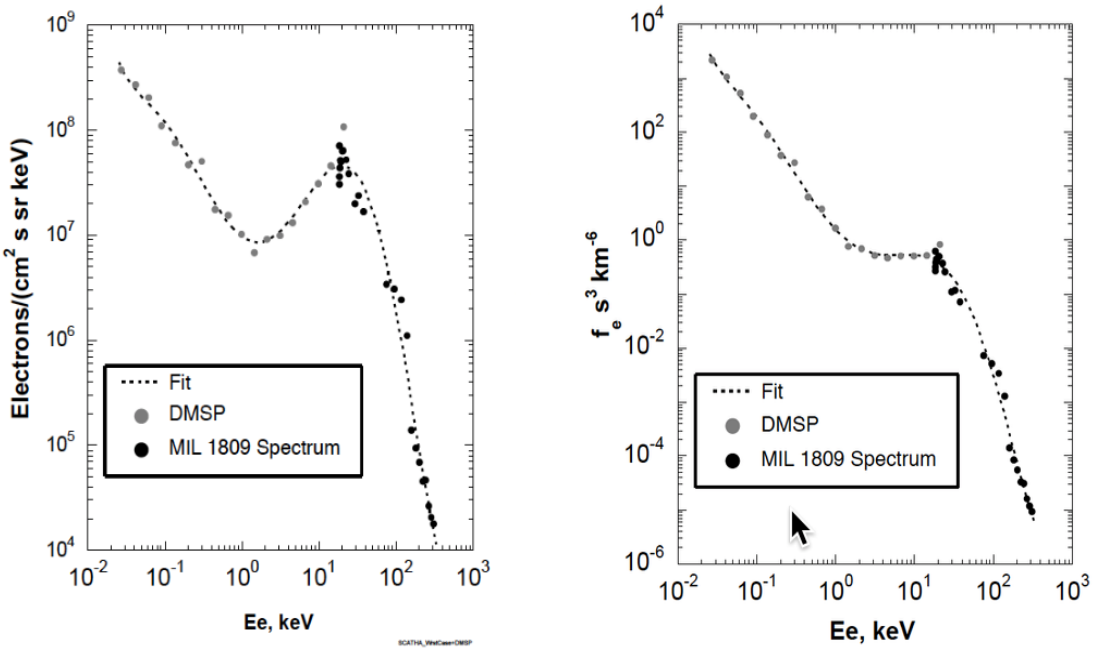

Figure 4. Left: combined DMSP and accelerated MIL-STD-1809 electron flux vs energy spectrum, showing the matched spectrum when MIL-STD-1809 at GEO is accelerated by 20 keV. Right: the electron phase space density corresponding to the surface charging flux at left.

Table 5. The Values of the Electron Flux vs Energy Fits from Figure 4. Note the Energy Spectrum is Staggered over Four Double Columns Separated by Double Vertical Lines.

E_e (keV)	Electron Flux electrons/(cm^2 sec sr keV)	E_e (keV)	Electron Flux electrons/(cm^2 sec sr keV)	E_e (keV)	Electron Flux electrons/(cm^2 sec sr keV)	E_e (keV)	Electron Flux electrons/(cm^2 sec sr keV)
2.51E-02	4.46E+08	2.82E-01	3.56E+07	3.16E+00	1.11E+07	3.55E+01	3.17E+07
2.99E-02	3.45E+08	3.35E-01	2.85E+07	3.76E+00	1.27E+07	4.22E+01	2.41E+07
3.55E-02	2.81E+08	3.98E-01	2.29E+07	4.47E+00	1.49E+07	5.01E+01	1.70E+07
4.22E-02	2.39E+08	4.73E-01	1.86E+07	5.31E+00	1.76E+07	5.96E+01	1.10E+07
5.01E-02	2.08E+08	5.62E-01	1.54E+07	6.31E+00	2.10E+07	7.08E+01	6.59E+06
5.96E-02	1.82E+08	6.68E-01	1.30E+07	7.50E+00	2.51E+07	8.41E+01	3.66E+06
7.08E-02	1.60E+08	7.94E-01	1.12E+07	8.91E+00	2.98E+07	1.00E+02	1.89E+06
8.41E-02	1.39E+08	9.44E-01	1.00E+07	1.06E+01	3.47E+07	1.19E+02	9.25E+05
1.00E-01	1.19E+08	1.12E+00	9.18E+06	1.26E+01	3.95E+07	1.41E+02	4.32E+05
1.19E-01	1.01E+08	1.33E+00	8.71E+06	1.50E+01	4.35E+07	1.68E+02	1.97E+05
1.41E-01	8.38E+07	1.58E+00	8.56E+06	1.78E+01	4.59E+07	2.00E+02	8.98E+04
1.68E-01	6.86E+07	1.88E+00	8.70E+06	2.11E+01	4.60E+07	2.37E+02	4.21E+04
2.00E-01	5.55E+07	2.24E+00	9.15E+06	2.51E+01	4.35E+07	2.82E+02	2.10E+04
2.37E-01	4.46E+07	2.66E+00	9.93E+06	2.99E+01	3.85E+07	3.35E+02	1.14E+04

The values from Table 5 can be used as inputs to surface charging tools, such as NASCAP2K, described in more detail in section 3.2.5.

2.5 Micrometeoroid and Orbital Debris (MMOD)

2.5.1 Overview

Risk assessment for spacecraft for particle impacts consists of two types of software: one to generate the environment (for both orbital debris and micrometeoroids) and the other to perform the risk assessment given the environment and a particular spacecraft. There are several models of the orbital debris environment that are available. NASA uses the Orbital Debris Engineering Model (ORDEM) as its primary tool for generating the orbital debris environment in the near-Earth environment, while ESA uses Meteoroid and Space Debris Terrestrial Environment Reference (MASTER). Aerospace also has the Aerospace Debris Environment Projection Tool (ADEPT) model, although this tool remains in house and is not available to the public. It is built to perform long-term projections but can also be used for survivability analysis in a limited way. For the micrometeoroids, NASA uses the Micrometeoroid Engineering Model (MEM), version 3.1. ESA's MASTER contains its own meteoroid model. Aerospace does not have its own meteoroid model but instead uses MEM. For risk assessment, NASA uses BUMPER and Aerospace uses MODRA.

Of course, if the debris environment changes drastically due to an on-orbit collision or fragmentation event, an assessment of the difference in debris environment for an in-development or on-orbit satellite is warranted.

2.5.2 ORDEM

The current version of ORDEM is 3.1 and is maintained by NASA Johnson Space Center's Orbital Debris Program Office (ODPO). It is available on the Microsoft Windows platform. The input is in the form of a GUI or command line interface that allows for the selection of the orbit (semi-major axis and eccentricity —alternatively apogee and perigee altitude—and inclination). The selectable time ranges from the years 2016 to 2050. The minimum size of generated particles is 0.01 mm. While the model will output files for orbits up through GEO, it is stated that the results for GEO orbits may only be valid for particles larger than 10 cm, as the small particle environment at GEO is largely unknown at the current time. The output from the environment consists of various files denoting the flux as a function of multiple parameters: size, relative velocity and direction, and particle density. Of greatest use in spacecraft risk assessment is the igloo file, which contain flux as a function of size, velocity, and direction for five populations: low density, medium density, high density, the sodium potassium population from the RORSAT satellites, and large intact objects. Certain plots of the parameters can be generated automatically as well. A single ORDEM run is performed for a specified orbit (altitude, eccentricity, inclination) and so multiple orbits require multiple runs. Once generated, the output files are used to perform risk assessments for spacecraft and individual components of spacecraft to assess survivability in codes such as BUMPER and MODRA.

ORDEM is an empirical model, basing its construction on radar observations and examinations of returned Space Shuttle radiators and windows from missions from 1997 to 2011. Since the in situ data comes from the Shuttle, it covers the altitude range of 400 to 600 km and ended with the termination of Shuttle flights in 2011. This source of data is therefore no longer current. Spectroscopic analysis of the radiators and windows performed by NASA showed the presence of small stainless-steel particles. These small stainless-steel particles were incorporated into ORDEM through a surface degradation model (SDM) where the rates in the SDM are coupled with particle decay and adjusted to match the observed STS impacts. However, a general SDM was assumed that allowed for all intact objects in orbit to produce steel particles. This produces some anomalistic results in that the predicted number of small steel particles at higher altitudes should be causing more satellite failures than is observed. The reason for this discrepancy between the historical in situ STS data and a lack of failures at higher altitudes has not yet

been determined. For this reason, users are recommended to evaluate the high-density results from the rest of the model when performing risk assessments.

ORDEM is developed and released by the Orbital Debris Program Office, Johnson Space Flight Center, and is available at https://www.orbitaldebris.jsc.nasa.gov/modeling/engrmodeling.html.

2.5.3 MASTER

ESA has developed a model to generate the flux environment in the near-Earth region, called MASTER. The latest version is MASTER 2009 although additional files updating the background environment were released in early 2020. It can be run on PC or Linux platforms. In contrast to ORDEM (which is largely based on empirical observations with some source physics), MASTER bases the orbital debris environment on particle sources (with some observational evidence). The particle sources that users can select are: explosion fragments, collision fragments, intact launch/mission objects, NaK droplets (sodium potassium from the RORSAT vehicles), solid rocket motor slag, solid rocket motor dust, paint flakes, ejecta, multi-layer insulation (MLI), and debris from certain specific collisions (Fengyun and Iridium/Cosmos). Each of these can be turned on or off at the desire of the user.

In addition to the man-made orbital debris flux, MASTER also contains the option of including micrometeoroids through the Divine-Staubach model to provide an estimate of the sporadic meteor environment [18][83]. Note that the meteoroid population is, at a high level, divided between the background sporadic meteors that are smoothly spread out in heliocentric space and the denser, but much shorter in duration, annual streams. The Divine/Staubach model uses observational data of interplanetary dust from various satellites (Pioneer, Helios, Galileo, and Ulysses) and the IAU meteor database to describe orbit characteristics and then groups the results into five sources: the core population (most numerous), asteroids, inclined, eccentric, and halo particles. The density of the individual particles is assumed to be 2 g/cm3. MASTER allows for the selection of two types of meteor stream models (Jenniskens 1994 [34] and McBride 1997 [45], or Cour-Palais 1969 [11]). The Jenniskens model is more comprehensive (50 streams versus 18 for Cour-Palais) and is much more recent than Cour-Palais. For this reason, the Jenniskens model is preferred.

MASTER is made available to the public by the Space Debris Office of the European Space Agency and is available at https://sdup.esoc.esa.int/.

2.5.4 ADEPT

Aerospace's ADEPT was built for the primary purpose of providing long-term estimates of the debris population growth due to collisions and explosions to support policy development and fulfillment of space debris assessment reporting (SDAR) requirements. Debris down to 1 cm is generated for explosions (based on historical likelihood) and collisions (identified through an orbit-trace-crossing method) using the hypervelocity code IMPACT. Multiple generations of debris can be created (i.e., the collision debris that arises from one run-through of the code can be fed back in to create a second generation of debris, and a third, and so on).

While built for long-term analysis and limited to particles of size 1 cm and greater, ADEPT results can be used to perform satellite risk assessment. For collision and explosion debris smaller than 1 cm, an extrapolation is performed using the results greater than 1 cm. For other small particle populations (sodium potassium droplets from RORSAT reactors, aluminum slag and liner particles from solid rocket motor firings, and the Westford needles), separate models have been developed similar in formulation to those used in MASTER. This allows a user to perform assessments for orbital debris down to about 0.1 mm in size (small enough to cover penetration threats to space vehicles).

The software is in house to Aerospace and as such is not available for general use. It can be utilized to perform risk assessment for smaller particles. For analysis or information requests, contact Marlon Sorge at Aerospace at marlon.e.sorge@aero.org.

2.5.5 Micrometeoroid Engineering Model (MEM)

NASA's MEM, version 3.1, is the current standard micrometeoroid model for spacecraft analysis and is maintained by Marshall Space Flight Center [50]. It is available on the PC and can be run through either a GUI or command line prompt. The input is a text file containing the desired orbit at user-specified time steps. Single-value files can be handled as well. MEM simply reads the file and does not expect a closed-form orbit. The output files describe the environment in various ways: flux (number of particles), velocity (magnitude and direction), and density (mass of the particle). Different coordinate frames can be selected as well: body-fixed, equatorial, or ecliptic. The center of the coordinate frame can be selected from various solar system bodies: Sun, Earth, Moon, Mercury, Venus, or Mars. As with ORDEM, these files (notably the igloo file) are then used as input to other code to compute risk. Note that ORDEM, MEM, and BUMPER were constructed to be compatible in terms of file format usage.

MEM uses a methodology based on the orbital characteristics of presumed sources and the physics of small particles to drive the flux and velocity distribution of the particles. The results are constrained by observations from the Canadian Meteor Orbit Radar (CMOR). It is a heliocentric model and does not contain the annual meteor showers. However, the annual showers do not contribute to the overall mean flux by more than a few percent and therefore are not necessary for pre-mission types of spacecraft risk assessment. If time-dependent anomalies are the subject of examination, then the meteor streams would be necessary (i.e., a model like Jenniskens in MASTER). The MEM model is limited to producing the flux for particles of 10^{-6} grams, but since particles smaller than 10^{-6} g are highly unlikely to penetrate spacecraft surfaces (and orbital debris in LEO dominates the micrometeoroids at this size), the lower limit of 10^{-6} grams is sufficient. The model is constructed to produce the flux for a requested input mass value. If mass variation is to be examined, separate runs must be performed.

MEM can be requested from the Office of Safety & Mission Assurance (SMA), Marshall Space Flight Center, at https://sma.nasa.gov/sma-disciplines/meteoroid-environments.

2.6 Atomic Oxygen (AO)

AO is a component of the neutral atmosphere. It is the dominant species by number density in the altitude range of roughly 300 to 700 km, and the density at a constant altitude varies strongly with solar activity. AO is a highly corrosive species and erodes polymers on surfaces of LEO spacecraft and those in elliptical or GEO-transfer orbits with low-altitude perigees. These polymers are often used on spacecraft as thermal control surfaces to manage the thermal balance of sensitive sensors or electronics. The erosion of these surfaces degrades their emissivity, putting sensitive components underneath at risk of over-heating.

One such polymer is Kapton, often used for thermal blankets. An experiment on the International Space Station (ISS) [16] determined the erosion yield to be 3.0×10^{-24} cm^3/AO atom by pre- and post-flight weighing of Kapton samples exposed to the LEO AO environment. Accordingly, spacecraft that fly through regions of high AO number density must account for this erosion and use thick enough polymers to sustain adequate thermal properties throughout the mission life.

Upper atmosphere models, such as NRLMSISE-00 model [67], are often used to provide estimates of the AO environment. At Aerospace, we use the version available within the International Radiation Belt Environment Model (IRBEM) library at https://github.com/prbem/irbem and have developed a method to

use the NRLMSISE-00 model to estimate AO confidence levels over the course of a mission. The empirical model takes solar activity (F10.7) and geomagnetic activity (Ap) indices as inputs and can provide estimates of the AO density, including NRLMSISE-00 outputs oxygen and "anomalous oxygen," per Picone et al. [67]. By repeatedly sampling a satellite orbit within a changing model atmosphere, these model estimates can be used to simulate spacecraft exposure to AO over a mission length, and the amount of polymer erosion can be calculated. Spacecraft thermal designers must then plan accordingly. See section 3.1.4 for details on the method used and results from this method.

3. Software Implementation, Methods, and Results

The current section describes the currently available software tools that are used to query the geophysical models discussed in the previous section. Here we describe the methods used to run or combine them into specifications and present worked examples of environment generation. This section is divided into two main subsections devoted to specifications of whole-mission accumulated quantities (section 3.1) and whole-mission worst-case quantities (Section 3.2).

3.1 Whole-Mission Accumulated Quantities

A primary use of an environment specification is to estimate the total mission accumulated environment for all particles that lead to long-term degradation effects. The design process can then include sufficient mitigation to ensure the satellite components are not adversely affected after exposure to these environments. These effects are listed in Table 6, and include total ionizing dose, displacement damage, catastrophic single-event effects, surface material dose, and surface material corrosion from atomic oxygen fluence in LEO orbits. Table 6 also lists the environments contributing to these hazards, spacecraft components at risk from those hazards, and typical mitigation strategies used to ensure the mission operates for its lifetime despite this environmental degradation.

Table 6. Example Spacecraft Hazards Stemming from Long-Term Environmental Accumulation, Including Typical At-Risk Components, and Mitigating Strategies

Hazard	Environments Contributing	Components at Risk	Mitigating Strategies
Total ionizing dose	Trapped protons, trapped electrons, solar proton fluence	EEE parts	Pick radiation-tolerant EEE parts, increase shielding
Displacement damage	Trapped protons, solar proton fluence	Solar cells, focal-plane arrays, optical fibers, EEE parts	Solar cells: choose radiation-tolerant cells, increase thickness of cover glass, FPA add shielding to limit dark current increase by EOL Optical fibers: choose radiation-tolerant fibers, add shielding
Single-event effects	Galactic cosmic ray LET spectra, trapped proton, solar particle LET spectra	Active devices, volatile memories	Error detection and correction (EDAC) system scrub frequency, redundant voting logic. Shielding not usually practical.
Surface material dose, degradation	Low-energy plasma protons, electrons	Surface paints, coatings, radiators	Choose or verify external material not damaged after exposure to mission-length plasma environment.
Surface polymer erosion in LEO	Atomic oxygen fluence	External polymers (e.g., Kapton) erode from corrosive atomic oxygen in LEO. Thinning makes thermal control surfaces less emissive.	Choose radiator material or thickness to ensure emissivity adequate to cool underlying components at EOL
Particulate impacts	Micrometeoroid/Orbital Debris	Surfaces, solar arrays, exposed propulsion lines	Multi-layer shielding for momentum dissipation of small impacts, judicious routing of harnesses internal to bus

In an appropriate environmental specification, these whole-mission accumulated quantities are calculated using the tools and methods described in the following sections. Worked examples are provided for many of the sections for two main reasons. First, the methodology is more clearly and comprehensively described if interim results are provided. Second, the reader can perform these calculations using their own installation of these tools and check the accuracy of the results with the values provided here. To enable worked examples, we performed a small orbit survey using the four orbits whose elements are provided in Table 7. These were the input orbits used to provide the results in the following sections.

Table 7. Orbital Elements for Worked Examples

Tag	Apogee (km)	Perigee (km)	Inclination (deg)	Eccentricity	Arg. Perigee (deg)	RAAN (deg)
GEO	35793	35793	0	0	0	0
HEO	38518	1863	63.4	0.690	270.0	60.0
LEO	800	800	98.0	0	270.0	10.7
GPS	20191	20191	55	0	0	0

3.1.1 Trapped Electron Fluence—AE9

In this section, we describe the process to determine a mission accumulated trapped electron fluence. This is done using the AE9-IRENE model. The basic process is to get the flux versus time for many perturbed mean scenarios (as described in section 2.1.4), accumulate those fluxes into fluence, then combine the results to compute confidence intervals. Most of these steps are handled automatically by the latest version of IRENE. In the case of multi-year mission integrated quantities, the AE9/AP9 models can be efficiently run using a short time period (approximately one week) then scaled up to the desired mission duration.

Although many effects tools require differential (in energy) particle flux or fluence as inputs, we recommend it as a best practice to compute confidence levels from integral (in energy) flux or fluence. This allows the percentile calculation that is included in the confidence-level determination to better reflect the cross-energy correlation present in the time-dependent variations in Monte Carlo scenarios and the energy-dependent uncertainties in both the perturbed mean and Monte Carlo scenarios. Ideally, one would perform these percentile calculations as the last step in any confidence-level estimation, but that is often not possible when the effect calculation step involves a complex code or one that cannot easily be performed automatically for each of many scenarios. Therefore, we compute the confidence levels on integral fluxes or fluences and then differentiate those. An integral flux $J_>(E)$ can be converted to a differential flux $j(E)$ using a derivative that treats the flux as having an inherently power-law spectrum:

$$j(E) = -\frac{\partial J_>(E)}{\partial E} = -\frac{\partial \log J_>(E)}{\partial \log E}\frac{J_>(E)}{E}$$

The derivative can be taken numerically, and it does not matter whether common (base 10) or natural logarithms are used in the rightmost expression. Of course, where $J_>(E) = 0$, $j(E)$ is also zero.

To illustrate this method of specification generation, we will use the example of computing the 95th percentile electron fluence for a GPS orbit. The most straightforward way to run the model is to use the IRENE GUI. Table 5 shows an example of the available GUI options. The *Satellite* tab allows for entry of the orbital parameters. Here, we have set it to run the GPS orbit (as shown in Table 7) for one week. The time step should be set according to section 2.1.6. For the GPS orbit, we use a timestep of 300 seconds.

The *Model* tab allows us to set the model parameters. In this example, we chose *Perturbed Mean* and ran 40 scenarios. Here we selected only the electron energies, so we will run only the AE9 model. However, if both electron and proton fluence are needed, they can both be selected and run simultaneously. We then have the option to choose differential or integral fluence. Here, we use *Integral Fluence*. Finally, *AccumInterval* sets the time steps where the fluence will be output. This can be set to 0 to output at the ephemeris cadence or -1 to just output the total mission fluence. The final panel is the advanced options tab. By default, the model will output the mean, 50%, 75%, and 95% confidence levels, which is appropriate in this example.

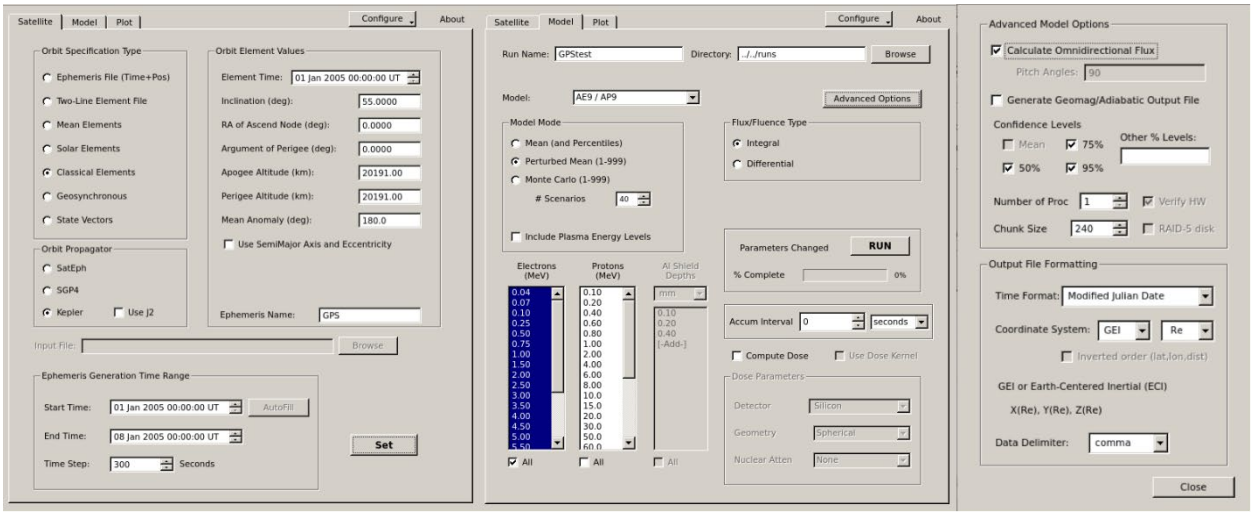

Figure 5. IRENE GUI options.

> CmdLineIrene.exe -i GPStest.AE9.input.txt

```
ModelType: AE9
FluxType: Integral
Energies: 0.04,0.07,0.1,0.25,0.5,0.75,1,1.5,2,2.5,3,3.5,4,4.5,5,5.5,6,6.5,7,8.5,10
OutFile: ../../runs/GPStest.AE9.output.txt
ModelDB: ../../modelData/AE9V15_runtime_tables.mat
MagfieldDB: ../../modelData/igrfDB.h5
AccumMode: Cumul
KPhiNNetDB: ../../modelData/fastPhi_net.mat
KHMinNNetDB: ../../modelData/fast_hmin_net.mat
FluxOut: Perturbed, 1-40
FluenceOut: true
Aggregate: Percent, 50, 75, 95
TimeSpec: MJD
CoordSys: GEI
CoordUnits: Re
DataDelim: comma
OrbitFile: ../../runs/ephem_GPS.dat
```

Figure 6. Input file for GPS electron fluence calculation.

The output files are the same format as described in section 3.1.1, with files named according to the following nomenclature: GPStest.AE9.output_pert_fluence_010.txt contains the fluence for each scenario

and GPStest.AE9.output_pert_fluence_conf_level_95.txt contains the combined 95th percentile fluence over all scenarios. An example of the 95th percentile output file is shown in Table 8.

Table 8. Electron Fluence Output File for GPS Example

MJD	posx(Re)	posy(Re)	posz(Re)	J(>.04 MeV)	J(>.07 MeV)	J(>0.1 MeV)	J(>8.5 MeV)
53371	-4.1691	0.0000	0.0000	0.00E+00	0.00E+00	0.00E+00	0.00E+00
53371.003	-4.1651	-0.1045	-0.1494	1.92E+10	1.46E+10	1.18E+10	5.51E+04
53371.007	-4.1531	-0.2090	-0.2985	3.81E+10	2.91E+10	2.35E+10	1.05E+05
53371.01	-4.1332	-0.3130	-0.4470	5.86E+10	4.33E+10	3.50E+10	1.48E+05
…	…	…	…	…	…	…	…
53378	-4.0507	-0.5653	-0.8073	1.95E+13	1.46E+13	1.17E+13	3.72E+07

Here we have output the fluence for a 1-week mission, so to scale up to a 10-year mission, we multiply by (10*365.25)/7 = 521.785. This scaling allows for a much faster calculation while still giving an accurate fluence spectrum. This is illustrated in Figure 7, which shows a comparison of the scaled 1-week fluence to a full 10-year 40-scenario Monte Carlo simulation. Good agreement implies that the variable space weather during a 10-year simulation largely averages out, and the results collapse to the perturbed mean (including model uncertainty only) results captured after a week.

Caution: While a seven-day simulation of a GPS orbit sampling the outer radiation belt sufficiently samples all regions of the radiation belts, this is not always the case. Orbits that experience long-term variation of the radiation environment to which the satellite is exposed over its entire mission life should not take advantage of this computational convenience and should rather simulate the entire mission. These cases include, but are not limited to:

- Non-station-kept science missions with orbital elements that slowly precess over the mission life
- Higher-order orbital perturbations (above J2) that cause critically inclined HEO perigees to wander in altitude.

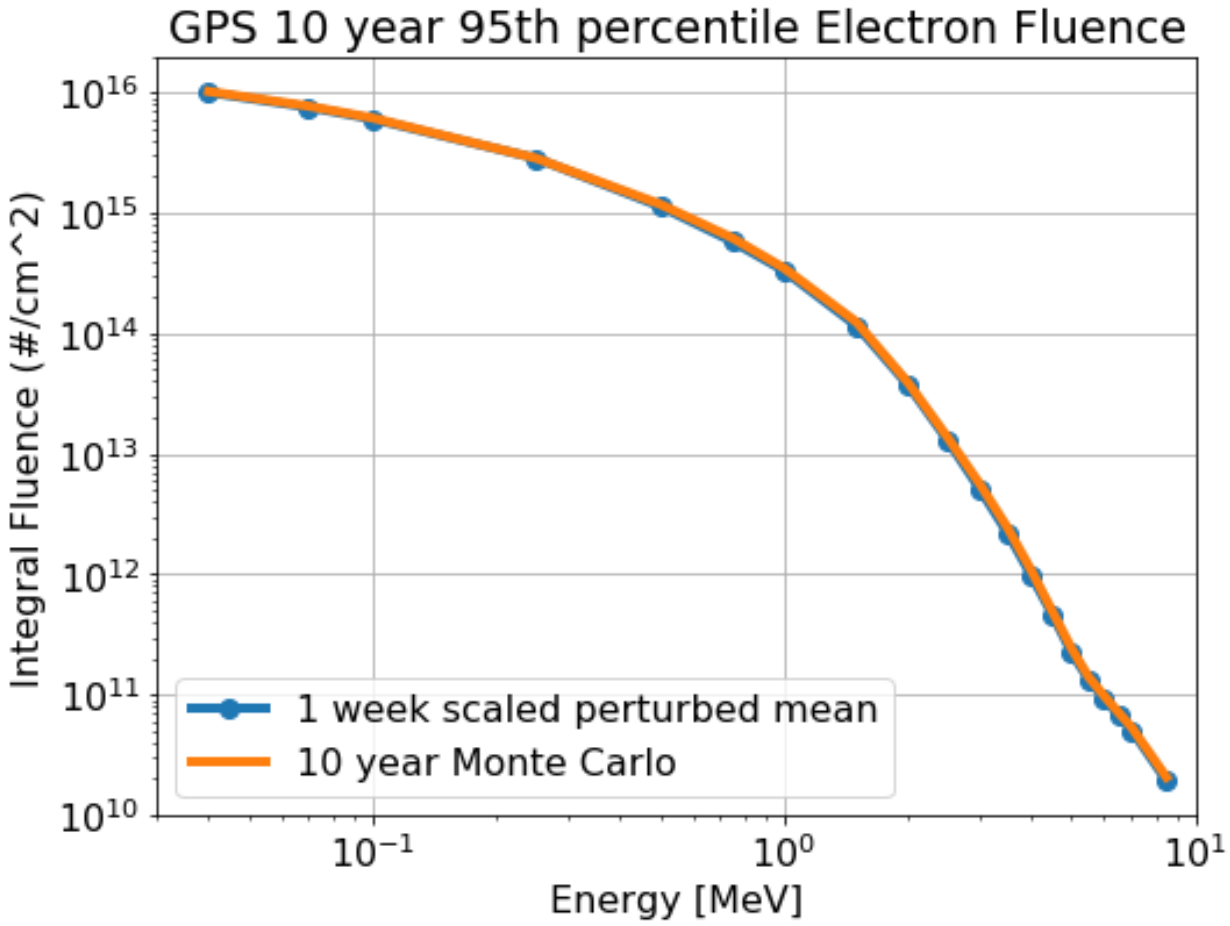

Figure 7. Comparison of scaled-up perturbed mean and mission-length Monte Carlo proton fluence.

This procedure is then repeated for each desired orbit. The 10-year integral electron fluence for each of the example orbits is shown in Figure 8. The mission-length electron fluence spectrum is one essential part of an adequate environment specification.

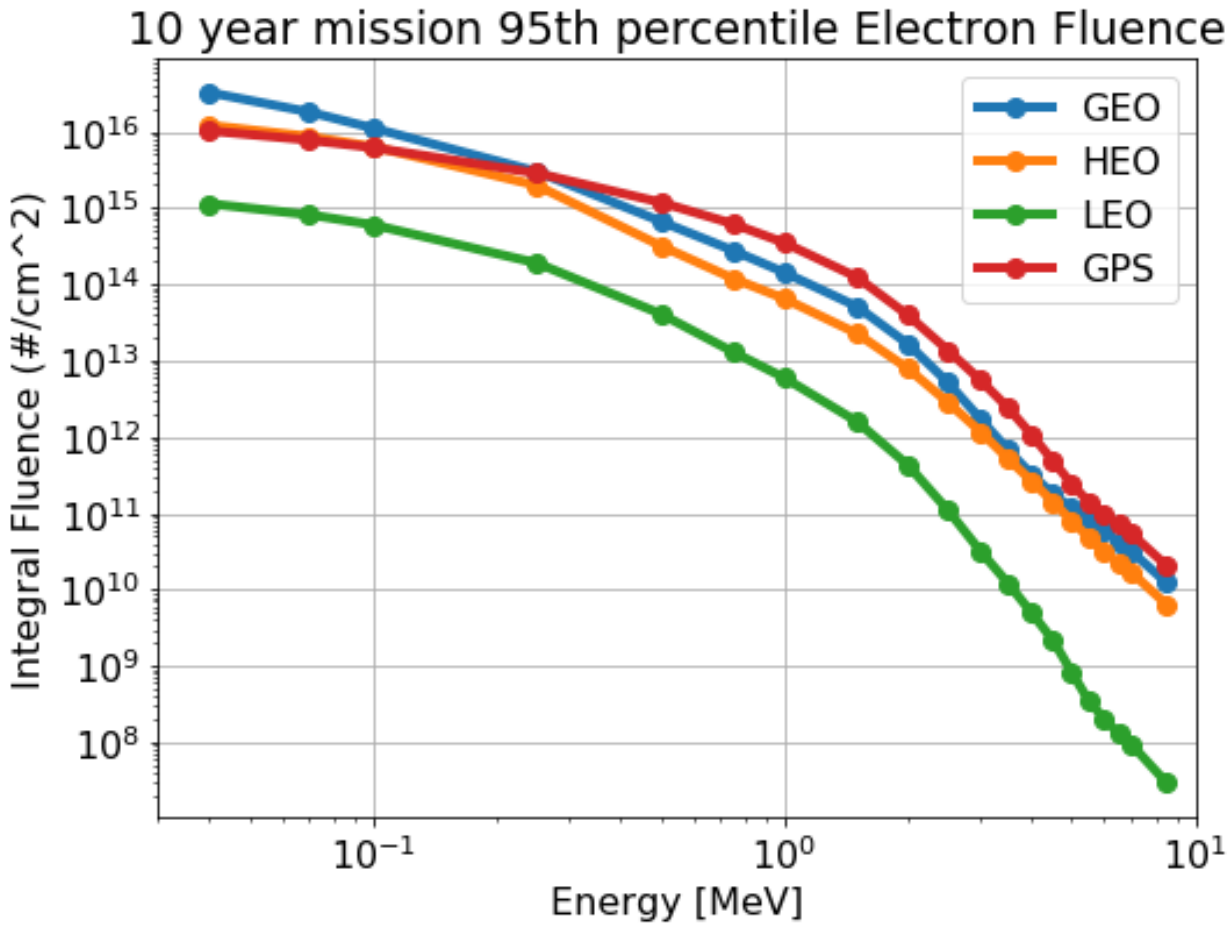

Figure 8. 95th percentile electron fluence for each of the example orbits.

3.1.2 Proton Fluence

Estimating the whole-mission-accumulated proton fluence is more difficult than the electron fluence because there are two sources of proton exposure: the trapped proton belt and solar protons. Orbits that intersect the trapped proton radiation belt are exposed to protons during every traversal, while only episodically do solar particle events occur, causing exposure outside a geomagnetic cutoff. This section describes how to generate each of the sources in turn and finishes by describing the method used to appropriately combine them into a mission-accumulated proton fluence.

3.1.2.1 Trapped Proton Fluence—AP9

To determine the mission-accumulated trapped proton fluence, we can again use IRENE-AP9. Much like the description of accumulating the trapped electron fluence in section 3.1.1, we describe the steps taken to produce the 95th percentile proton fluence for a HEO orbit.

Using the GUI, we input the appropriate orbital parameters on the *Satellite* tab to set it to run the HEO orbit (described in Table 7) for one week. The time step should be set according to section 2.1.6. For the HEO orbit, we use a timestep of 60 seconds. The *Model* tab allows us to set the model parameters. In this example, we again choose *Perturbed Mean* and run 40 scenarios. Here we selected only the proton energies, so we will run only the AP9 model. We then have the option to choose differential or integral fluence. Here, we use *Integral Fluence*. Finally, *AccumInterval* sets the time steps where the fluence will

be output. This can be set to 0 to output at the ephemeris cadence or -1 to just output the total mission fluence. Again, we leave the default Advanced options, so the model will output the mean, 50%, 75%, and 95% confidence levels, which is appropriate in this example. Running the GUI with these options will produce the input file `HEOtest.AP9.input.txt` that is shown in Figure 9.

```
ModelType: AP9
FluxType: Integral
Energies: 0.1,0.2,0.4,0.6,0.8,1,2,4,6,8,10,15,20,30,50,60,80,100,150,200,300,400,700,1200,2000
                                        OutFile: ../../runs/HEOtest.AP9.output.txt
ModelDB: ../../modelData/AP9V15_runtime_tables.mat
MagfieldDB: ../../modelData/igrfDB.h5
AccumMode: Cumul
KPhiNNetDB: ../../modelData/fastPhi_net.mat
KHMinNNetDB: ../../modelData/fast_hmin_net.mat
FluxOut: Perturbed, 1-40
FluenceOut: true
Aggregate: Percent, 50, 75, 95
TimeSpec: MJD
CoordSys: GEI
CoordUnits: Re
DataDelim: comma
OrbitFile: ../../runs/ephem_HEO.dat
DataDelim: comma
OrbitFile: ../../runs/ephem_HEO.dat
```

Figure 9. Input file for HEO proton fluence.

Running this will give output files for each scenario with names like `HEOtest.AP9.output_pert_fluence_010.txt` and a file with the 95th percentile fluence named `HEOtest.AP9.output_pert_fluence_conf_level_95.txt`. Each of these data files have the same format, giving the integral fluence (#/cm^2) at each energy value as a function of time. An example of the 95th percentile output file is as shown in Table 9. If *AccumInterval* is set to -1, there will be a single line containing the total mission fluence. Otherwise, the last line gives the total mission fluence.

Table 9. 95th Percentile Proton Fluence Output File for HEO Orbit

MJD	posx(Re)	posy(Re)	posz(Re)	J(>0.1 MeV)	J(>0.2 MeV)	J(>0.4 MeV)	J(>1200 MeV)	J(>2000 MeV)
53371	-3.523	-6.102	0.000	0.00E+00	0.00E+00	0.00E+00	0.00E+00	0.00E+00
53371.0007	-3.517	-6.105	-0.014	2.30E+08	7.86E+07	9.77E+06	0.00E+00	0.00E+00
53371.0014	-3.511	-6.109	-0.028	4.58E+08	1.56E+08	1.95E+07	0.00E+00	0.00E+00
53371.0021	-3.504	-6.112	-0.042	6.85E+08	2.34E+08	2.91E+07	0.00E+00	0.00E+00
…	…	…	…	…	…	…	…	…
53378	-3.335	-6.161	-0.384	3.17E+12	1.17E+12	1.65E+11	2.32E+04	0.00E+00

As with our IRENE-AE9 run above, here we have output the fluence for a 1-week mission, so to scale up to a 10-year mission, we multiply by (10*365.25)/7 = 521.785. This procedure can then be replicated for each desired orbit. The 10-year integral proton fluence for each of the example orbits (Table 7) is show in Figure 10.

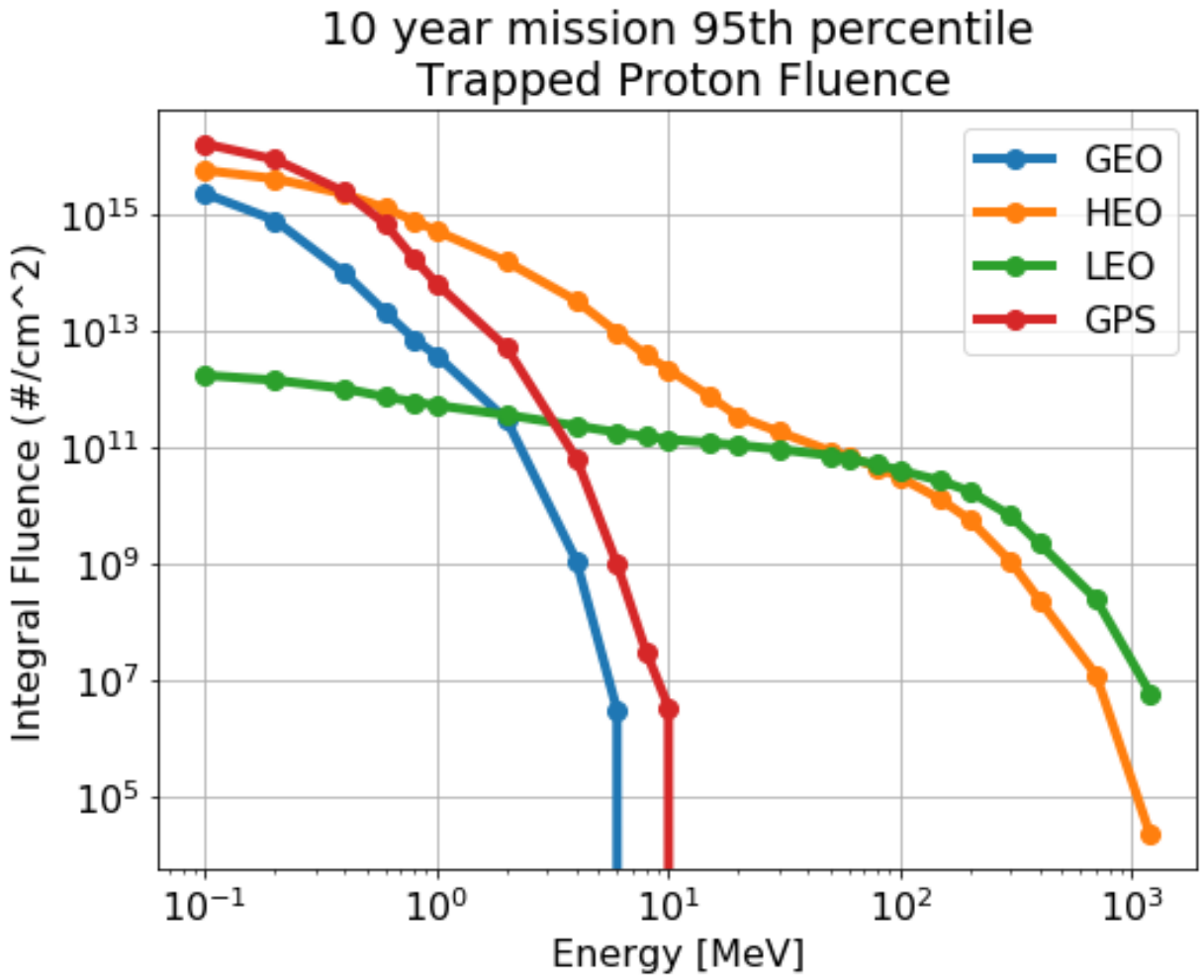

Figure 10. Trapped proton fluence for each example orbit.

Figure 10 illustrates a few general trends regarding orbital exposure to the inner belt protons. First, only LEO and HEO orbits that spend an appreciable amount of time traversing the inner belt (referred to as the South Atlantic Anomaly or SAA in LEO) encounter significant numbers of protons with energies above approximately 10 MeV. For GPS and GEO orbits that fly above the inner belt, the proton fluence becomes minimal above 10 MeV. Also, since the low-energy (1–10 MeV) extent of the inner belt extends to higher altitudes and is primarily limited to the equatorial regions, the 1–10 MeV proton fluence at HEO is far higher than at LEO.

3.1.2.2 Solar Proton Fluence

The whole-mission solar proton fluence can be constructed using any of the models described in section 2.3.1, but at Aerospace, we use ESP [91][92]. We use static tables of the ESP fluences for 10-year GEO missions that include 7 years of solar maximum conditions provided by M. Xapsos. The tables are included in 7.Appendix A, and represent the solar proton fluence versus energy at representative

confidence levels from 1% to 99%. The GEO environment is the same as having no geomagnetic shielding.

In our example, rather than running numerous orbits and attenuating that GEO fluence spectra through a separate calculation, we apply geomagnetic shielding to the GEO fluence and combine it with the trapped proton fluence according to the method described in the next section. To arrive at a consistent risk posture, we choose the same confidence level of solar protons as trapped protons from AP9 and add them, subject to the residence time outside the geomagnetic cutoff.

3.1.2.3 Combining Trapped and Solar Proton Specifications

Earth's magnetic field serves to trap protons inside a geomagnetic cutoff value and exclude solar protons from penetrating inside that cutoff. Accordingly, certain orbits that traverse these cutoffs have varied exposure to both trapped and solar proton environments. For aggregated quantities such as whole-mission proton-fluence exposure, both environments need to be added but modulated by the time spent inside or outside that cutoff.

For the examples provided here, we attenuate the solar protons as follows. We use the relationship determined by Mazur et al. [44], Figure 4, as an empirical method to "map" the ESP environment at GEO to lower orbits. This figure is reproduced in Figure 11 of this document, along with the tabulated values of adjusted invariant latitude as a function of proton energy. This relationship was derived from observations of various proton energies in solar particle events penetrating to different magnetic latitudes as a function of proton energy. The observations were made by the NASA mission SAMPEX, at a 600 km circular orbit. We tabulate this relationship of Mazur et al. [44] for protons (1H in the dashed red curve), transform it from invariant latitude (Λ) to L-shell assuming a dipole field ($L=1/\cos^2(\Lambda)$), and determine the fractional time the orbit spends outside (at a higher invariant latitude or L-Shell) the cutoff at each energy. The unattenuated differential-in-energy solar proton fluence at a given confidence level (Appendix A, Table 16) is multiplied by this fraction to reduce the flux encountered by the orbit. Because solar particle access is controlled by the incident particle rigidity, the differential flux needs to be attenuated prior to integrating in energy or calculating LET.

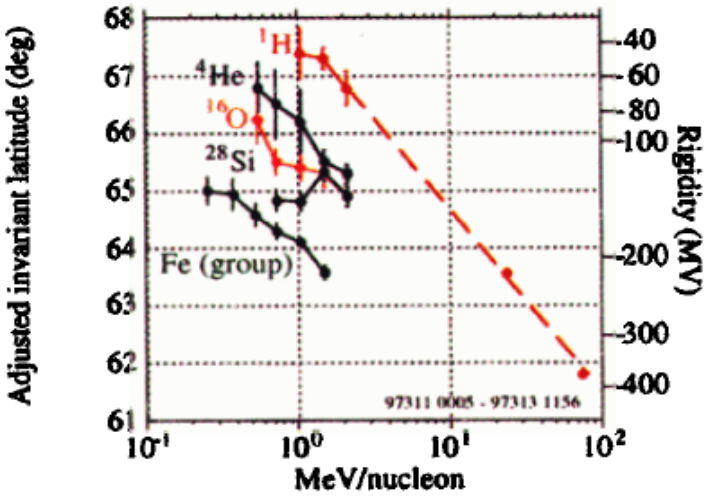

Proton Energy (MeV)	Adjusted Invariant Latitude (deg)	Dipole L-Shell
1.05	67.387	6.76
1.5	67.3	6.71
2.125	66.777	6.43
23.7	63.571	5.05
75.2	61.799	4.48

Figure 11. Empirical determination of the geomagnetic transmission function from Mazur et al. [44].

In our example, we ADD the output of AP9 (section 3.1.2.1) and solar protons (section 3.1.2.2), accounting for the geomagnetic attenuation according to the method discussed in this section to arrive at a

final total mission-length proton spectrum of an appropriate confidence level. The results for all four orbits in our survey are shown in Figure 12. The fluence spectra for the trapped proton population is plotted in dashed lines, while the total is given in solid lines for comparison. The mission-length proton-fluence spectrum is one essential part of an adequate environment specification.

Special note on combining confidence levels: In general, to compute the true confidence level of any derived quantity or effect that combines energies, species, or models, it is necessary to compute the desired confidence level from the statistics of the effects, rather than computing the effects from the flux at the desired confidence level. Nonetheless, it is a convenient, reasonable, and conservative approximation of adding the 95% confidence-level SEP fluence to a similar 95% confidence-level integral-fluence table for a trapped model like AP9. By the same logic, dose from the SEP fluence can be added to dose from the trapped fluence at the same confidence level. This adding procedure is conservative because it assumes that the sources of uncertainty in solar and trapped populations are perfectly correlated, which is untrue. In fact, much of the uncertainty in the trapped population is due to model uncertainty, which is necessarily uncorrelated with the uncertainty in the SEP model. The SEP model uncertainty is typically represented as being entirely due to dynamic uncertainty (variation between solar cycles), while the degree of SEP model uncertainty is assumed to be much smaller. Since uncertainties are not perfectly correlated, the true 95% confidence level of the combined solar plus trapped fluences is necessarily lower than the sum of the 95% confidence levels of the individual fluences (or doses). This paragraph is taken from O'Brien et al. [63]. One must take care when adding integral spectra with different energy ranges, especially when the lowest energies differ. For instance, if AP9 starts at 0.1 MeV and ESP starts at 1 MeV, then add the ESP 1 MeV fluence to all the AP9 channels below 1 MeV to avoid a jump in the 1 MeV summed spectrum.

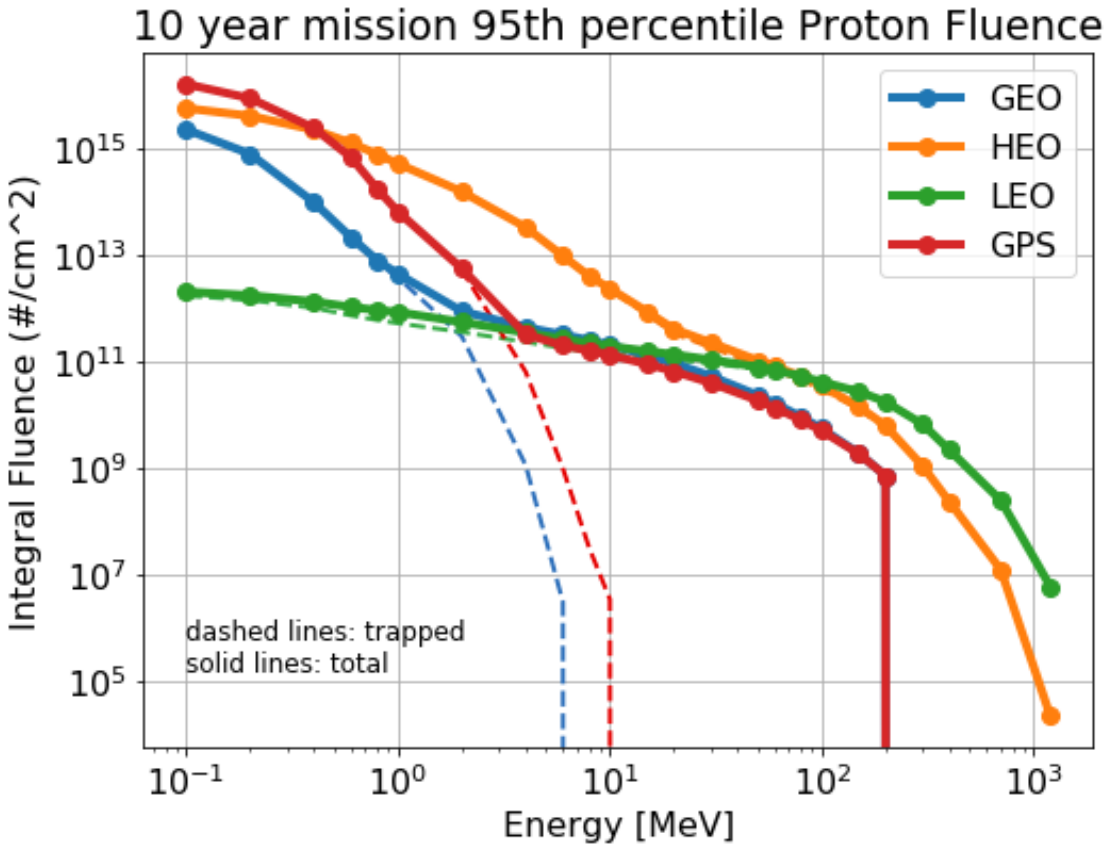

Figure 12. Proton fluence for each example orbit.

A comparison of Figure 12 (total proton fluence) with Figure 10 (trapped proton fluence) illustrates a few key differences. Adding the 95% confidence-level solar particle environment to the trapped environment of GEO and GPS orbits extends the fluence spectra for these orbits to high energies. There is still a steep drop-off in proton flux at 300 MeV, however. This is due to the ESP model [92] having a last valid energy at 300 MeV. Above this, for high-altitude orbits like GEO or GPS, there are no other trapped protons above this energy, so the flux goes to zero. We treat the low flux of GCR protons at these and higher energies separately in section 3.1.3.

Also note that the 95% confidence-level trapped proton fluence still exceeds the 95% confidence-level solar proton fluence for energies roughly greater than 30 MeV, and that difference increases with increasing proton energy.

3.1.2.4 Derived Radiation Effects for Reference

The mission-length electron (Figure 8) and proton (Figure 12) fluence spectra can be used in a variety of transport tools to estimate, for reference, the total ionizing or non-ionizing dose values of interest to the satellite engineering community. At the very outset of a satellite program, often the engineering organization does not yet have a detailed CAD model of the satellite in question, so we turn to simple tools to calculate dose and displacement damage as a function of depth through idealized geometries of aluminum shielding. The assumptions we use are simplified, but typically conservative to ensure the actual dose inside shielding doesn't increase with increasing satellite or modeling fidelity.

For the analysis we perform at Aerospace, we calculate dose for reference using Shieldose2 [77]. Shieldose2 supports three idealized shielding geometries (semi-infinite plane medium, finite-thickness slab, and hemisphere), and we typically double the third output "1/2 dose at the center of Al spheres" to arrive at 4π-steradian spherical shielding geometry with irradiation from all sides. This is a generally conservative assumption for satellites larger than CubeSats and is therefore a good starting point for beginning to procure EEE parts and perform a preliminary system design.

As an example, in Figure 13 we plot the 95% confidence-level total ionizing dose curves versus shielding depth for the 4 orbits considered in this report. To arrive at this result, we take the total mission fluence from protons and electrons from all 40 Monte Carlo scenarios, use Shieldose2 to calculate the dose/depth curve from those 40 scenarios, and take the 95th percentile one (38th out of 40 ranked from low to high) to highlight for reference in Figure 13.

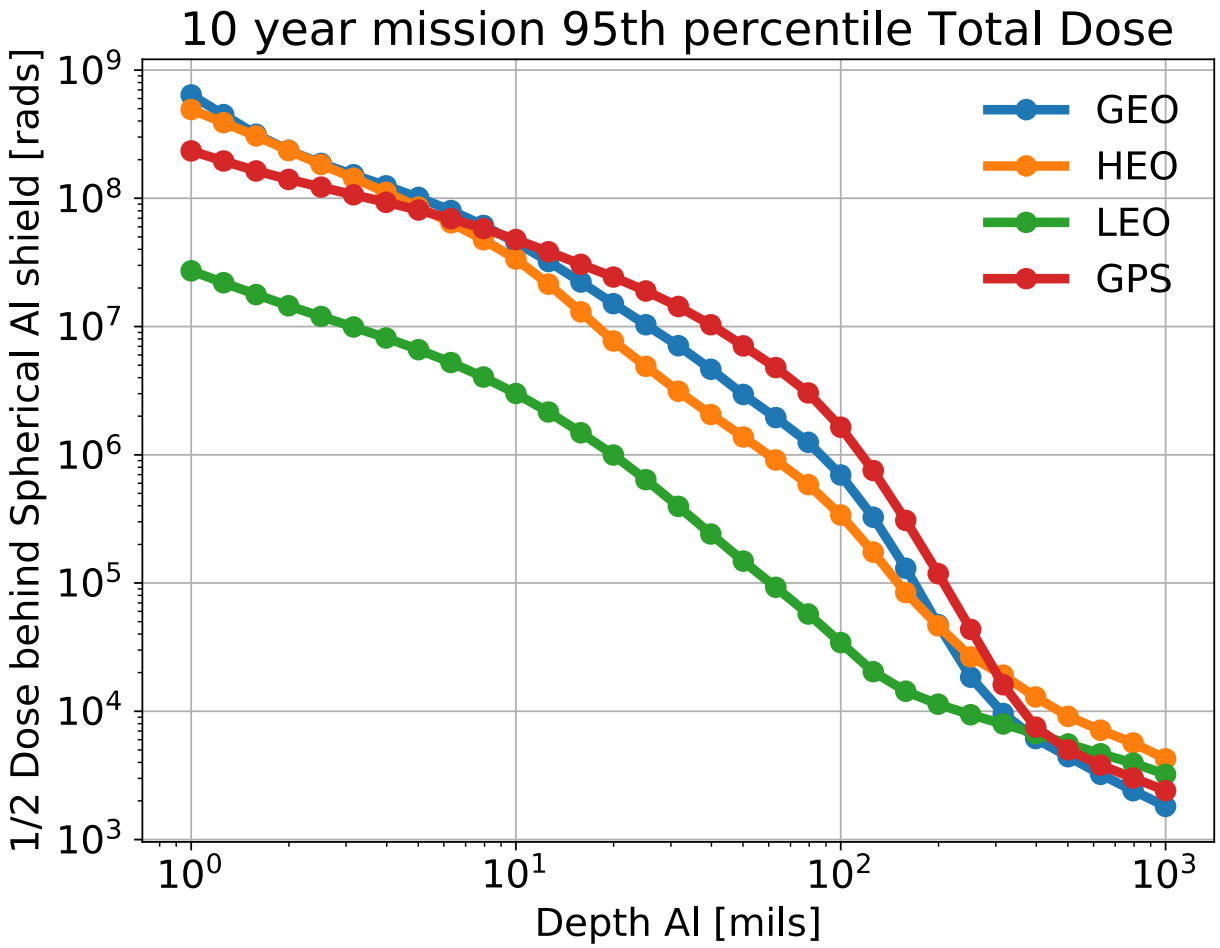

Figure 13. 95th percentile dose-depth curves for the example orbits.

NOTE: We do not apply a radiation design margin (RDM) to this 95% confidence-level dose-depth curve. The 95% confidence level of perturbed mean or Monte Carlo runs explicitly includes the environmental model's uncertainty; therefore, it is unnecessary to add more environmental margin. This is discussed in more detail in section 4.5.

In this analysis, we have specified integral fluxes/fluences for trapped environments outside the satellite. However, when fluxes across all energies involved in an effect are highly correlated, using differential quantities (differential flux or fluence) can be the better approximation than using integral quantities. Either expert knowledge of the underlying environmental phenomena or test runs would be required to determine when this is true on a case-by-case basis.

Similarly, we can compute a preliminary displacement damage dose specification. We use one of the AE9/AP9-IRENE precomputed kernels to approximate 1 MeV equivalent neutron fluence from the 40 Monte Carlo proton scenarios at the end of mission lifetime. These kernels approximate displacement damage dose either by using (1) the continuous slowing-down approximation and NIEL curves of incident protons in Si or GaAs [61] or (2) MULASSIS runs to estimate displacement damage in Si [57]. From those 40 end-of-mission displacement damage curves, we again choose the 95% confidence level (38th out of 40 ranked curves). This process results in the displacement damage dose curves show in Figure 14. These displacement damage kernels were developed at Aerospace and are slated for release in a future version of the AE9/AP9-IRENE model.

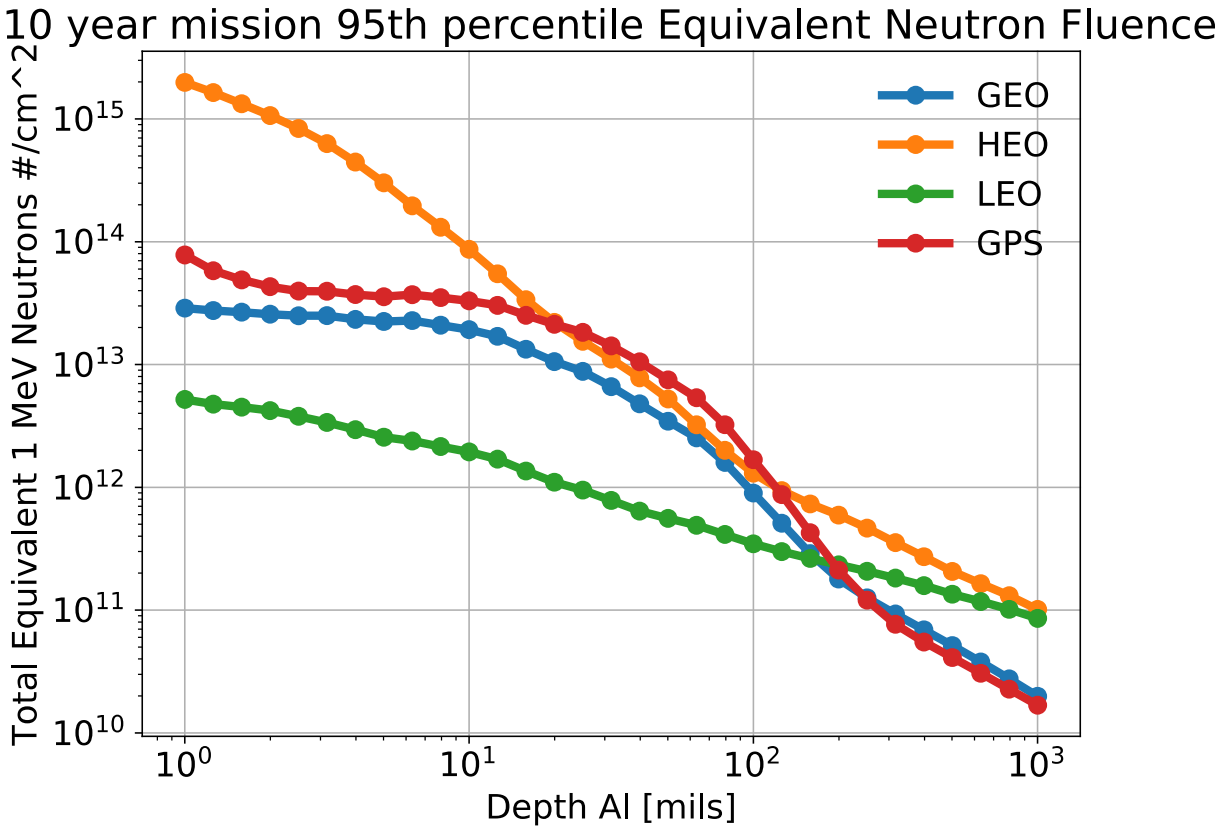

Figure 14. Equivalent neutron fluence for the example orbits.

While these simplified estimates of effects in idealized shielding geometries are useful in scoping parts hardness and end-of-life margins, often through the development of a satellite system, a higher-fidelity estimate is necessary. As the design of components, assemblies, and the space vehicle mature, these environment specifications should be revisited with a ray-tracing capability to estimate the dose/ displacement damage of individual components inside the as-designed geometry of the vehicle. Some of these more capable tools perform ray tracing of environmental impacts inside complex CAD representations that sometimes include the full-physics tracking of particles as they interact with matter are NOVICE, FASTRAD, MCNPX, and Geant4. For comparison among the total ionizing dose comparison computed via these tools, see Bongim et al., 2019 [11].

3.1.3 Mission-Accumulated Galactic Cosmic Ray (GCR) Fluence

The standard method to determine the mission GCR fluence is by using the FLUX module in the CREME tool (described in section 2.2.3). The GCR fluence is an output of the FLUX module, which often takes as an input the geomagnetic transfer function (an output of GTRN) and the trapped proton flux (an output of TRP).

The intensity of GCR flux is inversely proportional to the solar cycle. Primarily the low energy (less than 1GeV) portion of the GCR population is modulated by the solar cycle, and it varies about a factor of about 5 between solar minimum (largest) and solar maximum (smallest) in flux at the peak proton energy of approximately 400 MeV [51]. Regardless, it is recommended to use the solar minimum option to provide a conservative estimate of the GCR fluence and to avoid having a result that depends on the solar cycle. It is important to note that when the FLUX module is used while including a solar particle event

("worst day," "worst week," or "peak 5 minutes"), the GCR spectrum is not included in the particle spectrum. Therefore, when determining the particle flux during a solar event, the GCR flux from a solar quiet period needs to be added, with a stormy magnetic field or other such geomagnetic transfer function. We recommend simulating all atoms from Z=1 to Z=92 to cover all species. This can be important as the high Z atoms can be responsible for some of the very high LET events, and there is effectively no computational penalty in CREME to use the entire range of atoms.

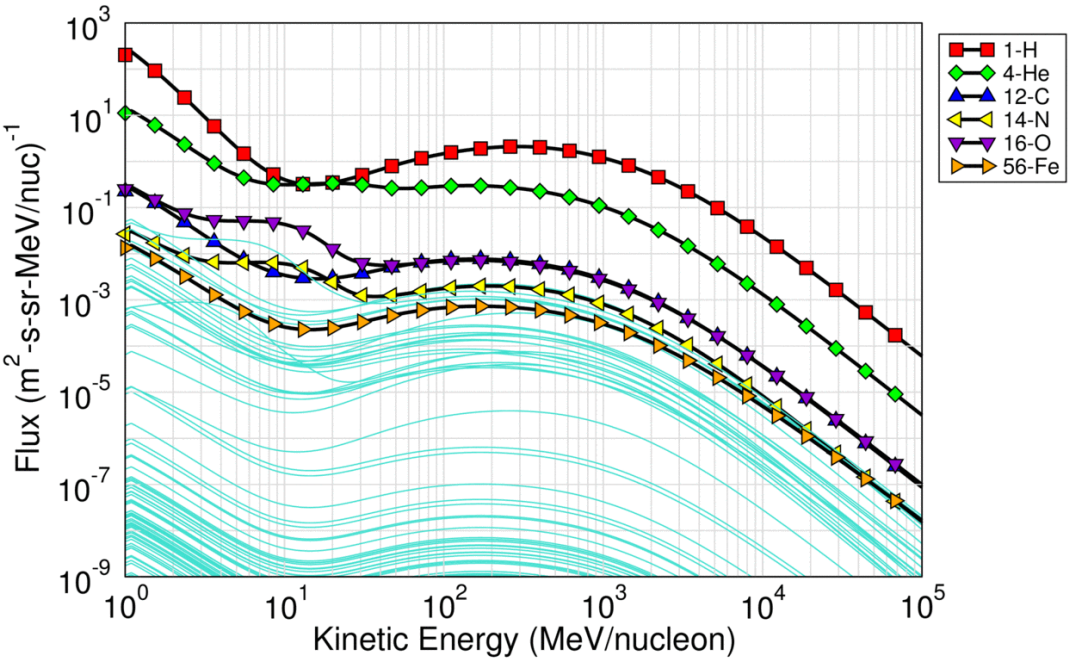

Figure 15. Output of the CREME's model of GCR particle flux at GEO during solar minimum.

An output of the CREME GCR evaluation is shown in Figure 15. Notable species are plotted with symbols, with the complement of all species with Z<92 shown as thin cyan lines. In general, the peak flux of GCR is in the few hundred MeV energies and dominated in flux by H and He. Note that this output is given as a differential flux, so if an integral fluence is need, the spectrum will need to be integrated over time and energy. It's also important to pay attention to the units as CREME and other codes may use different units.

3.1.4 Atomic Oxygen

In this section, we describe a methodology for estimating the atomic oxygen fluence a LEO vehicle will experience over a mission, with uncertainties. This methodology is applicable also to spacecraft in elliptic or GEO-transfer orbits with low-altitude perigees. We use the NRLMSISE-00 model [67] and approximately 60 years of historical solar activity (F10.7) and geomagnetic activity (Ap) indices to drive the NRLMSISE-00 model. The daily values (blue) and running averages of these quantities are shown in Figure 16.

We use an orbit propagator to determine the positions and velocities of a single LEO orbit for that approximately 60-year interval, evaluate the AO density including O and "anomalous O," per Picone et al. [67], and multiply by the satellite velocity to obtain the AO flux at all the times and positions in that

interval. We then sample 1-year periods randomly throughout the 60-year interval in Monte Carlo fashion. By integrating the AO flux in time for each of the 1-year samples into an annual fluence, we can build up a distribution of possible AO fluences based on historical atmospheric drivers. This cumulative distribution is shown for one example orbit (850 km circular orbit at 98.8° inclination) in Figure 17. Annual AO fluence is plotted on the x-axis and the percentile of the distribution is on the y-axis, where 0.5 corresponds to the median of the AO fluences in the Monte Carlo sampling, 0.9 the 90th percentile, and 0.99 the 99th percentile. We then compute the 50th, 95th, 90th, 95th, and 99th percentiles of the AO fluence of the entire distribution in units of AO/(cm^2 year) as shown in the inserted text box. All fluences are assumed to be in the forward-looking, or ram, direction.

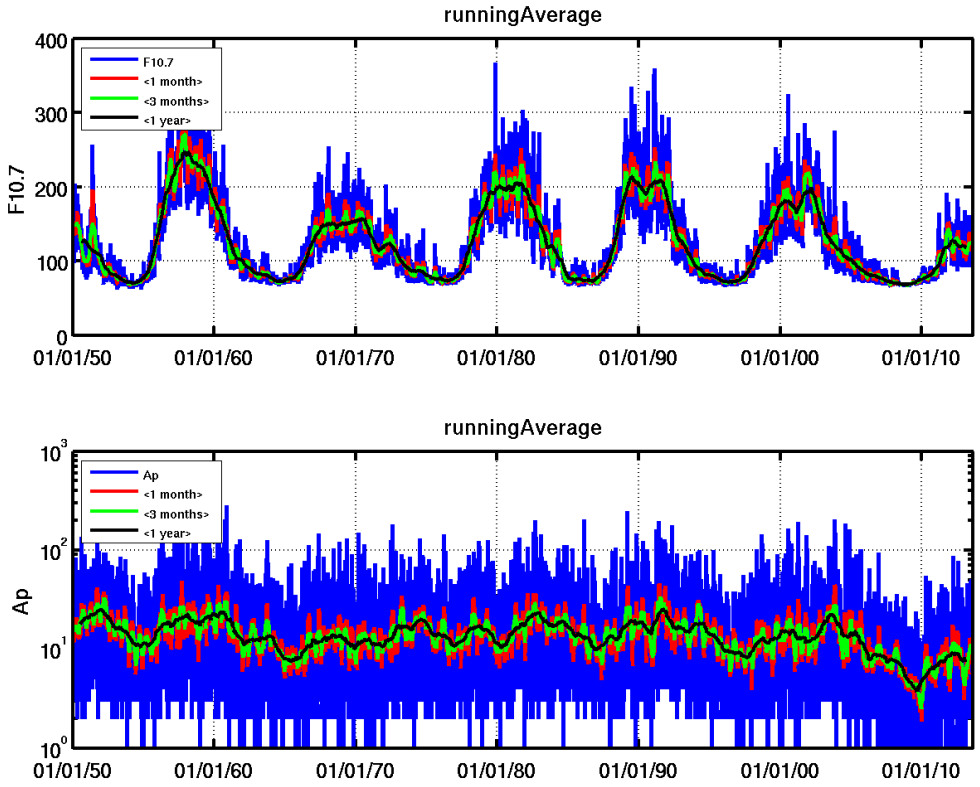

Figure 16. Long-term solar (F10.7, top panel) and geomagnetic activity (Ap, bottom panel) used to drive the analysis.

We extended this analysis by calculating the same values for many circular orbits with altitudes ranging from 150 to over 1000 km. Figure 18 illustrates the relationship between the circular orbit altitude (x-axis), annual AO fluence (y-axis), and percentile (colored curves). For each percentile, the AO fluence is a strongly decreasing function of altitude. The range between the median annual AO fluence (blue curve) and the 99th percentile annual AO fluence (magenta curve) changes with altitude from approximately a factor of 2 at 200 km to an order of magnitude at 500 km, to larger than an order of magnitude at 800 km. The small difference between the two symbols plotted at 500 kilometers altitude represents the inclination dependence of the AO fluence: one marker from a 50-degree inclination orbit, the other from a 98-degree inclination orbit. A listing of these fluence values are presented in Table 10.

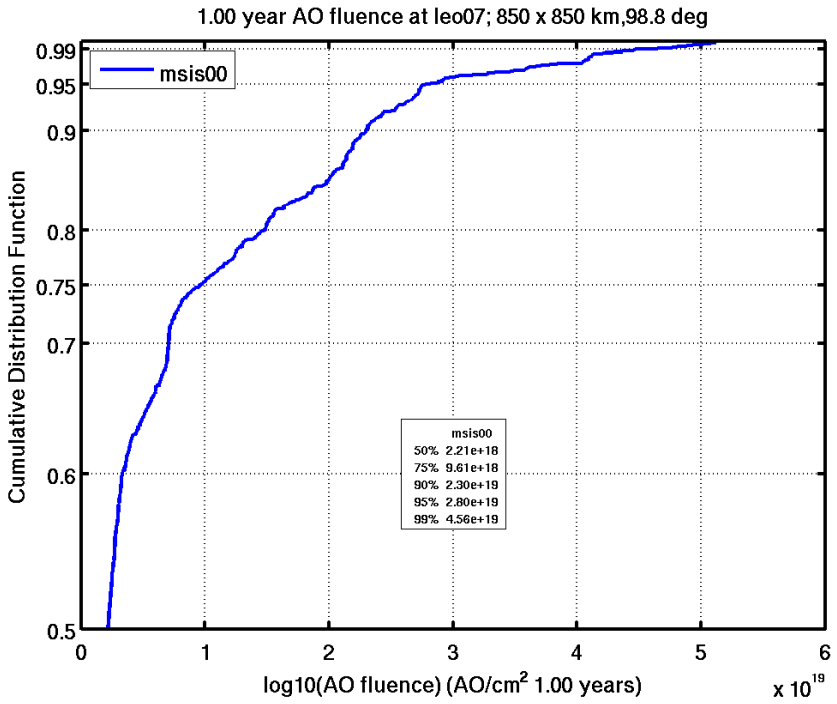

Figure 17. Cumulative distribution of annual AO fluences derived from a Monte Carlo sampling of many 1-year missions at a single orbit, but throughout the last ~60 years of changing solar and geomagnetic activity.

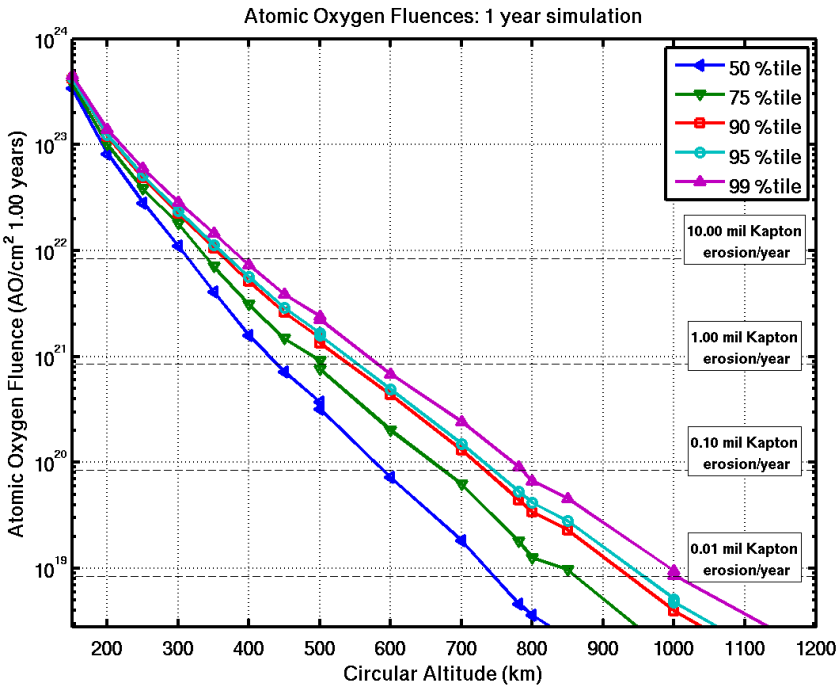

Figure 18. Altitude dependence on the annual AO fluence as a function of percentile. Kapton® erosion estimates based on certain AO fluences are given for context.

Table 10. Percentiles of Annual AO Fluences for Each Orbit Considered—AO Fluence Units Are AO/(cm^2 year).

		Percentile of the Annual AO Distribution (AO/(cm^2 year)				
Circular Altitude (km)	Inclination (degrees)	50th	75th	90th	95th	99th
150	90	3.40E+23	3.80E+23	4.20E+23	4.20E+23	4.50E+23
200	90	8.20E+22	1.00E+23	1.20E+23	1.20E+23	1.40E+23
250	90	2.80E+22	3.80E+22	4.80E+22	5.10E+22	6.00E+22
300	90	1.10E+22	1.80E+22	2.20E+22	2.40E+22	2.90E+22
350	90	4.10E+21	7.10E+21	1.00E+22	1.10E+22	1.50E+22
400	90	1.60E+21	3.10E+21	5.10E+21	5.60E+21	7.30E+21
450	90	7.20E+20	1.50E+21	2.60E+21	2.90E+21	3.80E+21
500	50	3.70E+20	9.10E+20	1.50E+21	1.70E+21	2.40E+21
500	98	3.20E+20	7.50E+20	1.30E+21	1.60E+21	2.20E+21
600	30	7.20E+19	2.00E+20	4.30E+20	4.90E+20	6.80E+20
700	10	1.80E+19	6.30E+19	1.30E+20	1.50E+20	2.40E+20
781	86.4	4.60E+18	1.80E+19	4.40E+19	5.30E+19	9.10E+19
800	70	3.60E+18	1.30E+19	3.40E+19	4.20E+19	6.70E+19
850	98.8	2.20E+18	9.60E+18	2.30E+19	2.80E+19	4.60E+19
1000	90	3.30E+17	1.50E+18	4.00E+18	5.10E+18	9.50E+18
1000	45	2.80E+17	1.60E+18	4.00E+18	4.80E+18	8.60E+18

For context, we include at certain fiducial AO fluence values the thicknesses of Kapton® eroded due to that fluence. As mention in section 2.6, [16] determined the erosion yield of Kapton to be 3.0 x 10^{-24} cm^3/AO atom by pre- and post-flight weighing of Kapton samples exposed on the International Space Station. Multiplying this value by the AO fluence and converting to mils, we arrive at the eroded thickness displayed in text boxes aligned with the dashed horizontal black lines on the right hand side of Figure 18. This method is more fully described in Guild et al, 2014 [30].

Given the altitude, inclination, duration, and risk tolerance (percentile) for a specific mission, the values in Table 10, as outlined above, could be used to calculate the expected erosion of a polymer like Kapton for the mission lifetime. The spacecraft designer would then need to ensure that the thickness Kapton blankets after a mission lifetime of polymer erosion will still adequately protect sensitive parts of the spacecraft.

One component of the Systema series of tools developed by Airbus Defence and Space is the Atomox application, which performs a similar type of analysis to the one described in this section. Rather than computing statistics over numerous solar cycles, it includes a CAD model of a spacecraft for individual estimates of material erosion at the end of a mission. More details can be found at this link: https://www.systema.airbusdefenceandspace.com/products/atomox.html.

3.1.5 MMOD

3.1.5.1 BUMPER

BUMPER is an MMOD probabilistic risk assessment code maintained by the Hypervelocity Impact Technology Group (HVIT) at NASA Johnson Space Center. It determines the probability of damage on

exposed spacecraft due to MMOD impacts. It reads in a finite-element model (FEM) of exposed spacecraft surfaces, which is generated using standard computer-aided design (CAD) software. The FEM accounts for surface orientation and any blockage of surfaces from MMOD by other surfaces. It uses output files from environment models such as ORDEM or MEM that contain information on MMOD flux versus mass/size, relative impact velocity, direction, and density (e.g., igloo files). From this data it produces a range of MMOD-on-surface impact scenarios. BUMPER contains a library of damage equations that it applies to the impact scenarios and determines whether damage (failure) occurs and the probability of damage. There are damage equations for simple metallic surfaces, dual-wall metallic configurations, glass (e.g., crew vehicle windows or sun sensors), and reentry thermal tiles. Damage can be defined as complete or partial penetration or exceeding a crater size.

In the BUMPER input file, the user will specify the name of the FEM files, which environment model to use, and the names of various output files to be produced. Outputs from BUMPER include total probability of damage for the spacecraft, probability of damage by element identification number (EID), and percentage of total probability for each EID. This allows the user to determine which spacecraft surfaces have the highest MMOD risk and may be the most efficient candidates for implementation of additional shielding, such as multi-layer insulation (MLI). The code also outputs number of damaging impacts and critical particle diameters (size of MMOD impactor that causes damage) versus impact velocity and angle for ranges of EIDs.

A copy of the BUMPER executable can be requested by contacting:

NASA Johnson Space Center
Technology Transfer & Commercialization Office
2101 NASA Parkway
Mail Code: XP
Houston, TX 77058

Website: https://technology-jsc.ndc.nasa.gov

Email: jsc-techtran@mail.nasa.gov

Phone: (281) 483-3809

3.1.5.2 Meteoroid and Orbital Debris Risk Assessment (MODRA)

MODRA is a code developed at and used by Aerospace for MMOD probabilistic risk assessment. It loops through the entire range of MMOD-on-surface impact scenarios defined by impactor mass or size, density, impact velocity, and angle relative to surface normal. For each of these impact scenarios, it determines the flux of cases that cause damage (penetration to a certain depth or exceedance of a crater-sized threshold) and computes total damage fluence and probability of damage for spacecraft faces and the total spacecraft. MODRA uses empirical damage equations to determine whether damage occurs for a specific impact scenario. There are single-wall and dual-wall equations. Single-wall equations modeling penetration determine the critical wall thickness needed to stop an impactor in a given impact scenario. If the critical wall thickness is greater than the input wall thickness of a surface, damage is flagged. This will generally be used for exposed metallic surfaces. Single-wall equations modeling crater formation determine the diameter of a crater created by an impactor in a given impact scenario. If the crater diameter is greater than an input threshold for the surface, damage is flagged. This will generally be used for glass and optical surfaces, such as on-sun sensors. Dual-wall equations modeling penetration determine the critical inner-wall thickness needed to stop an impactor in a given impact scenario. If the critical inner-wall thickness is greater than the input inner-wall thickness of a surface, damage is flagged.

This will generally be used for exposed metallic surfaces covered by MLI or honeycomb. A reentry thermal tile penetration equation has been used for crew vehicle analysis. There are several versions of each of these classes of damage equation available, and the code is setup to be easily modifiable to accept new damage equations as long as the classic parameters (wall thickness, density, spacing, yield stress) are used. The single-wall Modified Cour-Palais equation, which uses Brinell hardness, is also available. There is also a damage model for harnesses that determines damaging impactor kinetic energy.

MODRA reads in environment files that contain information on MMOD flux versus mass or diameter; flux versus relative velocity, azimuth, and elevation in the local vertical local horizontal (LVLH) frame; density versus mass or size; and optionally a meteoroid density histogram from MEM. MODRA can use environment files from ORDEM3.1, ORDEM3.0, ORDEM2000, MASTER, ADEPT, and MEM. It can read in igloo files in the ORDEM3.1/3.0 format. There is a preprocessor that converts MASTER *.sei files into igloo format. It also reads in a user-generated file surface data file. Each line in the file corresponds to a flat spacecraft face and contains common data needed by damage equations. For single-wall configurations, the data includes surface normal vector in LVLH, area of exposed surface, and inner-wall thickness and density. For dual-wall configurations, additional information included is outer-wall thickness and density, spacing between the inner and outer wall, and yield stress of the inner wall. MODRA does not have the capability to read CAD FEM files as does BUMPER. It also does not model blockage of surfaces by other surfaces, but the surface data file has a column for a view factor supplied by the user if the user has an estimate of the overall blockage of a face. MODRA also reads in a file that contains a varying attitude profile of spacecraft faces in the LVLH frame. Each profile has a line for an attitude and a fraction of total time spent in that attitude. This has been used, for example, to model GPS yaw steering as well as attitude flips performed by another spacecraft. The general input file for MODRA specifies mission duration, which input file formats are used, and binning information for output files. Output files contain total damage fluence and probability of damage for the spacecraft, damage fluence per spacecraft face (defined in the surface data input file), histograms of damage over impactor mass or diameter, impact velocity, impact angle, and impact kinetic energy. These histograms can be generated for individual faces, for groups of faces, or the entire spacecraft. These output files can be useful in identifying the faces with highest MMOD risk, allowing for identification of the most efficient candidates for implementation of additional shielding such as MLI.

MODRA analysis requests can be requested by contacting Alan Jenkin at Aerospace at Alan.B.Jenkin@aero.org.

3.1.6 Plasma Fluence

The mission-length-accumulated plasma fluence can be computed by the AE9/AP9-IRENE modules for plasma electrons (SPME) and plasma protons (SPMH). The procedure to do this is exactly like the one for computing the trapped electron fluence, shown in section 3.1.1, but replacing the model AE9 with SPME, then SPMH. Once you have a mission-length spectrum of protons and electrons at the appropriate confidence level, it can be combined with the higher-energy spectra of AE9 or AP9 at the same confidence level. In future versions of IRENE, the capability will be included to automatically combine these models into a single spectrum. For now, AE9/AP9-IRENE provides an IntegralPlasma utility to combine SPM and AE9/AP9 model fluxes and fluences into unified integral spectra when those are desired. The graphical user interface invokes this utility automatically, but the user can (must) invoke it manually when performing runs using the command line interface.

3.2 Whole Mission Worst-Case Quantities

3.2.1 Introduction

In contrast to the whole-mission-accumulated hazards listed in section 3.1, some spacecraft hazards are driven by the worst environment the satellite will likely experience on orbit during its lifetime. This could be due to the catastrophic nature of a hazard or an availability requirement to operate through even the worst expected space environments. Examples of worst-case spacecraft hazards are single-event upsets from heavy ions during a severe solar particle event, a proton-related SEE from a severe trapped proton belt, internal electro-static discharges (ESDs) driven by a severe outer-zone energetic-electron enhancement, or surface ESD due to a severe substorm injection occurring near eclipse. These hazards, the environments leading to them, examples of spacecraft components at risk, and mitigation strategies are included in Table 11. This is not a comprehensive list.

Table 11. Example Spacecraft Hazards Stemming from Whole-Mission Worst-Case Environments, Including Typical At-Risk Components, and Mitigating Strategies

Hazard	Environments Contributing	Components at Risk	Mitigating Strategies
Single-event effects	Worst-case trapped proton flux, solar proton flux, solar particle heavy ion fluxes	Active devices, volatile memories that perform critical functions or cannot have outages	Radiation-tolerant parts selection, adequate parts testing, redundant voting logic, error detection, and correction schemes
Internal charging	Worst-case trapped electron fluxes	Internal dielectrics, cabling, or floating conductors with inadequate shielding, conductivities, or grounding strategies	Choosing adequate shielding to attenuate internal current to dielectrics or floating conductors
Surface charging	Worst-case electron, ion plasma spectra, illumination conditions, surface material conductivity to ground	Solar arrays, external transmitters/recievers, unfiltered components	Grounding external materials, choosing conductive external materials, filtering transients out of component inputs

To adequately determine these whole-mission worst-case environments, we recommend the tools and methods described in the following sections.

3.2.2 Worst-Case Electron Flux

To determine this mission-length worst-case trapped electron flux, we can use IRENE-AE9. For electrons, we are concerned with the internal charging hazard, caused by a temporary interval of very high electron flux in the outer zone. These outer-zone enhancements often follow geomagnetic storms, can last for several weeks, and can happen throughout the solar cycle but are more prevalent during the declining phase (between solar maximum and minimum). Internal charging becomes a hazard when energetic

electrons can penetrate thermal blankets or box walls and deposit charge on internal components faster than the charge can be bled away to vehicle ground, leading to an internal electrostatic discharge risk. In this section, we walk through the calculation of the worst 24-hour electron fluxes for a 10-year GEO orbit.

It is important to note the meaning of the percentiles for these worst-case transient effects. For example, the 95% confidence level for the worst-case 24-hour averaged electron fluence means that threshold will not be exceeded in 95% of the missions at any time during those missions. That is different from and usually much higher than the threshold that will be exceeded approximately 5% of the time during every mission.

To accurately determine the confidence intervals for transient effects, we need to use Monte Carlo scenarios covering the full mission duration. Recall the Monte Carlo scenarios are varied with model uncertainty and space weather variability. The latest version of IRENE (v1.56) includes built-in tools to do this calculation. If working with an older version of the model, these worst-case fluxes can be calculated following the method described in O'Brien, 2014 [58]. The transient effects of interest typically depend on a range of energies that penetrate a given depth of shielding, so we recommend using integral fluxes.

Here we provide steps to compute the worst-case 24-hour electron flux for a 10-year GEO mission. Using the GUI, we input the appropriate orbital parameters on the satellite tab, using a time range that covers the full mission duration. For the GEO orbit, a time step of 3600 seconds is used. In the model tab, we select *Monte Carlo* for the Model Mode and select 40 scenarios (more can be used if desired). We then select all the electron energies and chose *Integral* for the Flux/Fluence type. Since we are interested in the worst-case 24-hour fluxes, we set *AccumInterval* to 86400 seconds. Then, in the Advanced Options, under Additional Accum for Flux Averages, we select *Boxcar* and *MC Worst Case*. Choosing these options will give the input file `GEOtest.AE9_input.txt`, as shown in Figure 19.

```
ModelType: AE9
FluxType: Integral
Energies: 0.04,0.07,0.1,0.25,0.5,0.75,1,1.5,2,2.5,3,3.5,4,4.5,5,5.5,6,6.5,7,8.5,10
OutFile: ../../runs/GEOtest.AE9.output.txt
ModelDB: ../../modelData/AE9V15_runtime_tables.mat
MagfieldDB: ../../modelData/igrfDB.h5
AccumMode: Interval
AccumIntervalSec: 86400
KPhiNNetDB: ../../modelData/fastPhi_net.mat
KHMinNNetDB: ../../modelData/fast_hmin_net.mat
FluxOut: MonteCarlo, 1-40
FluenceOut: true
Aggregate: Percent, 50, 75, 95
AccumMode: Boxcar
AccumIncremSec: 0
MCWorstCase: true
TimeSpec: MJD
CoordSys: GEI
CoordUnits: Re
DataDelim: comma
OrbitFile: ../../runs/ephem_GEO.dat
```

Figure 19. Input file for GEO 24-hour worst-case electron flux.

The calculation of the worst-case flux utilizes several steps that are shown schematically in Figure 20. Beginning with the integral flux (#/cm^2/s) versus time for each scenario (1st year shown with blue line), a 24-hour boxcar average is applied (orange line). At each time, the "worst case" is the highest boxcar average flux recorded up to that point (green line). These worst-case fluxes from each scenario are given in output files `LEOtest.AP9.output_mcWC_fluxRunAvg_035.txt` where 035 is the scenario number.

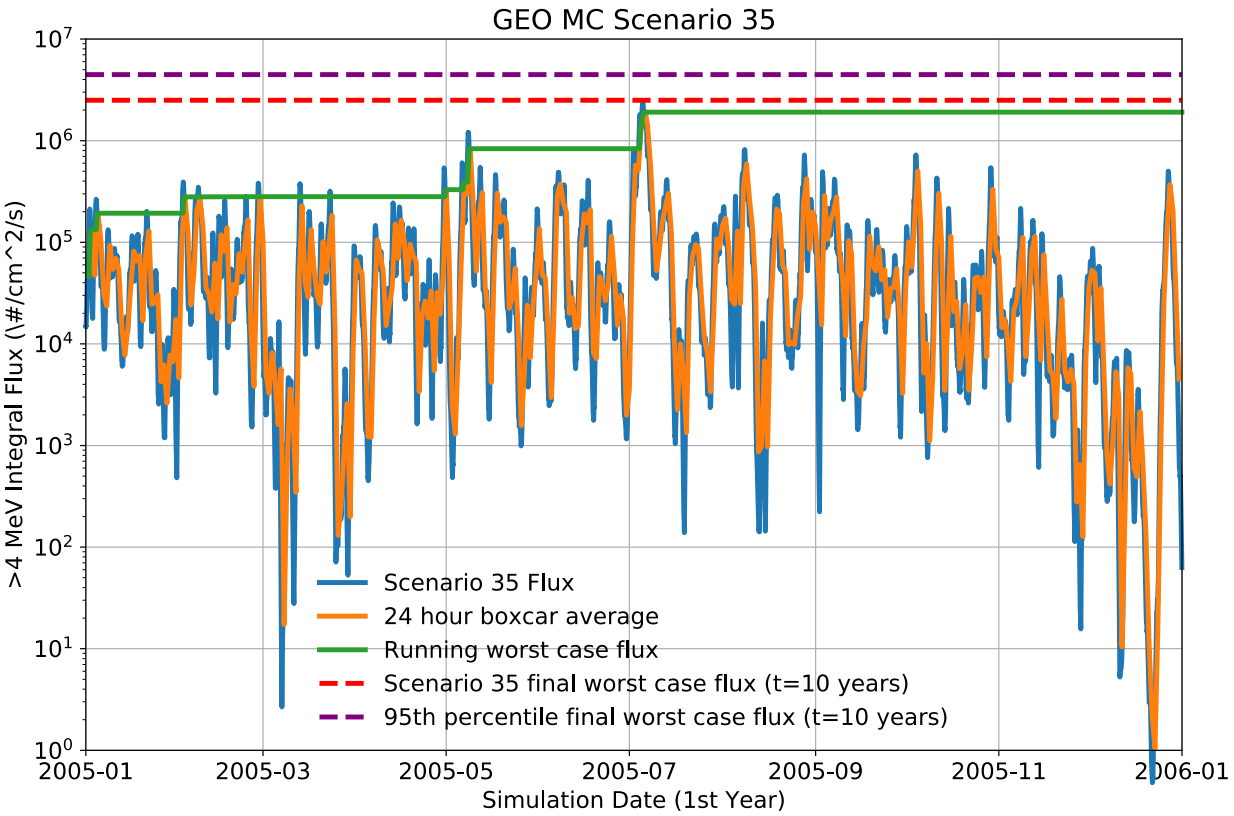

Figure 20. Diagram of worst-case flux calculation.

The final value for the scenario (at t=10 years, off the plot to the right) is shown with the dashed red line. Combining these results for all the scenarios gives the 95th percentile worst-case flux, shown as the purple dashed line, which is written to file `GEOtest.AE9.output_mcWC_fluxRunAvg_conf_level_95.txt`, shown in Table 12. Selecting the last line (shown in Table 12) gives the worst-case for a 10-year mission.

Table 12. 95th Percentile Monte Carlo Worst-Case Output File for GEO Electrons

MJD	posx(Re)	posy(Re)	posz(Re)	j(>.04 MeV)	j(>.07 MeV)	j(>.1 MeV)	j(>8.5 MeV)	j(>10 MeV)
53372	0	0	0	3.05E+08	1.56E+08	8.91E+07	3.33E+02	0.00E+00
53372.04	0	0	0	3.05E+08	1.62E+08	8.93E+07	3.33E+02	0.00E+00
53372.08	0	0	0	3.05E+08	1.69E+08	8.94E+07	3.33E+02	0.00E+00
53372.13	0	0	0	3.05E+08	1.75E+08	8.96E+07	3.33E+02	0.00E+00
…	…	…	…	…	…	…	…	…
57024.5	0	0	0	3.31E+10	1.70E+10	3.01E+09	4.06E+03	3.71E+03

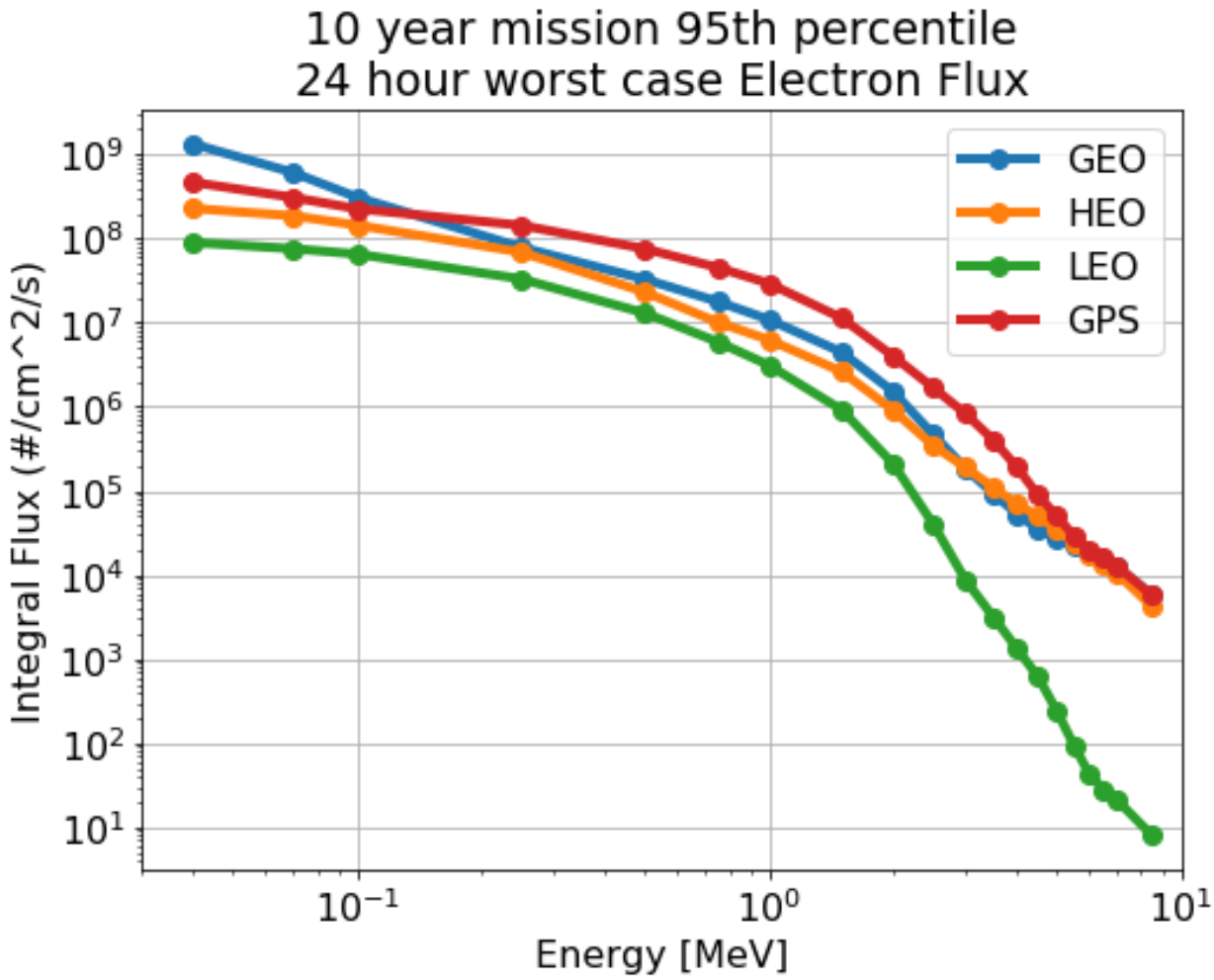

Figure 21. Worst-case electron flux for the example orbits.

This process can then be repeated for each desired orbit and used to characterize the internal charging hazard. The results for each of the example orbits is shown in Figure 21. The mission-length worst-case electron flux spectra is one essential part of an adequate environment specification.

We choose 24 hours for an averaging interval because it is a reasonable, yet convenient, duration that samples integer numbers of orbits for commonly used orbits (GEO-1, HEO-2, GPS-2, LEO-many). If the design has an internal charging bleed-off time constant very different than 24 hours, more appropriate averaging intervals should be used.

3.2.3 Worst-Case Proton Flux

In the following sections, we describe the method to determine a worst-case trapped proton flux, a worst-case solar proton flux, and the method to combine them into a complete worst-case proton flux specification.

3.2.3.1 Worst-Case Trapped Proton Flux

Determining the worst-case proton flux follows a similar procedure to the calculation of the worst-case electron flux described in section 3.2.2. To determine this worst-case trapped proton flux, we can also use

IRENE-AP9 and simulate Monte Carlo scenarios covering the full mission duration. For protons, we are concerned with single-event upset rates, which are caused by temporary high fluxes. In this section, we walk through the calculation of the worst 1-minute proton fluxes for a 10-year Polar LEO orbit.

The Monte Carlo scenarios are varied with model uncertainty and space weather variability. For trapped protons, the space weather variability primarily comes from the episodic, long-lived changes in the outside edge of the trapped proton belt at roughly equatorial altitudes of 6,000 km to 12,000 km (2<L<3). These quick changes could either be due to trapping of solar protons during geomagnetic storms, leading to a sudden increase in proton fluxes that last for many months to years, or a sudden, permanent loss of inner-belt protons during a geomagnetic storm (for a survey of both, see Selesnick et al., 2010 [76]). Both serve to make specifying the proton flux in the slot region of the magnetosphere more uncertain for long-term satellite exposure planning.

As described above, the latest version of IRENE (v1.56) includes built-in tools to do this calculation, and our description follows those steps. If working with an older version of the model, these worst-case fluxes can be calculated following the method described in O'Brien, 2014 [58]. The transient effects of interest typically depend on a range of energies, so we recommend using integral fluxes.

Using the GUI, we input the appropriate orbital parameters on the satellite tab, using a time range that covers the full mission duration. For the LEO orbit, a time step of 10 seconds is used. In the model tab, we select *Monte Carlo* for the Model Mode and select 40 scenarios (more can be used if desired). We then select all the proton energies and chose *Integral* for the Flux/Fluence type. Since we are interested in the worst-case 1-min fluxes, we set *AccumInterval* to 60 seconds. Then, in the Advanced Options, under Additional Accum for Flux Averages, we select *Boxcar* and *MC Worst Case*. Choosing these options will give the input file `LEOtest.AP9_input.txt` shown below:

```
ModelType: AP9
FluxType: Integral
Energies: 0.1,0.2,0.4,0.6,0.8,1,2,4,6,8,10,15,20,30,50,60,80,100,150,200,300,400,700,1200,2000
OutFile: ../../runs/LEOtest.AP9.output.txt
ModelDB: ../../modelData/AP9V15_runtime_tables.mat
MagfieldDB: ../../modelData/igrfDB.h5
AccumMode: Interval
AccumIntervalSec: 60
KPhiNNetDB: ../../modelData/fastPhi_net.mat
KHMinNNetDB: ../../modelData/fast_hmin_net.mat
FluxOut: MonteCarlo, 1-40
FluenceOut: true
Aggregate: Percent, 50, 75, 95
AccumMode: Boxcar
AccumIncremSec: 0
MCWorstCase: true
TimeSpec: MJD
CoordSys: GEI
CoordUnits: Re
DataDelim: comma
OrbitFile: ../../runs/ephem_LEO.dat
```

Figure 22. Input file for LEO 5-minute worst-case electron flux.

Running this calculation will output files with names similar to `LEOtest.AP9.output_mcWC_fluxRunAvg_032.txt` containing the worst-case fluxes as a function of time from each scenario. The file `LEOtest.AP9.output_mcWC_fluxRunAvg_conf_level_95.txt` gives the 95th percentile worst-case fluxes. Selecting the last line (shown in Table 13) gives the worst, 95th percentile, 1-minute averaged proton flux for a 10-year mission.

Table 13. 95th Percentile Monte Carlo Worst-Case Proton Flux Output File for LEO Example

MJD	posx(Re)	posy(Re)	posz(Re)	j(>0.1 MeV)	j(>0.2 MeV)	j(>0.4 MeV)	j(>1200 MeV)	j(>2000 MeV)
53371.0006	0	0	0	0.00E+00	0.00E+00	0.00E+00	0.00E+00	0.00E+00
53371.0008	0	0	0	0.00E+00	0.00E+00	0.00E+00	0.00E+00	0.00E+00
…	…	…	…	…	…	…	…	…
53735.999	0	0	0	1.09E+06	8.36E+06	4.66E+05	1.69E+01	0.00E+00
53736.0	0	0	0	1.09E+06	8.36E+06	4.66E+05	1.69E+01	0.00E+00
…	…	…	…	…	…	…	…	…
57024.5	0	0	0	2.48E+06	2.48E+06	2.48E+06	5.48E+01	0.00E+00

3.2.3.2 Worst-Case Solar Proton Flux

When a vehicle is outside the geomagnetic shielding of Earth's magnetosphere, it can be exposed to the unattenuated flux of solar protons from a solar particle event. Although interplanetary space is often devoid of such particles, estimating a worst-case solar proton flux should include a flux commensurate with a large confidence level of not being exceeded. As discussed in section 2.3.2, the current state of practice is to continue using the "worst-observed" solar particle fluxes, derived from the October 1989 series of observed solar particle events [87]. CREME96 includes a "peak 5-minute averaged flux," a "worst day," or a "worst week" solar proton specification, all based on the series of solar particle events that occurred in October 1989. Instructions to generate a GEO solar proton spectra from CREME96 are provided at the CREME site: https://creme.isde.vanderbilt.edu.

For our example here, we're aiming to provide a worst-case five-minute proton flux, which is the fastest timescale practically present in the solar energetic particle environment. We therefore pick the CREME96 "peak 5 minute" flux to specify. This is often the most appropriate worst-case flux value because most Earth orbits have intervals when they are exposed to the interplanetary flux for at least five minutes. GEO orbits are always exposed, HEO orbits dwell high above the geomagnetic cutoffs, and even polar LEO orbits spend fractions of their orbits over the poles, directly exposed.

3.2.3.3 Combining Trapped and Solar Worst-Case Proton Fluxes

In section 3.1.2.3, we discussed combining both trapped and solar protons to determine whole-mission-accumulated fluence values from both. We introduced the concept of the geomagnetic cutoff, which sorts orbital positions to be exposed to one or both environments. For the accumulated fluence, we *added* these separate fluences since the satellite will sample both environments for its mission length. However, to estimate the whole-mission worst-case proton flux over a short interval, we take advantage of the fact that a single vehicle will never experience the worst proton flux from both the trapped and solar proton population at the same time: they occur in different locations along an orbit. In this case, we take the

maximum of either the worst-case trapped proton flux, or the worst-case solar proton flux, not adding them together. This is reasonable for worst-case proton flux levels averaged over short durations such as 10 minutes or less.

We combine the trapped and solar proton flux in the following way. The worst, 95th percentile, 1-minute averaged proton flux for a 10-year mission that we determined in section 3.2.3.1 is compared, at every energy, to the CREME96 peak 5-min proton flux, and the larger of the two fluxes at each energy is retained. We've converted the CREME96 flux (in protons/(m^2 s sr MeV)) to the units that have been output from AP9 (protons / (cm^2 s)) by integrating in energy and converting from unidirectional flux to omnidirectional flux (multiply by 4pi).

This process can then be repeated for each desired orbit and used to characterize the SEE hazard. The results for each of the example orbits is shown in Figure 23.

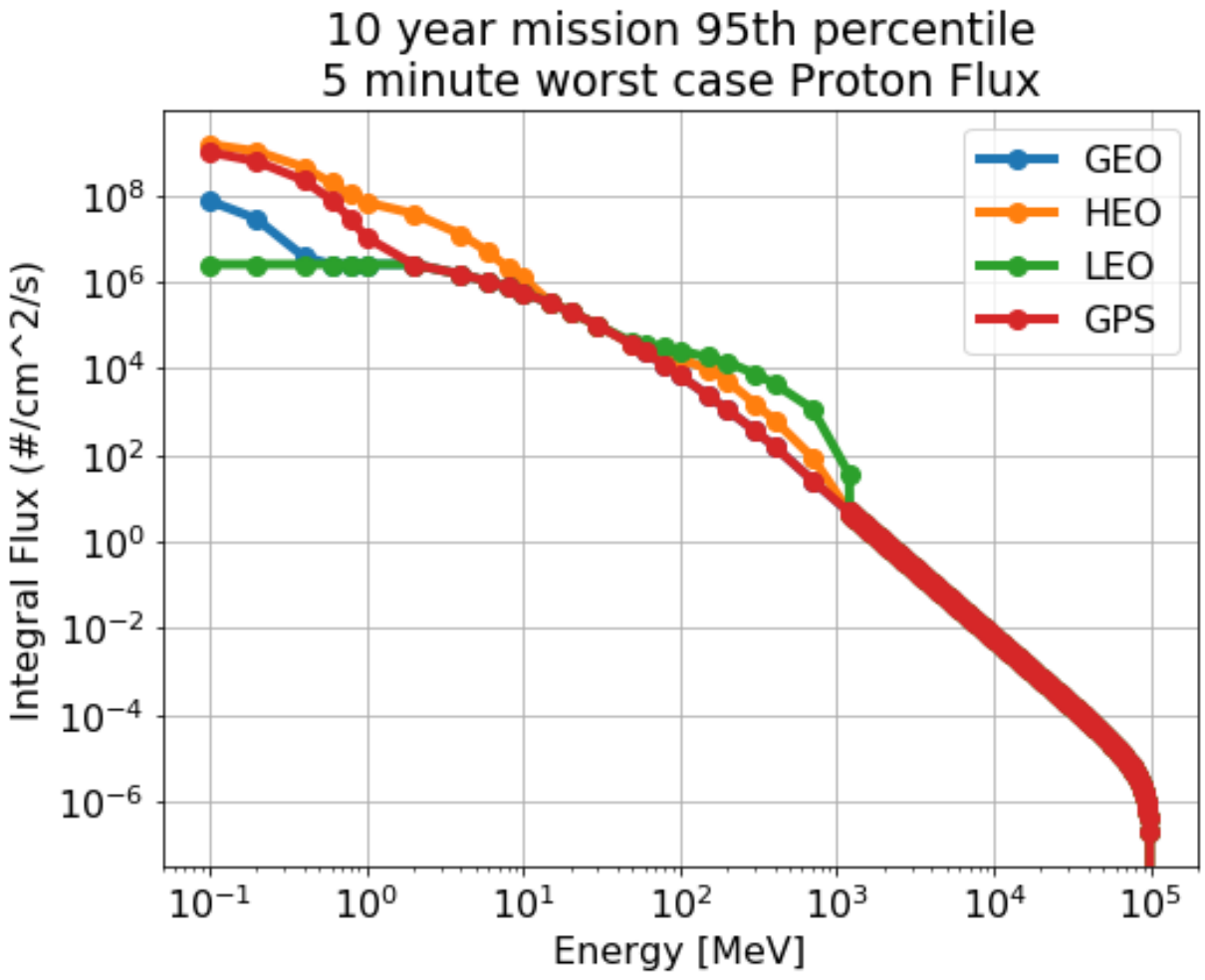

Figure 23. Worst-case 5-minute electron flux for the example orbits.

Note our combined trapped/solar 95th percentile worst-case integral particle flux now spans 6 orders of magnitude in energy, but above the highest energy of AP9 (1.2 GeV), the fluxes from all orbits are identical. This is because each of these orbits spends time outside the geomagnetic cutoff, with the potential of experiencing the same worst five-minute solar proton environment taken from CREME96.

We attenuate solar protons for worst-case durations only greater than 30 minutes, which is a reasonable upper bound of the duration of time that polar LEO orbits spend in the polar cap above the cutoff.

Again, a caveat for these worst-case proton fluxes is warranted. The 95% confidence level for the worst-case 5-minute proton fluence means that threshold will not be exceeded in 95% of the missions *at any time* during those missions. That is different from and usually much higher than the threshold that will be exceeded approximately 5% of the time during every mission.

3.2.4 Worst-Case LET in SPE

Ideally, the worst-case LET from a SPE would be tied to a confidence interval similar to how it is in trapped proton models such as IRENE. The PSYCHIC component of the ESP/PSYCHIC model can help provide the expected heavy ion particle spectrum to a certain confidence interval, but then the end user is required to transport the spectrum to the intended orbit, transport the spectrum through shielding, and then convert the particle spectrum to LET. As discussed in section 3.1.2.3, care must be taken when adding spectra with different energy ranges, especially when the lowest energies differ. For instance, if AP9 starts at 0.1 MeV and ESP starts at 1 MeV, then add the ESP 1 MeV fluence to all the AP9 channels below 1 MeV to avoid a jump in the 1 MeV summed spectrum.

Practically, an end user will often use the "peak 5-minute averaged flux," "worst day," or "worst week" in CREME96 to generate the expected LET spectrum. Not only will this provide the highest LET spectrum that could be possible but can tie this LET spectrum to the particle rate in order to help understand how the intensity changes above a given LET threshold. Using CREME96 also allows for an easy way to generate the upset rate for a part during these severe intervals (5 minutes, day, week). For softer parts, the upset rate from the SPE can be quite high and can defeat mitigations such as error detection and correction (EDAC) code.

It is important to note that CREME96 does not combine the GCR contribution with the SPE contribution. This means that while CREME96 says the maximum LET for a SPE is a certain value, this does not include the GCR maximum LET, which is often higher than a SPE's LET. An example LET spectrum is shown in Figure 24. In this spectrum, the SPE does not necessarily produce higher LETs, but does increase the flux over the entire LET spectrum. Also for context, Figure 25 plots proton flux from GCR ("Solar Quiet") along with a worst-week proton spectrum, where we show the SPE doesn't contribute higher energies but does provide far more protons at energies less than a few GeV.

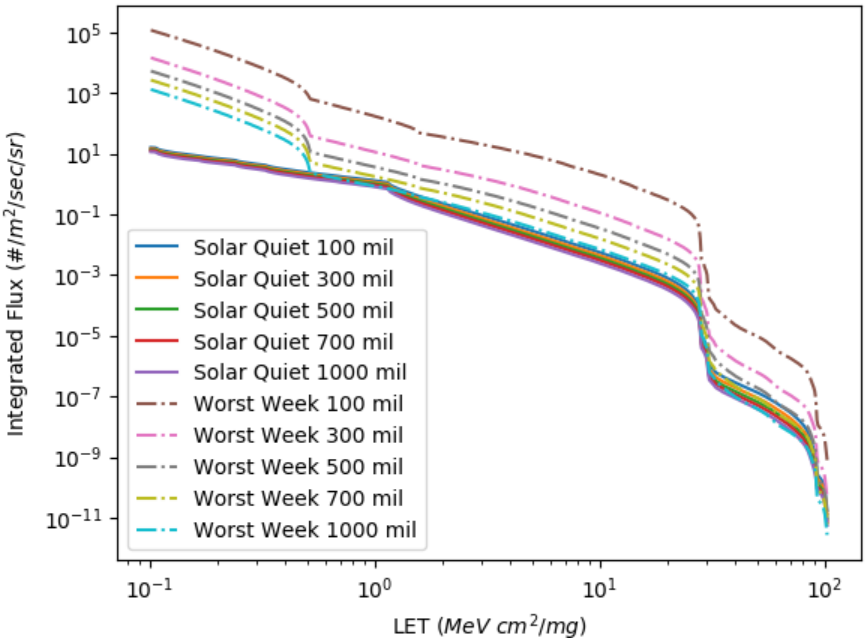

Figure 24. LET spectrum at high latitudes with minimal geomagnetic shielding for a solar quiet period or the CREME96 worst week with different levels of physical shielding in mils of Al.

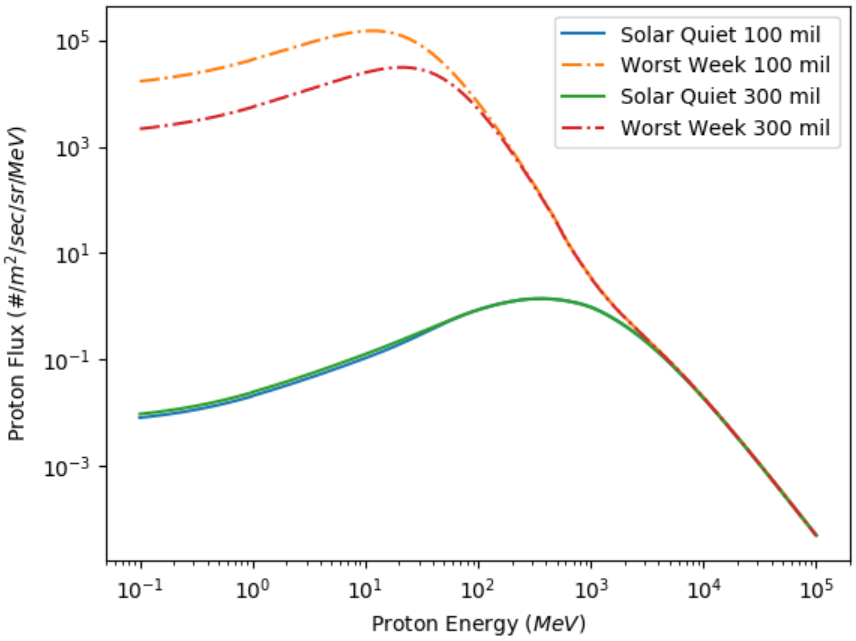

Figure 25. Proton energy spectrum at high latitudes with minimal geomagnetic shielding for a solar quiet period or the CREME96 worst week with different levels of physical shielding in mil of Al.

3.2.5 Surface Charging

With a worst-case charging specification in hand from section 2.4.2, a satellite designer next needs a CAD description of the spacecraft in question and a simulation tool to calculate surface charging

quantities on the surface of their satellite geometry. The simulation tool recommended at present is NASCAP2K [43]. Rather than going through a NASCAP2K example here, we direct the reader to the download site at https://software.nasa.gov/software/MFS-32056-1 and an extensive user guide [15], available at DTIC: https://apps.dtic.mil/sti/pdfs/AD1064754.pdf.

Some third-party tools, such as EMA-3D, provide some CAD importing/re-gridding tools to facilitate getting a model into more complex tools such as NASCAP2K or SPIS: https://www.ema3d.com/blog/nascap-spacecraft-charging/.

4. Other Considerations

4.1 Uniform, Traceable Documentation

Environment specifications as derived in this report are foundational to the organizations using them to design spacecraft. As such, these specifications should be clearly traceable to design choices made in the program (such as mission lifetime or orbits) or assumptions made, and versions of, the tools used to generate these environments and effects for design. Environment specifications are also typically reviewed by both internal and external auditing groups to verify the appropriate choices have been made. If not enough detail is included in these environment specifications about the origin of the numerical values, reviews are difficult or impossible to perform. Finally, revisions of environment specifications are sometimes warranted when environment models are updated or excursions around a prior orbit are likely in a follow-on block for a program. Both situations require re-running the environment models used to make the specification with different choices of model, tool, or orbit to provide a "delta" used to inform decisionmakers of the consequence of that change. This requires that a skilled practitioner have enough details to exactly reproduce the prior environment specification and allow deltas to be made for the current changes of interest.

For all the above reasons, enough information to reproduce environment specifications is essential. We propose in Table 14 one possible format that could be used as adequate documentation to clearly record all the models, assumptions, and post-processing steps for generating environment specifications. The details contained within are succinct, human-readable descriptions of the derivations of the worked examples of section 3 and should be retained in any environment specification to facilitate the traceability, reproducibility, and auditability of an adequate environmental specification.

The format in Table 14 is only an example. We encourage organizations to exceed this level of documentation if warranted.

Table 14. Example of Concise, Traceable Environmental Specifications to Facilitate Review and Updating

Environment Input	Models	Notes
Trapped proton	AP9 V1.50.001 95%, Monte Carlo for total dose, displacement damage, and single event effects	40 scenarios, 10-year orbit simulations for all runs described in this report.
Trapped electron	AE9 V1.50.001 95%, Monte Carlo for total dose, displacement damage. and internal charging	
Solar proton	ESP-PSYCHIC 95%, CREME96 5-minute worst case	ESP-PSYCHIC used for fluence, CREME96 used for worst-case transient
Solar proton cutoffs	Mazur et al, 1998 [44]	Method described in section 3.1.2.3
Method for joining trapped and solar proton environments	Sum for TID and DDD, max for SEE	Solar particles added to TID and DDD after calculating percentiles in AP and ESP models (AP9/AE9 does not include solar particles)

Effects tools using the environment specification to contribute to spacecraft design also have choices, model settings, and model versions. Accordingly, each effect calculated from the environment specification, either for reference or in follow-on mission design or analysis, should be captured completely with the tools and assumptions made in the analysis. Examples for the effects calculated in this report are given in Table 15.

Table 15. Example of Concise, Traceable Derived Effects Calculations to Facilitate Review and Updating

Hazard Calculation	Models/Setup Parameters	Notes
Total Ionizing Dose		
Effects code	Shieldose2	Silicon target
Geometry	2 x “1/2 dose at center of solid aluminum spheres” (full 4π sr)	
Shielding	1 – 1000 mils Al	
Displacement Damage Dose		
Effects code	Displacement damage kernel	Described in [61] for protons and [62] for electrons
Geometry	Full sphere, protons, and electrons	
Shielding	1 – 1000 mils Al	
Internal Charging Current		
Effect code	Internal charging kernel	Described in [60]
Geometry	Half sphere, electrons only, no electrons from back side	
Shielding	1 – 1000 mils Al	
Proton SEE Rate		
Effect code	Single event effect kernel	Proton SEE rate Weibull kernel with slim = 4.5e-14, E0=1, W=20, S=1.546. [4]. Described in TOR-2015-02707 [59]
Geometry	Full sphere, protons only	
Shielding	1 – 1000 mils Al	

As environment specification models become more complex, it may be useful to capture more run-specific information than can be stored in a table like Table 15. Toward this end, it may be prudent to store the environmental run settings files in addition to facilitate re-generating the specifications easily. These run settings files can be included as embedded files within an environment specification and will serve to exactly reproduce the specification if revised, updated, or audited.

4.2 The Difference between Geophysical Models and Software

The space environment survivability community sometimes suffers from nomenclature that impedes clear communication. A designer often turns to "models" to produce environment specifications; however, models can be of two main types: a geophysical model of some aspect of the environment or a software used to run one or more geophysical models. AE9/AP9-IRENE is a geophysical model. It comes bundled with software (GUI) to facilitate running the geophysical model or is bundled in other software packages (SPENVIS) to facilitate combining its output with separate geophysical models. The CREME software and its geophysical models of the solar particle environment (worst 5-minute, worst-day, worst-week) also suffer from this lack of distinction.

4.3 How to Deal with Evolving Models in Satellite Design

As has been shown in this document, the natural environment specification for a space or launch system depends on many different geophysical models and the software tools used to evaluate a system design. A question many designers and program managers often ask is how to react to upgrades on a minor or major component of that ecosystem of models and software. The best answer we can provide is to update system requirements on the natural development cadence of the program—do not interrupt the program lifecycle to redo the environment specification or qualification simply because of the update of a geophysical model or associated software. This guidance is primarily because increasing an environment specification during the design or assembly of a spacecraft or block could necessitate re-qualification of just-qualified hardware, an expensive undertaking. This large cost is not often justified to accommodate typically small environmental changes with new versions of geophysical models.

Once the system specifications have been set, any subsequent changes to the environment models or software should not trigger a response from the program unless the domain subject matter experts indicate a catastrophic problem with the models or software has occurred. An example of such a catastrophic problem would be introduction of substantial new debris field after a collision or explosion in space.

An important related issue that often arises is how to deal with legacy hardware on a new contract. For example, can hardware that was qualified for a geosynchronous orbit for AE8/AP8 be used on a new contract that specifies AE9/AP9? The authors believe the answer is yes. There is no evidence that previously designed systems that adequately followed contemporary qualification practices with contemporary models were especially vulnerable to the natural environment. A simple assessment should be performed to ensure that the previous qualification was complete—did it consider all the relevant environments? If so, then the prior qualification should be accepted even if a geophysical model update has occurred since acceptance. However, new or modified hardware should use the updated models specified on the contract, and specifications themselves should be updated to incorporate the newer geophysical models with exceptions allowed for prior qualifications. This approach should enable development and use of long-lived product lines concurrent with ongoing updates to geophysical models and associated software.

4.4 Transfer Orbits

The advent of electric propulsion has offered satellite hosts the opportunity to increase bus mass in place of carrying an apogee kick motor to quickly circularize a spacecraft's orbit ending at geosynchronous orbit. However, this mass benefit comes at the cost of many months transit through the heart of the radiation belts to raise perigee or spiral the entire orbit. In the worked examples of this report, we did not include the effect of a lengthy transfer orbit on the environment specifications. If this were an option, a designer could separate the transfer orbit and operational orbit and follow the methods of section 3 to sum or take the maximum of both for a composite environment specification.

4.5 Retiring Radiation Design Margin

Decades ago, survivability engineers had one simple model of the trapped radiation environment to generate environment specifications: AE8/AP8. These were median models; therefore, each mission had an equal chance of exceeding the AE8/AP8 specification as it has of falling short. Survivability engineers rightly adopted a multiplier to account for the long-term environment model's uncertainty, referred to as a radiation design margin (RDM). RDM is often defined as a ratio of a part's radiation capability (failure level), to the expected mission dose at the part [40]. A minimum RDM, often 2x, is typically required on all parts in a spacecraft. This one-size-fits-all approach intrinsically covered some environmental and some parts hardness uncertainty without accounting for how much of each. In retrospect, this practice seems to have been sufficient, since satellite EEE component failures due to the long-term aggregated radiation environment (TID and DDD) have been extremely rarely observed and only after missions exceed their design lives many times over.

The AE9/AP9-IRENE models now explicitly include environmental uncertainty in their perturbed mean and Monte Carlo modes. Rather than specifying AE8/AP8 and an RDM multiplier of 2, we recommended specifying the AE9/AP9-IRENE 95 percent confidence level with an RDM of 1.0. This appropriately captures the environmental uncertainty, since the 95 percent CL gives every mission only a 5 percent chance of exceeding this threshold.

In decades of use, RDM became associated with program requirements and sometimes radiation hardness assurance (RHA) methodologies. For instance, TOR-2011(8591)-21 [37] lists RDM levels expected for certain classes of missions, and RDM appears numerous times in the Aerospace Mission Assurance Handbook (TOR-2006(8583)-5236 Rev B [69]). Further, some programs specify a threshold RDM beyond which radiation lot acceptance testing (RLAT) can be waived. These RLAT RDMs are typically larger factors, like 5x to 10x. As RLAT testing is expensive, buying harder parts can save money in testing costs. The lowly RDM factor that started as a poorly quantified guess has graduated to become heritage practice, then design guidance, and now a mission assurance requirement in the intervening decades of use.

Programs are rightly wary of reducing radiation margin on new systems. However, current practice is often to include radiation margin at numerous steps during a satellite design, without careful accounting of that margin. The aggregate effect of margin upon margin ends up as a large, unknown amount of *implicit* margin. For instance, (1) specifications are generated as 95 percent confidence level, (2) when ray-tracing to sensitive parts to estimate the dose, large amounts of material are neglected because the ray-tracing setup is easier without it, (3) programs require large RDMs when RLAT testing is not desirable, (4) parts that require RLAT testing apply a one-sided tolerance limit (KTL factor) on what constitutes acceptable parts, and (5) when the design team performs a failure modes, effects, and criticality analysis (FMECA), circuits will likely still perform adequately when the degraded part is only slightly out of spec. This illustrates five possible sources of margin related to the radiation environment in standard space vehicle designs. Perhaps this is why we know of no known recent examples of dose-related failures before vehicles last many times their design lives. In pursuit of more transparent spacecraft radiation design, with less blanket margin, we suggest more carefully harvesting margin out of steps 2–5 above, instead of continuing to add margin to the radiation environment. With the advent of rigorous statistical models of radiation environments, we suggest derating the parts rather than inflating the environment.

We also suggest the community retire the term "radiation design margin" in its current form, described above. In its place, we propose to define a new, more itemized factor we refer to as the radiation derating factor (RDF). The RDF applies only to a single part (not the entire environment specification), refers to the "total dose pass level," and there may be a separate RDF for DDD. If a program requires RLAT

testing, it can take advantage of the parts' full rating (TID level), whereas if not, derating the TID pass level is an option. RDFs could take unique values for parts tested on the ground, flown, or commercial off-the-shelf (COTS) parts in the design. This aims to more clearly separate parts-level margin from environmental margin in the quest to safely walk back the margin-upon-margin conservatism of past programs, retaining *adequate* survivability.

A practical but conservative approach to separating parts margin from environmental margin is provided here. Prior guidance required that without RLAT, a large RDM (denoted RDM_{TOT}, at least 4) was required, representing a combined uncertainty for part variation and environmental variation or model errors, and with RLAT, a smaller RDM (denoted RDM_{ENV}, at least 2) was required, representing only the environmental uncertainties. RDM_{TOT} includes an implicit radiation derating factor for parts uncertainty covering lot-to-lot and testing uncertainties. Absent other information, multiplicative errors are typically representative of a log-normal distribution, independent errors add in a log-sum-of-squares sense:

$$\ln(RDM_{TOT})^2 = \ln(RDF)^2 + \ln(RDM_{ENV})^2$$

Although RDM_{TOT} is often somewhat arbitrary, we can still use it to estimate an RDF if we do not have data on which to base an RDF:

$$RDF = e^{\sqrt{\ln(RDM_{TOT})^2 - \ln(RDM_{ENV})^2}}$$

For typical values of RDM_{TOT}=4 and RDM_{ENV}=2, we have $RDF = 2^{\sqrt{3}} = \sim 3.3$. We note that while it is conservative to assume that design margin factors are correlated, and so combine them multiplicatively ($RDM_{TOT} = RDM_{ENV} * RDF$) when creating a total from two component errors, it is conservative (and correct) to assume they are uncorrelated when decomposing the total into constituent sources of uncertainty, as we have done here. There is no reason to expect that the uncertainty in the environment (RDM_{ENV}) is correlated with the uncertainty in the parts (RDF).

Despite the estimate of RDF consistent with prior guidance above, there have been better RHA methods proposed in the professional literature that take advantage of radiation environment confidence levels. Xapsos et al., 2017 [93] used both the confidence levels of the environment with parts TID/DDD failure distributions to inform failure probabilities in a new RHA methodology. Building on Xapsos et al.'s method, Ladbury and Carstens [40] developed methods based on KTL factors and maximum likelihood estimation to translate margin to probability of success. Both methods are more rigorous than the heritage RDM factor approach, are less conservative (and more correct) than our RDF estimate above, and are recommended in new programs' RHA methodologies. Producing success/failure probabilities, these new methods are more aligned with traditional engineering reliability models, offering the promise of more fully incorporating radiation reliability with other systems in a more transparent risk posture.

4.6 Effects Tools

This report discusses appropriate methods to generate the environments outside a space vehicle for an environment specification. But the process of satellite design necessarily propagates these external environments to radiation effects, often inside the satellite. Radiation effects are the consequences that adequate spacecraft design need to mitigate for the duration of the mission, through all expected severities of the space environment.

An in-depth review or tutorial of all these radiation effects tools is outside the scope of this report. In addition, there are often many tools that accomplish the same effects calculations or software suites that wrap many effects tools and provide a convenient user interface. It is up to the design organization to

choose the tools that work best for them. A brief outline of tools is given below with links to websites for more information:

- Radiation transport through shielding
  - NOVICE: https://empc.com/novice-software/.
  - Geant4: https://geant4.web.cern.ch/node/1
  - MCNP: https://mcnp.lanl.gov/
  - FASTRAD: https://www.fastrad.net/
  - SHIELDOSE-2: https://www.nist.gov/publications/updated-calculations-routine-space-shielding-radiation-dose-estimates-shieldose-2.
    - Note the original NIST version suffered from an error in the original publication. In the elbrbas2.dat file, the Bremsstrahlung finite-slab and semi-infinite slab data tables, with the exception of the Al detector targets, had been switched (Heynderickx, 2013).
    - This error has been corrected in at least the versions of SHIELDOSE-2 included in SPENVIS and AE9/AP9-IRENE.
    - A discussion of the fix is provided in 7.Appendix B.
- Specific effects calculations
  - Displacement damage from MULASSIS: https://essr.esa.int/project/mulassis
  - Internal charging can be calculated by a simple capacitor model as in Bodeau, 2010, Figure 5. Internal charging can also be estimated from the MOBE-DIC model [33], hosted within SPENVIS.
  - Solar cell degradation: EQFLUX originally published in The Solar Cell Radiation Handbook, JPL publication 82-69 and the GaAs Solar Cell Radiation Handbook, JPL Publication 96-9. Available to download from https://opensource.gsfc.nasa.gov/projects/eqflux/index.php
- Software suites facilitating spacecraft environmental design
  - SPENVIS: SPENVIS is the European Space Agency's web-based software suite used to compute a number of space environments and effects for satellite design. It is available at https://www.spenvis.oma.be/ and includes a comprehensive collection of tools discussed in this report.
  - OMERE: OMERE is the TRAD tool that computes the space environment for satellite design. It is available at https://www.trad.fr/en/space/omere-software/.
  - EMA3D: Tools produced by EMA that simulate electromagnetic coupling to cables in complex CAD geometries.

- Systema: Series of tools developed by Airbus Defence and Space to simulate many aspects of the space environment for satellite design. Available at https://www.systema.airbusdefenceandspace.com/products/systema.html.

4.7 Environments Not Considered Here

There are numerous environments necessary for a space environment specification. This report covers many but not all of them. A partial listing of other environments that have not been extensively discussed in this report are below. They include the solar irradiance, the neutral density for drag considerations, and nuclear detonation-induced environments. More details are provided in the subsections below.

4.7.1 Solar Irradiance, Including Ultraviolet Environment

The solar spectral irradiance contributes to spacecraft thermal design, testing of surface material degradation, and photocurrent calculation for surface charging design. The most current international standard, which contains the zero air mass solar spectral irradiance table, is ASTM-E490-00a(2019). The most recently approved version is available at http://www.astm.org/cgi-bin/resolver.cgi?E490.

4.7.2 Neutral Density

Although not strictly considered a spacecraft design issue, neutral density and spacecraft drag are of importance directly to mission planning and indirectly to spacecraft design (attitude control propulsion tanks need to be sized to maintain altitude for the mission life). An approach similar to how mission length AO exposure was calculated in section 3.1.4 could be used to determine the impact of satellite drag. First you would run the NRLMSISE-00 model [67] using approximately 60 years of historical solar activity (F10.7) and geomagnetic activity (Ap) indices to calculate mass density (instead of number density used in the AO calculation) throughout the 60-year span, then sample mission-length periods (or times between orbital adjustment burns) randomly throughout the 60-year interval in Monte-Carlo fashion. Next propagate the orbit through each of the periods and determine the orbital decay at the end of the period for every interval of a given mass density. Finally, build up a cumulative distribution of possible orbit decays based on historical atmospheric drivers. This can then be used to determine if a particular orbit and propulsion system will satisfy mission duration requirements.

4.7.3 Artificial Radiation Environments

While the natural space radiation environment of trapped proton and electron belts and episodically solar particle events exists in space much of the time, there are sometimes perturbations to that natural environment caused by human activities. During the dawn of the space age, nuclear weapons were detonated above the atmosphere by the U.S. and then USSR, leading to intense, long-lived electron radiation belts produced by beta-decay of fission fragments.

The detonation of a nuclear weapon above the atmosphere generates two main environmental challenges for space system design: (1) withstanding prompt effects of photons and particles escaping the fission reaction and (2) enduring a potential, persistent new radiation belt comprising energetic beta-decay electrons. Both types of environments are typically highly uncertain, subject to the initial conditions of the nuclear weapon type and detonation location. A recent academic review of artificial radiation environments is contained in Gombosi et al., 2017 [29].

Developing satellite design tools to specify the environmental impacts of high-altitude nuclear detonations (HANDs) is the goal the U.S. Defense Threat Reduction Agency. Other U.S. organizations (LANL, LLNL, Sandia, and AFRL) contribute to research involving HAND environments and ultimately

contribute to DTRA design tools. To obtain DTRA tools or expertise, please contact Bruce Wilson (bruce.c.wilson14.civ@mail.mil), David Kulp (william.d.kulp.civ@mail.mil), or Mark Sward (mark.l.sward.civ@mail.mil).

5. Future Enhancements

5.1 IRENE Development Plans

The IRENE model continues to incorporate new datasets while releasing significant updates approximately every 2 years. IRENE is also adding new capabilities. One important new capability is integration of SAPPHIRE/VESPER solar protons with the trapped AP9 protons. This integration is part of an architectural change that will enable tighter runtime combinations of the different sub-models (or modules) that make up the environment. Additional improvements will add local time dependence of the plasma populations and better longitude dependence of the low-altitude populations. Another important feature will be historical sample solar cycles, which will allow designers to fly a satellite through a reconstructed past solar cycle to provide a single, hyper-realistic mission scenario. These developments will be rolled out over the next several years. Once all these new capabilities are incorporated, IRENE will settle on a 5-year routine update cadence, simply incorporating new datasets.

5.2 Virtual Time Series SPE Models

Recent advances in solar energetic particle models such as SAPPHIRE [35] or VESPER [6] have more closely aligned these models with the Monte Carlo capabilities of AE9/AP9-IRENE. As such, soon it may be possible to combine the solar and trapped environments in a consistent, statistically rigorous way. As suggested in O'Brien et al. [63], the anticipated future best practices could include a composite (solar and trapped) whole-mission fluence spectrum, along with a modification of the peak flux environment for SEE considerations. Rather than use CREME96's arbitrary "peak 5 minutes," "worst day," or "worst week" specifications, the proton flux could be computed not to be exceeded in a month with 50 percent confidence or 95 percent confidence, or the proton flux not to be exceeded in the entire mission with 95 percent confidence level. These correspond to a typical month (50 percent CL), a severe month (95 percent CL), or the mission worst case. These thresholds are likely more meaningful than the CREME96 thresholds.

5.2.1 Space Ionizing Radiation Environment and Effects (SIRE2)

A new development on the single event effects (SEEs) front is the SIRE2 toolkit [3], which promises to eventually replace the CREME series of tools. SIRE2 provides solar, trapped, and cosmic ray proton and ion models as well as various methods of computing single event effects. SIRE2 is progressively including more updated models of geomagnetic cutoffs and how they are influenced by solar and geomagnetic activity. SIRE2 is also continuing to upgrade its models of particle populations.

5.3 Improvements in SEE Rate Models

SEE rate models are based on the idea that there is a certain amount of deposited or free charge, called the critical charge, which will cause an upset in a device. This concept works well for most types of SEE, although the topology of the deposited charge is also important for some effects like single-event latchups (SELs), burnout (SEB), or gate rupture (SEGR). The fundamental idea of critical charge has been a driver for SEE testing using non-particle beam sources, such as lasers or x-rays, to generate a known amount of charge in certain locations to probe device upsets.

Ideally, accelerator test data would show at what critical charge and topology an upset will happen and the particle environment as a function of critical charge and topology. Unfortunately, it is difficult to determine the critical charge needed for an upset from beam testing without some assumptions about the device structure. These same assumptions are needed to also translate the LET spectrum into a charge distribution. The issue is that while a quantity like LET is a property of the incident particles, the critical

charge is a function of both the incident particle and the device's "sensitive area." The sensitive area is the area in which deposited charge can cause an upset. The assumption is that any charge deposited outside the sensitive region will not cause any upsets, except if due to a charge funnel intersecting the sensitive region.

The typical assumption used is the rectangular parallelepiped (RPP) model. This model assumes that the sensitive volume is a box and that particles of a certain LET will generate critical charge in the volume based on the particle pathlength. The actual size of the RPP is left to the user, although the surface area perpendicular to the test beam is usually picked to be the same area as the measured saturation cross section. The thickness or depth of the RPP is usually a free parameter that the user can pick. Historically this has been set at 1 micron as older technologies had much thicker substrates, but smaller depths will lead to a higher upset rate. It is important to point out that beam testing is done at a known LET, not a known critical charge. Therefore, if an upset is seen at a given LET, then the critical charge for that upset is smaller when the depth is smaller. Unless a user knows the depth for a technology (e.g., silicon-on-insulator technology), a small depth should be picked to be conservative.

Note that the area of the sensitive volume is based on experimental data and may be very different from the actual transistor node size. For example, a SRAM cell has four to six MOSFETs. The actual cell upset area is a combination of various transistors and possible other areas on the die where charge can leak in. More complicated upsets can be tied to multiple sites in a circuit or, especially for angular effects, to multiple hits in multiple areas. This is exacerbated by the actual size of the "charge column" from the incident ions. In particular, the topology of the deposited charge can be different based on the incident particle's energy, which may cause certain upset types to be less common for lower energy particles.

Given the uncertainties mentioned above, the overall effect is that the RPP method approximates an unknown sensitive volume that is based on empirical data and a user's choice for the thickness. Such an approach was largely sufficient for older, planar technologies where the area was usually very large compared to the thickness. The angular effects on these RPPs were easier to understand, especially the "effective LET" methods. A few deviations from the RPP, such as a cylinder shape, or general rules of thumb, such as using a certain ratio between area and thickness, were used to help tune the model to different upset modes.

With newer technologies containing different, non-planar topologies, the RPP method is being seriously questioned. For example, how is the RPP represented for a 3D FinFET technology? If the dimensions of the FinFET are taken as a starting point, what is the appropriate thickness? How does the tested angular effects correspond to the constructed RPP, and how is charge sharing properly modeled if the critical charge is in the "fin" instead of the bulk? In addition, most planar devices assume a square for the area unless there is some known data. FinFETs can be very asymmetrical, which drives questions about which angular areas the FinFETs are most sensitive in and how that data can be properly integrated into the upset rate model. As expected, going to other topologies like nanowire or gate-all-around will only make the situation worse.

One option is to remove the concept of sensitive volume and instead use a simulation chain starting with particle interactions with Geant4 [5] Monte Carlo code, moving towards a transistor-level simulation to determine how the electric fields will move charge deposited by the particle, then moving to a part-level simulation to determine how that charge will move throughout the device. Such a simulation would need manufacturer level of detail as well as beam tests to calibrate for each device. As expected, such a tool is very limited and is of more interest to R&D or academic efforts.

A more empirical method is to collect more beam testing for each part. Testing the device at many beam angles (azimuth and elevation) relative to device normal help determine where the expected "effective

LET" would fail. The gathered data can be used as a replacement for the RPP method by no longer needing critical charge but relating upsets as a function of LET and angle. This would require more data than typically taken and would require some newer models that will take angular data as an input.

Overall, the community does not currently have a clear path to making a better upset rate model. With the increasing complexity of device topologies, attempting a more data-driven empirical method would appear to be most useful, but the added costs and difficulties in angular testing complex devices may prove to be too much of a hurdle. For now, the best method is to continue to use the RPP, but spot check high angles and attempt to push for conservatism in areas like the thickness of the RPP to provide some margin.

6. Table of Acronyms

ADEPT	Aerospace Debris Environment Projection Tool
AE	Auroral Electrojet
AFRL	Air Force Research Laboratory
AIAA	American Institute for Aeronautics and Astronautics
AMS	Alpha magnetic spectrometer
AO	Atomic oxygen
AP index	Planetary A magnetometer index
ASEC	Applied Space Environments Conference
ASTM	American Society for Testing and Materials (now ASTM International)
ATOMOX	Atomic Oxygen Tool in Systema suite (produced by Airbus Defence and Space)
ATR	Aerospace Technical Report
BON	Badhwar-O'Neill galactic cosmic ray model
BRAM	Block random access memory
BUMPER	NASA tool for analyzing micrometeoroid and debris risk
CAD	Computer-aided design
CAMMICE	Charge and Mass Magnetospheric Ion Composition Experiment (sensor on NASA's Polar mission)
CL	Confidence level
CME	Coronal mass ejection
CMOR	Canadian Meteor Orbit Radar
COTS	Commercial off-the-shelf
CREME	Cosmic Ray Effects on Micro-Electronics (software tool)
DDD	Displacement damage dose
DMSP	Defense Meteorological Satellite Program
DTIC	Defense Technical Information Center
DTRA	Defense Threat Reduction Agency
EDAC	Error detection and correction
EEE	Electrical, electronic, and electromechanical
EMA	Electro Magnetic Applications, Inc.
EOL	End of life (of a satellite)
EQFLUX	NASA solar cell radiation degradation tool
ESA	European Space Agency
ESD	Electro-static discharge
ESP	Emission of Solar Protons ([93], solar particle model)
FASTRAD	3D CAD tool for radiation shielding analysis
FEM	Finite element model
FLUX	Module within CREME tool
FMECA	Failure modes, effects, and criticality analysis
FOM	Figure of merit
FPA	Focal-plane array
GCR	Galactic cosmic ray

GEO	Geosynchronous equatorial orbit
GPS	Global Positioning System
GTRN	Geomagnetic Transmission Routine (module within CREME)
GUI	Graphical user interface
HAND	High-altitude nuclear detonation
HEO	Highly elliptical orbit
HUP	Heavy Ion Upset (module within CREME)
HVIT	Hypervelocity Impact Technology Group (at NASA Johnson Space Center)
IAU	International Astronomical Union
IEEE	Institute of Electrical and Electronics Engineers
IMP	International Monitoring Platform (a series of satellites to monitor sun/Earth environment)
IMPACT	The Aerospace Corporation's hypervelocity impact code
IRBEM	International Radiation Belt Environment Modeling software library
IRENE	International Radiation Environment Near Earth (new name for AE9/AP9)
ISS	International Space Station
JPL	Jet Propulsion Laboratory (NASA Center)
JSC	Johnson Space Center (NASA)
KTL factor	K-factor for one-sided tolerance limits
LANL	Los Alamos National Laboratory
LEO	Low Earth orbit
LET	Linear energy transfer
LLNL	Lawrence Livermore National Laboratory
LVLH	Local-vertical, local-horizontal (spacecraft coordinate system)
MASTER	Meteoroid and Space Debris Terrestrial Environment Reference
MC	Monte Carlo
MCNP(X)	Monte Carlo N-Particle (eXtended) Radiation Transport Code
MEM	Micrometeoroid Engineering Model (NASA software)
MEO	Medium Earth orbit
MICS	Magnetospheric Ion Composition Sensor (part of CAMMICE experiment on Polar)
MISSE	Materials International Space Station Experiment
MJD	Modified Julian date
MLI	Multi-layer insulation
MMOD	Micro-meteoroid and orbital debris
MOBE-DIC	Model of Outer Belt Electrons for Dielectric Internal Charging
MODRA	Meteoroid and Orbital Debris Risk Assessment
MPA	Magnetospheric Plasma Analyzer (LANL sensor)
MRED	Monte Carlo Radiative Energy Deposition
MSM	Magnetospheric Shielding Model
MSSREM	Mission-Specific Solar Radiation Environment Model
MULASSIS	Multilayered shielding simulation software tool
NAS	National Academy of Sciences
NASA	National Air and Space Administration

NASCAP	NASA/Air Force Spacecraft Charging Analyzer Program
NIEL	Non-ionizing energy loss
NIST	National Institute of Standards and Technology
NOVICE	Radiation Transport Code from EMPC, Inc.
NRL	Naval Research Laboratory
NRLMSISE	Naval Research Laboratory Mass Spectrometer and Incoherent Scatter Radar, Extended through Exosphere
NSSDC	NASA Space Science Data Coordinated Archive
ODPO	Orbital Debris Program Office (NASA JSC)
OMERE	Outil de Modelisation de l'Environnement Radiatif Externe (TRAD model of environment)
ORDEM	Orbital Debris Engineering Model (NASA software)
PAMELA	Payload for Antimatter Matter Exploration and Light-nuclei Astrophysics
PC	Personal computer
PEACE	Polymer Erosion and Contamination Experiment (on MISSE-2)
POLAR	NASA satellite hosting
PSYCHIC	Prediction of Solar particle Yields for Characterizing Integrated Circuits ([92], 2007 model)
PUP	Proton Upset (module withing CREME)
RAAN	Right ascension of the ascending node (orbital element)
RDF	Radiation derating factor
RDM	Radiation design margin
RDM_{ENV}	Radiation design margin due to the environment
RDM_{TOT}	Radiation design margin, total
R_E	Earth radius
RHA	Radiation hardness assurance
RLAT	Radiation lot acceptance testing
RORSAT	Radar Ocean Reconnaissance Satellites (contributing unique LEO debris population)
RPP	Rectangular parallelepiped (assumed geometry for SEU calculations)
SAA	South Atlantic Anomaly
SAMPEX	Solar Anomalous Magnetospheric Particle Explorer (NASA satellite)
SAPPHIRE	Solar Accumulated and Peak Proton and Heavy Ion Radiation Environment
SCATHA	Spacecraft Charging at High Altitudes (NASA/AF satellite)
SDAR	Space Debris Assessment Reporting
SDM	Surface Degradation Model (module within ORDEM)
SEB	Single-event burnout
SEE	Single-event effect
SEFI	Single-event functional interrupt
SEGR	Single-event gate rupture
SEL	Single-event latchup
SEP	Solar energetic particle (also SPE)
SEU	Single-event upset
SHIELDOSE	Tool for computing dose from electron/proton fluxes

SMA	Semi-major axis
SOPA	Synchronous Orbit Particle Analyzer (LANL sensor)
SPE	Solar particle/proton event (also SEP)
SPENVIS	Space Environment Information System (ESA tool)
SPM	Space Plasma Model (including SPME (electron) SPMH (protons), SPMHe (Helium) and SPMO (oxygen))
SRAM	Static random-access memory
STS	Space Transportation System (Shuttle)
TID	Total ionizing dose
TOR	Technical Operating Report (Aerospace report)
TRAD	Test and Radiations (company that produces FASTRAD and OMERE)
UV	Ultraviolet
VESPER	Virtual Enhancements−Solar Proton Event Radiation Model
VIRTEX	Type of FPGA sold by Xilinx

7. References

[1] Adams, J. H., Jr., "Cosmic Ray Effects on Micro-Electronics (CREME), Part IV," Naval Research Laboratory Memorandum Report 5901, December 31, 1986.

[2] Adams, J. H. et al., "CRÈME: The 2011 Revision of the Cosmic Ray Effects on Micro-Electronics Code," in IEEE Transactions on Nuclear Science, vol. 59, no. 6, pp. 3141–3147, December 2012.

[3] Adams, J. H. et al., "The SIRE2 Toolkit," Space Weather, 2020. doi:10.1029/2019SW002364

[4] Allen, G.; G. Swift; and C. Carmichael, "VIRTEX - 4 VQ static SEU characterization summary," JPL Tech Report 08-16 4/08, Jet Propulsion Laboratory, National Aeronautics and Space Administration, Pasadena, CA, 2008.

[5] Allison, J. et al., "Recent developments in Geant4," Nuclear Instruments and Methods in Physics Research Section A: Accelerators, Spectrometers, Detectors and Associated Equipment, vol. 835, pp. 186–225, ISSN 0168-9002, 2016. https://doi.org/10.1016/j.nima.2016.06.125.

[6] Aminalragia-Giamini S.; I. Sandberg; C. Papadimitriou; I. A. Daglis; and P. Jiggens. "The virtual enhancements: solar proton event radiation (VESPER) model," J. Space Weather Space Clim. 8: A06, 2018.

[7] Anderson, P. C., "Characteristics of Spacecraft Charging in Low Earth Orbit," J. Geophys. Res., 117, A07308, 2012. doi:10.1029/2011JA016875.

[8] Anderson, P. C., and H. C. Koons, "A Spacecraft Charging Anomaly on a DMSP Satellite in an Aurora," J. Spacecraft. Rockets, 33, 734, 1996. doi:10.2514/3.26828.

[9] ASTM E490-00a(2019), Standard Solar Constant and Zero Air Mass Solar Spectral Irradiance Tables, ASTM International, West Conshohocken, PA, 2019. Retrieved from www.astm.org.

[10] Bodeau, J., "High Energy Electron Climatology that Supports Deep Charging Risk Assessment in GEO," AIAA 2010-1608. 48th AIAA Aerospace Sciences Meeting Including the New Horizons Forum and Aerospace Exposition. January 2010. https://doi.org/10.2514/6.2010-1608.

[11] Bongim, J.; L. M. M. Sierra; B. X. Zhu, Brian X.; and I. Jun, "Comparison of Total Ionizing Doses from Representative Space Radiation Shielding Analysis Tools," Applied Space Environments Conference: ASEC 2019, Los Angeles, California, May 13–17, 2019, http://hdl.handle.net/2014/50738.

[12] Cour-Palais, B. G., "Meteoroid environment model 1969," NASA SP-8013, NASA JSC, Houston, Texas, 1969.

[13] CREME, https://creme.isde.vanderbilt.edu/.

[14] Davis, V. A. et al., "Validation of NASCAP-2K Spacecraft-Environment Interactions Calculations," 8th Spacecraft Charging Technology Conference, Huntsville, AL, 2004.

[15] Davis, V. A. et al, "NASCAP-2K Version 4.3 User's Manual," AFRL Technical Report AFRL-RV-PS-TR-2017-0002, 2016. https://apps.dtic.mil/sti/pdfs/AD1064754.pdf.

[16] de Groh, K. K.; B. A. Banks; C. E. Mccarthy; R. N. Rucker; L. M. Roberts; and L. A. Berger, "MISSE 2 PEACE Polymers Atomic Oxygen Erosion Experiment on the International Space Station," High Performance Polymers, 20(4–5), 388–409, 2008. https://doi.org/10.1177/0954008308089705

[17] de Groh, K. K. et al., 2010, MISSE-2 PEACE Polymers Experiment Atomic Oxygen Erosion Yield Error Analysis, NASA/TM-2010-216903, 2010.

[18] Denton, M. H.; M. F. Thomsen; H. Korth; S. Lynch; J. C. Zhang; and M. W. Liemohn, "Bulk plasma properties at geosynchronous orbit," J. Geophys. Res., 110, A07223, 2005. doi:10.1029/2004JA010861.

[19] Department of the Air Force, Military Standard: Space Environment for USAF Space Vehicles, MIL-STD-1809, Washington, D.C., February 15, 1991.

[20] Divine, N., "Five Populations of Interplanetary Meteoroids," Journal of Geophysical Research, 98, 17029-17048, 1993.

[21] Dyer, C.; K. Hunter; S. Clucas; and A. Campbell, "Observation of the Solar Particle Events of October and November 2003 From CREDO and MPTB," IEEE Transactions on Nuclear Science, vol 51, no 6, December 2004.

[22] Edmonds, L., "Upper Bound SEU Rate for Devices in an Isotropic or Nonisotropic Flux." NASA-CR-189765, JPL-PUBL-91-32, NAS 1.26:189765, Jet Propulsion Laboratory, California Institute of Technology, 1991.

[23] Fennell, J. F.; H. C. Koons; M. W. Chen; and J. B. Blake, "Internal charging: a preliminary environmental specification for satellites," in IEEE Transactions on Plasma Science, vol. 28, no. 6, pp. 2029–2036, December 2000. doi: 10.1109/27.902230.

[24] Fennell, J. F.; P. C. Anderson; and J. B. Blake, *Electron Environment for Surface Charging at SBIRS-Low Altitudes*, Aerospace Report No. TOR-2002(1033)-1, The Aerospace Corporation, El Segundo, CA, 2002.

[25] Feynman, J.; A. Ruzmaikin; and V. Berdichevsky, "The JPL proton fluence model: an update," J. Atmospheric and Solar-Terrestrial Physics, 64, 1679-86, 2002.

[26] Feynman, J.; G. Spitale; J. Wang; and S. Gabriel, "Interplanetary proton fluence model: JPL 1991," Journal of Geophysical Research 98, 13, 281-94, 1993.

[27] Flegel, S., "Master-2009 Software User Manual," June 7, 2011.

[28] Ginet, G. P. et al., "AE9, AP9 and SPM: New models for specifying the trapped energetic particle and space plasma environment," Space Sci. Rev., 179, 579-615, 2013.

[29] Gombosi, T. I.; D. N. Baker; A. Balogh, et al., Anthropogenic Space Weather, Space Sci Rev 212, 985–1039, 2017. https://doi.org/10.1007/s11214-017-0357-5.

[30] Guild, T. B.; T. P. O'Brien; and J, E. Mazur, *A Method for Statistically Determining the Atomic Oxygen Fluence on LEO Spacecraft*, Aerospace Report No. TOR-2014-02863, The Aerospace Corporation, El Segundo, CA, August 29, 2014.

[31] Guild, T. B.; T. P. O'Brien; B. P. Kwan; and J. E. Mazur, *Satellite Natural and Nuclear Environment Standard – Appendix B: Natural Environment Method and Results*, Aerospace Report Number TOR-2014-03250, The Aerospace Corporation, El Segundo, CA, September 20, 2014.

[32] Gussenhoven, M. S.; D. A. Hardy; F. Rich; W. J. Burke; and H. C. Yeh, "High Level Charging in the Low-Altitude Polar Auroral Environment," J. Geophys. Res., 90, 11000, 1985.

[33] Hands, A. D. P; K. A. Ryden; I. Sandberg; D. Heynderickx; G. Provatas; S. Aminalragia-Giamini; A. Tsigkanos; C. Papadimitriou; D. Rodgers; and H. Evans, "An Update to MOBE-DIC Using Current Monitor Measurements from Galileo," IEEE Transactions on Nuclear Science, vol. 67, no. 1, January 2020. https://doi.org/10.1109/TNS.2019.2944699.

[34] Jenniskens, P., "Meteor Stream Activity – I. The annual meteor streams," Journal of Astronomy and Astrophysics, 287, 990-1013, 1994.

[35] Jiggens, P.; A. Varotsou; P. Truscott; D. Heynderickx; F. Lei; H. Evans; and E. Daly, "The Solar Accumulated and Peak Proton and Heavy Ion Radiation Environment (SAPPHIRE) model," IEEE Trans. Nucl. Sci., 65 (2), 2018.

[36] Jiggens, P.; D. Heynderickx; I. Sandberg; P. Truscott; O. Raukunen; and R. Vainio, "Updated Model of the Solar Energetic Proton Environment In Space," J. Space Weather Space Climate, 2018, 8, A31, https://doi.org/10.1051/swsc/2018010.

[37] Johnson-Roth, G., *Mission Assurance Guidelines for A-D Mission Risk Classes*, Aerospace Report Number TOR-2011(8591)-21, The Aerospace Corporation, El Segundo, CA, June 3, 2011.

[38] Johnston, W. R.; T. P. O'Brien; S. L. Huston; T. B. Guild; and G. P. Ginet, "Recent updates to the AE9/AP9/SPM radiation belt and space plasma specification model," IEEE Trans. Nucl. Sci., 62(6):2760-2766, 2015.

[39] Koons, H. C.; P. F. Mizera; J. L. Roeder; and J. F. Fennell, "Severe spacecraft-charging event on SCATHA in September 1982," J. Spacecraft and Rockets, 25, 239, doi.org/10.2514/6.1987-475, 1988.

[40] Ladbury, R., and T. Carstens, "Development of TID Hardness Assurance Methodologies to Capitalize on Statistical Radiation Environment Models," in IEEE Transactions on Nuclear Science, vol. 68, no. 8, pp. 1736–1745, August 2021. doi: 10.1109/TNS.2021.3055694.

[41] Lear, D. M.; E. L. Christiansen; and J. L. Hyde, "BUMPER: A Tool for Analyzing Spacecraft Micrometeoroid and Orbital Debris Risk," First International Orbital Debris Conference, December 2019.

[42] Lei, F., ESHIEM Project Technical Note 2A, Issue 1.5, RADMOD/TN/201401, ESA Contract: 4000107025/12/NL/GLC, July 2017.

[43] Mandell, M. J.; V. A. Davis; D. L. Cooke; A. T. Wheelock; and C. J. Roth, "Nascap-2k Spacecraft Charging Code Overview," in IEEE Transactions on Plasma Science, vol. 34, no. 5, pp. 2084–2093, October 2006. doi: 10.1109/TPS.2006.881934.

[44] Mazur, J. E.; G. M. Mason; M. D. Looper; R. A. Leske; and R. A. Mewaldt, "Charge states of solar energetic particles using the geomagnetic cutoff technique: SAMPEX measurements in the 6 November 1997 solar particle event," Geophys. Res. Lett., 26 (2) 173-6, 1999.

[45] McBride, M., "The Importance of the Annual Meteor Streams to Spacecraft and Their Detectors," Advances in Space Research, 20, 8, 1513-1516, 1997.

[46] McPherson, D. A.; D. P. Cauffman; and W. R. Schober, "Spacecraft charging at high altitude: SCATHA satellite program," J. Spacecraft. Rockets, 12, doi.org/10.2514/3.57027, 1975.

[47] Mendenhall, M. H., and Robert A. Weller, "A probability-conserving cross-section biasing mechanism for variance reduction in Monte Carlo particle transport calculations," Nucl. Inst. & Meth. A, Volume 667, Pages 38–43, March 1, 2012. doi:10.1016/j.nima.2011.11.084.

[48] Meshishnek, M., "MEO Space Radiation Environment, Issues for Programs: Spacecraft External Surfaces vs Shielded Materials," Aerospace Report Number ATR-2007(5174)-1, The Aerospace Corporation, El Segundo, CA, December 30, 2006.

[49] Messenger, G. C., and S. A. Milton, *Single Event Phenomena*. Chapman & Hall, 1997.

[50] Morehead, A. V., "NASA Micrometeoroid Engineering Model (MEM) version 3," NASA, July 22, 2019.

[51] Mrigakshi, A. I.; D. Matthiä; T. Berger; G. Reitz; and R. F. Wimmer-Schweingruber, "Assessment of galactic cosmic ray models," J. Geophys. Res., 117, A08109, 2012. doi:10.1029/2012JA017611.

[52] NASCAP-2K, NASA/Air Force Spacecraft Charging Analyzer Program, Version 4.3, Ref. MFS-32056-1, https://software.nasa.gov/software/MFS-32056-1.

[53] National Air and Space Administration, Mitigating In-Space Charging Effects – A Guideline, NASA-HDBK-4002A, 2017. Retrieved from https://standards.nasa.gov/standard/nasa/nasa-hdbk-4002.

[54] Neal, J. J.; C. J. Rodger; and J. C. Green, "Empirical determination of solar proton access to the atmosphere: Impact on polar flight paths," Space Weather, 11, 420– 433, 2013. doi:10.1002/swe.20066.

[55] Neergaard, L. E. et al., "Comparison of the NASCAP/GEO, POLAR, SEE Charging Handbook, and NASCAP-2K.1 Spacecraft Charging Codes," 7th Spacecraft Charging Technology Conference, Noordwijk, 2001.

[56] Nymmik, R. A.; M. I. Panasyuk; T. I. Pervaja; and A.A. Suslov, "A Model of Galactic Cosmic Ray Fluxes," Nucl. Tracks Radiat. Meas. 20, 427, 1992.

[57] O'Brien, T. P., and B. P. Kwan, *Using pre-computed kernels to accelerate effects calculations for AE9/AP9: A displacement damage example*, Aerospace Report No. TOR-2013-00529, The Aerospace Corporation, El Segundo, CA, 2013.

[58] O'Brien, T. P., *AE9/AP9 Guidance for Third-Party Developers*, Aerospace Report No. TOR-2014-01204, The Aerospace Corporation, El Segundo, CA, March 25, 2014.

[59] O'Brien, T. P., *AE9/AP9 Proton Single-Event Effect Kernel Utility*, Aerospace Report No. TOR-2015-02707, The Aerospace Corporation, El Segundo, CA, September 2, 2015.

[60] O'Brien, T. P.; J. L. Roeder; and M. D. Looper, *AE9/AP9 Internal Charging Kernel Utility—Beam-Slab Geometry Adapted to Hemispherical Shell for Aluminum Shields*, Aerospace Report No. TOR-2016-01203, The Aerospace Corporation, El Segundo, CA, March 3, 2016.

[61] O'Brien, T. P., *AE9/AP9 Proton Displacement Damage Kernels (version 2)*, Aerospace Report No. ATR-2016-03268, The Aerospace Corporation, El Segundo, CA, October 12, 2016.

[62] O'Brien, T. P.; B. P. Kwan; and J. R. Srour, *AE9/AP9 Electron Displacement Damage Kernels*, Aerospace Report No. TOR-2017-00514, The Aerospace Corporation, El Segundo, CA, October 11, 2017.

[63] O'Brien. T. P., and B. P. Kwan, "Incorporating Radiation Effects Into AE9/AP9," in IEEE Transactions on Nuclear Science, vol. 65, no. 1, pp. 457-461, January 2018. doi: 10.1109/TNS.2017.2758322.

[64] O'Brien, T. P.; W. R. Johnston; S. L. Huston; C. J. Roth; T. B. Guild; Y.-J. Su; and R. A. Quinn, "Changes in AE9/AP9-IRENE version 1.5," IEEE Trans. Nucl. Sci., 65(1):462-466, doi:10.1109/TNS.2017.2771324, 2018.

[65] O'Brien, T. P.; J. E. Mazur; S. C. Davis; B. P. Kwan; and B. A. Morgan, *Current and Evolving Practices for Use of Solar Energetic Particle Climatology Models in Satellite Environment Specifications*, Aerospace Report No. TOR-2019-01714, The Aerospace Corporation, El Segundo, CA, July 1, 2019.

[66] Petersen, E., *Single Event Effects in Aerospace*. IEEE Press, 2011.

[67] Picone, J. M.; A. E. Hedin; D. P. Drob; and A. C. Aikin, "NRLMSISE-00 empirical model of the atmosphere: Statistical comparisons and scientific issues," *Journal of Geophysical Research*, 107(A12), 1468. doi:10.1029/2002JA009430,2002.

[68] Reed, R. A. et al., "Physical Processes and Applications of the Monte Carlo Radiative Energy Deposition (MRED) Code," in IEEE Transactions on Nuclear Science, vol. 62, no. 4, pp. 1441–1461, August 2015.

[69] Robertson, S. R.; L. I. Harzstark; J. P. Siplon; D. M. Peters; P. H. Hesse; M. J. Engler; R. J. Ferro; W. A. Martin; G. G. Cuevas; M. H. Cohen; J. H. Sokol; K. N. Feistel; S. R. Nuccio; and G. J. Ewell, *Technical Requirements for Electronic Parts, Materials, and Processes Used in Space Vehicles*, Aerospace Report Number TOR-2006(8583)-5236 Rev B, The Aerospace Corporation, El Segundo, CA, March 6, 2013.

[70] Robinson, Z. D.; J. H. Adams Jr.; J. H. Fisher; J. H. Nonnast; and D. C. Terry, "Mission Specific Solar Radiation Environment Model (MSSREM): Peak Flux Model," 2020. doi:10.1029/2019SW002361.

[71] Robinson, Z. D., "New probabilistic model for episode integrated fluences of protons using episodes from 1973-2013," Masters Thesis, The University of Alabama in Huntsville, 2015.

[72] Roeder, J. L., *Specification of the Plasma Environment at Geosynchronous Orbit in the Energy Range 87 eV to 288 keV*, Aerospace Report Number TR-94(4940)-6; WMD-TR-96-9, 1994.

[73] Roeder, J. L.; M. W. Chen; J. F. Fennell; and R. Friedel, "Empirical models of the low-energy plasma in the inner magnetosphere," Space Weather, 3, S12B06, 2005. doi:10.1029/2005SW000161

[74] Roeder, J. L. "Advanced Spacecraft Charging Models: Progress and Challenges," seminar, The Aerospace Corporation, 2007

[75] Sawyer, D. M., and J. I. Vette, "AP-8 Trapped Proton Environment for Solar Maximum and Solar Minimum," Tech. rep., NSSDC/WDC-A-R&S 76-06, 1976.

[76] Selesnick, R. S.; M. K. Hudson; and B. T. Kress, "Injection and loss of inner radiation belt protons during solar proton events and magnetic storms," J. Geophys. Res., 115, A08211, 2010. doi:10.1029/2010JA015247.

[77] Seltzer, S. "Updated Calculations for Routine Space-Shielding Radiation Dose Estimates: SHIELDOSE-2, NIST Interagency/Internal Report (NISTIR)," National Institute of Standards and Technology, Gaithersburg, MD, 1994. https://tsapps.nist.gov/publication/get_pdf.cfm?pub_id=103635, accessed September 7, 2021.

[78] Shea, M. A., and D. F. Smart, "A five by fifteen degree world grid of calculated cosmic-ray vertical cutoff rigidities for 1965 and 1975," 14th International Cosmic Ray Conference. Conference Papers, 4, pp. 1298-1303, 1975.

[79] Slaba, T. C., and K. Whitman, K., "The Badhwar-O'Neill 2020 GCR model," Space Weather, 18, e2020SW002456, 2020. https://10.3847/10.1029/2020SW002456

[80] Smart, D. F., and M. A. Shea, "A comparison of the Tsyganenko model predicted and measured geomagnetic cutoff latitudes," Advances in Space Research, 28(12), 1733–1738, 2001.

[81] SPENVIS, https://www.spenvis.oma.be/intro.php.

[82] Stansbery, E. G.; M. J. Matney; and P. H. Krisko, "NASA Orbital Debris Engineering Model ORDEM 3.0 – User's Guide," NASA/TP-2014-217370, NASA/Johnson Space Center, April 2014.

[83] Staubach, P., "Numerische Modellierung von Mikrometeoriden und ihre Bedeutung für interplanetare Raumsonden und geozentrische Satelliten," Thesis at the University of Heidelberg, April 1996.

[84] Stevens J. R., and A. L. Vampola, "Description of the space test program P78-2 spacecraft (SCATHA) and payloads," SAMSO TR-78-24, 1978.

[85] Thomsen, M. F.; M. H. Denton; B. Lavraud; and M. Bodeau, "Statistics of plasma fluxes at geosynchronous orbit over more than a full solar cycle," Space Weather, 5, S03004, 2007. doi:10.1029/2006SW000257.

[86] Tylka, A. J.; J. H. Adams, Jr.; P. R. Boberg; B. Brownstein; W. F. Dietrich; E. O. Flueckiger; E. L. Petersen; M. A. Shea; D. F. Smart; and E. C. Smith, "CREME96: A Revision of the Cosmic

Ray Effects on Micro-Electronics Code," IEEE Trans. Nucl. Sci., vol. 44, no. 6, pp. 2150–2160, December 1997.

[87] Tylka, A. J.; W. F. Dietrich; and P. R. Bobery, "Probability distributions of high-energy solar-heavy-ion fluxes from IMP-8: 1973-1996," in IEEE Transactions on Nuclear Science, vol. 44, no. 6, pp. 2140–2149, December 1997. doi: 10.1109/23.659029.

[88] United States Department of Defense, System Safety, Department of Defense Standard Practice, MIL-STD-882E, May 11, 2012.

[89] Vette, J. I., "The AE-8 trapped electron model environment," NASA STI/Recon Technical Report N, 92, 24,228–+, 1991.

[90] Weller, R. A.; M. H. Mendenhall; R. A. Reed; R. D. Schrimpf; K. M. Warren; B. D. Sierawski; and L. W. Massengill, "Monte carlo simulation of single event effects," IEEE Trans. Nucl. Sci., vol. 57, no. 4, pp. 1726–1746, August 2010.

[91] Xapsos, M. A.; G. P. Summers; J. L. Barth; E. G. Stassinopoulos; and E. A. Burke, "Probability model for cumulative solar proton event fluences," IEEE Trans. Nucl. Sci., 47 (3), 486-90, 2000.

[92] Xapsos, M. A.; C. Stauffer; T. Jordan; J. L. Barth; and R. Mewaldt, "Model for cumulative solar heavy ion energy and linear energy transfer spectra," IEEE Trans. Nucl. Sci., 54, 1985-9, 2007.

[93] Xapsos, M. A. et al., "Inclusion of Radiation Environment Variability in Total Dose Hardness Assurance Methodology," IEEE Trans. Nucl. Sci., vol. 64, no. 1, pp. 325–331, January 2017.

Appendix A. ESP GEO Proton Fluences

Tabulated below are results derived from the ESP model [Xapsos et al., 2001 [92] calculated for 10 years at GEO, including 7 years in solar maximum conditions. Integral fluences were provided to us by M. Xapsos in 2015. We added the 25th and 75th percentiles by linearly interpolating the percentiles in log(energy) and numerically differentiated the integral fluxes provided to arrive at the table of fluences below. Fluences are in units of protons / (cm^2 MeV). Aerospace personnel use these fluences, attenuate for geomagnetic shielding, and add to the trapped proton fluences at a given confidence level to generate statistically consistent satellite environment specifications.

Table 16. 10-Year GEO Solar Proton Fluences with Units of Protons / (cm2 MeV) and as a Function of Energy (columns, MeV) and Confidence Level (rows)

Diff Energy (MeV)	6	C = 5%	C = 10%	C = 20%	C = 25%	C = 30%	C = 40%	C = 50%	C = 60%	C = 70%	C = 75%	C = 80%	C = 90%	C = 95%	C = 99%
1	3.90E+11	4.48E+11	4.79E+11	5.18E+11	5.31E+11	5.45E+11	5.68E+11	5.88E+11	6.08E+11	6.26E+11	6.36E+11	6.45E+11	6.64E+11	6.70E+11	6.50E+11
3	2.60E+10	3.52E+10	4.11E+10	4.94E+10	5.27E+10	5.62E+10	6.24E+10	6.87E+10	7.53E+10	8.28E+10	8.73E+10	9.20E+10	1.05E+11	1.15E+11	1.30E+11
5	7.18E+09	1.07E+10	1.32E+10	1.68E+10	1.83E+10	1.99E+10	2.30E+10	2.62E+10	2.98E+10	3.39E+10	3.65E+10	3.92E+10	4.73E+10	5.42E+10	6.58E+10
7	2.82E+09	4.54E+09	5.80E+09	7.79E+09	8.64E+09	9.58E+09	1.14E+10	1.34E+10	1.56E+10	1.83E+10	2.01E+10	2.20E+10	2.79E+10	3.34E+10	4.40E+10
10	9.55E+08	1.67E+09	2.25E+09	3.19E+09	3.61E+09	4.09E+09	5.04E+09	6.11E+09	7.38E+09	9.00E+09	1.01E+10	1.13E+10	1.52E+10	1.92E+10	2.83E+10
15	2.51E+08	4.87E+08	6.91E+08	1.05E+09	1.22E+09	1.41E+09	1.82E+09	2.29E+09	2.88E+09	3.68E+09	4.23E+09	4.85E+09	7.05E+09	9.50E+09	1.59E+10
20	9.37E+07	1.96E+08	2.90E+08	4.63E+08	5.47E+08	6.46E+08	8.58E+08	1.12E+09	1.45E+09	1.91E+09	2.23E+09	2.62E+09	4.03E+09	5.71E+09	1.06E+10
25	4.24E+07	9.41E+07	1.43E+08	2.38E+08	2.86E+08	3.42E+08	4.66E+08	6.20E+08	8.23E+08	1.11E+09	1.32E+09	1.58E+09	2.54E+09	3.73E+09	7.52E+09
30	2.19E+07	5.08E+07	7.95E+07	1.36E+08	1.65E+08	2.00E+08	2.78E+08	3.77E+08	5.10E+08	7.03E+08	8.48E+08	1.02E+09	1.71E+09	2.59E+09	5.55E+09
35	1.23E+07	2.98E+07	4.76E+07	8.36E+07	1.02E+08	1.25E+08	1.77E+08	2.43E+08	3.35E+08	4.69E+08	5.72E+08	6.96E+08	1.20E+09	1.86E+09	4.19E+09
40	7.47E+06	1.87E+07	3.03E+07	5.44E+07	6.72E+07	8.29E+07	1.19E+08	1.65E+08	2.30E+08	3.28E+08	4.03E+08	4.95E+08	8.71E+08	1.38E+09	3.25E+09
45	4.78E+06	1.23E+07	2.03E+07	3.71E+07	4.61E+07	5.72E+07	8.28E+07	1.17E+08	1.64E+08	2.37E+08	2.93E+08	3.63E+08	6.53E+08	1.06E+09	2.57E+09
50	3.20E+06	8.42E+06	1.41E+07	2.61E+07	3.27E+07	4.08E+07	5.97E+07	8.50E+07	1.21E+08	1.76E+08	2.19E+08	2.73E+08	5.00E+08	8.21E+08	2.06E+09
55	2.22E+06	5.96E+06	1.01E+07	1.90E+07	2.39E+07	3.00E+07	4.42E+07	6.36E+07	9.13E+07	1.34E+08	1.68E+08	2.10E+08	3.91E+08	6.51E+08	1.68E+09
60	1.59E+06	4.35E+06	7.44E+06	1.42E+07	1.79E+07	2.26E+07	3.36E+07	4.88E+07	7.07E+07	1.05E+08	1.32E+08	1.66E+08	3.14E+08	5.29E+08	1.40E+09
70	8.67E+05	2.45E+06	4.26E+06	8.31E+06	1.06E+07	1.34E+07	2.02E+07	2.97E+07	4.35E+07	6.54E+07	8.30E+07	1.05E+08	2.03E+08	3.50E+08	9.60E+08
80	5.14E+05	1.49E+06	2.63E+06	5.22E+06	6.68E+06	8.54E+06	1.30E+07	1.93E+07	2.85E+07	4.34E+07	5.55E+07	7.09E+07	1.40E+08	2.44E+08	6.91E+08
90	3.23E+05	9.57E+05	1.71E+06	3.44E+06	4.42E+06	5.69E+06	8.74E+06	1.31E+07	1.95E+07	2.99E+07	3.85E+07	4.94E+07	9.89E+07	1.75E+08	5.10E+08
100	1.77E+05	5.50E+05	1.00E+06	2.08E+06	2.71E+06	3.53E+06	5.53E+06	8.42E+06	1.28E+07	2.01E+07	2.61E+07	3.40E+07	7.04E+07	1.29E+08	3.98E+08
125	7.96E+04	2.51E+05	4.62E+05	9.70E+05	1.27E+06	1.65E+06	2.61E+06	4.00E+06	6.13E+06	9.68E+06	1.26E+07	1.65E+07	3.47E+07	6.39E+07	2.01E+08
150	4.47E+04	1.41E+05	2.60E+05	5.45E+05	7.12E+05	9.30E+05	1.47E+06	2.25E+06	3.45E+06	5.44E+06	7.11E+06	9.29E+06	1.95E+07	3.59E+07	1.13E+08
175	2.69E+04	8.47E+04	1.56E+05	3.28E+05	4.28E+05	5.59E+05	8.83E+05	1.35E+06	2.07E+06	3.27E+06	4.27E+06	5.58E+06	1.17E+07	2.16E+07	6.81E+07
200	1.72E+04	5.43E+04	1.00E+05	2.10E+05	2.74E+05	3.58E+05	5.66E+05	8.67E+05	1.33E+06	2.10E+06	2.74E+06	3.58E+06	7.51E+06	1.38E+07	4.36E+07
225	1.16E+04	3.64E+04	6.72E+04	1.41E+05	1.84E+05	2.40E+05	3.79E+05	5.82E+05	8.91E+05	1.41E+06	1.84E+06	2.40E+06	5.03E+06	9.29E+06	2.93E+07
250	8.15E+03	2.57E+04	4.74E+04	9.94E+04	1.30E+05	1.70E+05	2.68E+05	4.10E+05	6.29E+05	9.93E+05	1.30E+06	1.69E+06	3.55E+06	6.55E+06	2.06E+07
275	5.86E+03	1.85E+04	3.41E+04	7.15E+04	9.34E+04	1.22E+05	1.93E+05	2.95E+05	4.52E+05	7.14E+05	9.32E+05	1.22E+06	2.55E+06	4.71E+06	1.48E+07
300	4.23E+03	1.33E+04	2.46E+04	5.16E+04	6.74E+04	8.81E+04	1.39E+05	2.13E+05	3.27E+05	5.16E+05	6.73E+05	8.80E+05	1.85E+06	3.40E+06	1.07E+07

Appendix B. SHIELDOSE2 Swapped Data Tables

During the development of AE9/AP9-IRENE, the development team became aware of an error in the NIST-distributed version of SHIELDOSE2. The problem lies in the swapping of Bremsstrahlung data tables of different geometries. In the original elbrbas2.dat file, the Bremsstrahlung finite-slab and semi-infinite slab data tables, with the exception of the Al detector targets, were mistakenly switched. Daniel Heynderickx found and fixed this error first and described the fix in an email excerpted below.

> As promised, here is my analysis of the bug I found in SHIELDOSE-2 many years ago. I had signalled this to Seltzer, but never received a reply. I don't know if the NIST version has ever been updated, but from the fact that your implementation appears to exhibit the same error as before, I guess it hasn't.
>
> The error is in the elbrbas2.dat file: except for Al targets, the finite and semi-infinite slab data for Bremsstrahlung have been reversed. To illustrate this, I attach Al and Si results obtained with the source code downloaded from the NIST ftp site (ftp://ftp.nist.gov/pub/shieldose/) using their sample inputs. Also attached are the same results obtained with my corrected code.
>
> The results for Al are identical, proving that no correction is needed for Al. For Si, you can see that the Bremsstrahlung doses are indeed interchanged. This has the additional effect that the sphere doses are also wrong; in fact, I noticed the problem when I saw the negative Si sphere doses! In the file obtained with my corrected code, the slab Bremsstrahlung doses are in the right order, and the sphere doses are no longer negative.
>
> The change required is minimal: if you compare the two versions, you will see that the only change occurs at line 178, where I added an if clause checking on the target material, and inverting the Bremsstrahlung data for materials other than Al. That's all!
>
> It looks trivial, but it took me a while way back when to figure this out...

Figure 26. Heyndrickx 2013, personal communication.

Appendix C. AE9/AP9-IRENE Environment Data Tables

Table 17. 10 year integral 95th percentile electron fluence with units of electrons / (cm2) as a function of energy (MeV) for the example GEO, HEO, LEO and GPS orbits (as defined in Table 7). This data is shown in Figure 8.

Energy (MeV)	GEO	HEO	LEO	GPS
0.04	3.24E+16	1.21E+16	1.13E+15	1.02E+16
0.07	1.80E+16	8.60E+15	8.12E+14	7.71E+15
0.1	1.11E+16	6.34E+15	6.00E+14	6.15E+15
0.25	2.99E+15	1.97E+15	1.90E+14	2.85E+15
0.5	6.67E+14	3.20E+14	4.11E+13	1.18E+15
0.75	2.77E+14	1.19E+14	1.30E+13	6.19E+14
1	1.43E+14	6.48E+13	5.96E+12	3.49E+14
1.5	5.13E+13	2.28E+13	1.60E+12	1.24E+14
2	1.65E+13	7.83E+12	4.26E+11	3.92E+13
2.5	5.15E+12	2.84E+12	1.10E+11	1.36E+13
3	1.72E+12	1.17E+12	3.19E+10	5.54E+12
3.5	6.76E+11	5.19E+11	1.21E+10	2.41E+12
4	3.21E+11	2.62E+11	4.92E+09	1.06E+12
4.5	1.79E+11	1.42E+11	2.18E+09	4.85E+11
5	1.17E+11	7.95E+10	8.32E+08	2.42E+11
5.5	8.27E+10	4.80E+10	3.49E+08	1.40E+11
6	5.88E+10	3.14E+10	2.05E+08	9.79E+10
6.5	4.20E+10	2.22E+10	1.30E+08	7.13E+10
7	3.13E+10	1.66E+10	9.29E+07	5.35E+10
8.5	1.24E+10	6.42E+09	2.97E+07	2.07E+10

Table 18. 10 year integral 95th percentile proton fluence with units of protons / (cm2) as a function of energy (MeV) for the example GEO, HEO, LEO and GPS orbits (as defined in Table 7). This data is shown in Figure 10.

Energy (MeV)	GEO	HEO	LEO	GPS
0.1	2.20E+15	5.51E+15	2.01E+12	1.56E+16
0.2	7.69E+14	3.95E+15	1.72E+12	8.45E+15
0.4	9.56E+13	2.18E+15	1.32E+12	2.35E+15
0.6	2.10E+13	1.23E+15	1.04E+12	6.59E+14
0.8	7.71E+12	7.57E+14	9.13E+11	1.67E+14
1	4.35E+12	5.03E+14	8.38E+11	6.33E+13
2	8.71E+11	1.51E+14	5.46E+11	5.47E+12
4	4.36E+11	3.26E+13	3.47E+11	3.23E+11
6	3.18E+11	9.45E+12	2.65E+11	1.98E+11
8	2.49E+11	3.95E+12	2.19E+11	1.58E+11
10	2.02E+11	2.31E+12	1.92E+11	1.32E+11
15	1.31E+11	8.53E+11	1.56E+11	8.91E+10
20	9.26E+10	4.06E+11	1.35E+11	6.53E+10
30	5.32E+10	2.25E+11	1.08E+11	3.96E+10
50	2.31E+10	1.04E+11	7.89E+10	1.86E+10
60	1.65E+10	8.12E+10	6.87E+10	1.37E+10
80	9.16E+09	5.23E+10	5.29E+10	7.98E+09
100	5.55E+09	3.48E+10	4.15E+10	5.05E+09
150	1.89E+09	1.42E+10	2.71E+10	1.85E+09
200	7.29E+08	6.29E+09	1.77E+10	7.29E+08
300	0.00E+00	1.09E+09	6.65E+09	0.00E+00
400	0.00E+00	2.38E+08	2.21E+09	0.00E+00
700	0.00E+00	1.27E+07	2.52E+08	0.00E+00
1200	0.00E+00	2.32E+04	6.15E+06	0.00E+00

Table 19. 10 year 95th percentile total dose with units of Rads as a function of spherical Al shielding depth in mils for the example GEO, HEO, LEO and GPS orbits (as defined in Table 7).
This data is shown in Figure 13.

Depth mils Al	GEO	HEO	LEO	GPS
1	6.40E+08	4.92E+08	2.72E+07	2.34E+08
1.25893	4.49E+08	3.89E+08	2.20E+07	1.95E+08
1.58489	3.16E+08	3.07E+08	1.78E+07	1.63E+08
1.99526	2.37E+08	2.36E+08	1.45E+07	1.40E+08
2.51189	1.87E+08	1.84E+08	1.20E+07	1.22E+08
3.16228	1.53E+08	1.44E+08	9.92E+06	1.07E+08
3.98107	1.25E+08	1.11E+08	8.15E+06	9.32E+07
5.01187	1.02E+08	8.54E+07	6.61E+06	8.10E+07
6.30957	8.04E+07	6.44E+07	5.24E+06	6.93E+07
7.94328	6.15E+07	4.75E+07	4.04E+06	5.81E+07
10	4.53E+07	3.36E+07	3.01E+06	4.77E+07
12.5893	3.22E+07	2.14E+07	2.16E+06	3.83E+07
15.8489	2.23E+07	1.30E+07	1.48E+06	3.06E+07
19.9526	1.51E+07	7.71E+06	9.96E+05	2.43E+07
25.1189	1.03E+07	4.90E+06	6.40E+05	1.89E+07
31.6228	7.09E+06	3.13E+06	3.96E+05	1.43E+07
39.8107	4.64E+06	2.06E+06	2.41E+05	1.03E+07
50.1187	2.95E+06	1.38E+06	1.48E+05	7.07E+06
63.0957	1.95E+06	9.10E+05	9.27E+04	4.79E+06
79.4328	1.25E+06	5.85E+05	5.74E+04	3.04E+06
100	6.96E+05	3.39E+05	3.43E+04	1.64E+06
125.893	3.26E+05	1.74E+05	2.03E+04	7.54E+05
158.489	1.30E+05	8.43E+04	1.43E+04	3.08E+05
199.526	4.73E+04	4.64E+04	1.14E+04	1.18E+05
251.189	1.84E+04	2.65E+04	9.40E+03	4.35E+04
316.228	9.61E+03	1.92E+04	7.96E+03	1.61E+04
398.107	6.12E+03	1.29E+04	6.69E+03	7.53E+03
501.187	4.43E+03	9.13E+03	5.56E+03	5.01E+03
630.957	3.22E+03	7.12E+03	4.66E+03	3.81E+03
794.328	2.40E+03	5.67E+03	3.94E+03	3.02E+03
1000	1.81E+03	4.26E+03	3.22E+03	2.40E+03

Table 20. 10-Year 95th Percentile Total Equivalent 1 MeV Neutron Fluence with Units of Neutrons / (cm2) as a Function of Al Shielding Depth (mils) for the Example GEO, HEO, LEO and GPS Orbits (as Defined in Table 7). This data is shown in Figure 14.

Depth mils Al	GEO	HEO	LEO	GPS
1	2.88E+13	1.99E+15	5.20E+12	7.81E+13
1.25893	2.75E+13	1.64E+15	4.76E+12	5.81E+13
1.58489	2.67E+13	1.33E+15	4.50E+12	4.89E+13
1.99526	2.57E+13	1.07E+15	4.22E+12	4.31E+13
2.51189	2.50E+13	8.37E+14	3.79E+12	3.97E+13
3.16228	2.50E+13	6.30E+14	3.38E+12	3.95E+13
3.98107	2.33E+13	4.46E+14	2.95E+12	3.72E+13
5.01187	2.24E+13	3.02E+14	2.56E+12	3.57E+13
6.30957	2.28E+13	1.96E+14	2.39E+12	3.71E+13
7.94328	2.09E+13	1.31E+14	2.15E+12	3.51E+13
10	1.92E+13	8.68E+13	1.94E+12	3.30E+13
12.5893	1.70E+13	5.49E+13	1.70E+12	3.04E+13
15.8489	1.33E+13	3.37E+13	1.36E+12	2.52E+13
19.9526	1.06E+13	2.20E+13	1.10E+12	2.13E+13
25.1189	8.80E+12	1.55E+13	9.50E+11	1.83E+13
31.6228	6.61E+12	1.11E+13	7.82E+11	1.42E+13
39.8107	4.79E+12	7.80E+12	6.41E+11	1.05E+13
50.1187	3.45E+12	5.25E+12	5.59E+11	7.51E+12
63.0957	2.53E+12	3.23E+12	4.91E+11	5.37E+12
79.4328	1.59E+12	2.00E+12	4.13E+11	3.24E+12
100	8.98E+11	1.30E+12	3.47E+11	1.68E+12
125.893	5.10E+11	9.40E+11	3.00E+11	8.73E+11
158.489	2.89E+11	7.32E+11	2.63E+11	4.27E+11
199.526	1.79E+11	5.94E+11	2.34E+11	2.12E+11
251.189	1.26E+11	4.66E+11	2.07E+11	1.21E+11
316.228	9.30E+10	3.55E+11	1.82E+11	7.67E+10
398.107	6.91E+10	2.72E+11	1.58E+11	5.50E+10
501.187	5.14E+10	2.07E+11	1.35E+11	4.11E+10
630.957	3.79E+10	1.64E+11	1.18E+11	3.06E+10
794.328	2.76E+10	1.31E+11	1.01E+11	2.27E+10
1000	1.99E+10	1.01E+11	8.57E+10	1.68E+10

Table 21. 10-Year 24-Hour Worst-Case Integral Electron Flux with Units of Electrons / (cm2 s) as a Function of Energy (MeV) for the Example GEO, HEO, LEO and GPS Orbits (as Defined in Table 7). This data is shown in Figure 21.

Energy (MeV)	GEO	HEO	LEO	GPS
0.04	1.34E+09	2.29E+08	8.99E+07	4.68E+08
0.07	6.10E+08	1.87E+08	7.61E+07	3.09E+08
0.1	3.11E+08	1.45E+08	6.57E+07	2.27E+08
0.25	7.91E+07	6.91E+07	3.33E+07	1.44E+08
0.5	3.29E+07	2.31E+07	1.30E+07	7.58E+07
0.75	1.79E+07	1.01E+07	5.93E+06	4.55E+07
1	1.09E+07	6.26E+06	3.12E+06	2.94E+07
1.5	4.47E+06	2.63E+06	9.21E+05	1.14E+07
2	1.52E+06	9.13E+05	2.11E+05	4.01E+06
2.5	4.72E+05	3.48E+05	4.07E+04	1.70E+06
3	1.84E+05	1.90E+05	8.66E+03	8.28E+05
3.5	9.37E+04	1.10E+05	3.18E+03	4.05E+05
4	5.29E+04	7.02E+04	1.33E+03	1.91E+05
4.5	3.48E+04	4.99E+04	6.12E+02	8.86E+04
5	2.65E+04	3.43E+04	2.39E+02	4.99E+04
5.5	2.17E+04	2.41E+04	9.34E+01	2.91E+04
6	1.81E+04	1.78E+04	4.23E+01	1.97E+04
6.5	1.50E+04	1.35E+04	2.81E+01	1.58E+04
7	1.24E+04	1.04E+04	2.10E+01	1.28E+04
8.5	5.82E+03	4.23E+03	8.01E+00	5.72E+03

Table 22. 10-Year 5-Minute Worst-Case Integral Proton Flux with Units of Protons / (cm2 s) as a Function of Energy (MeV) for the Example GEO, HEO, LEO and GPS Orbits (as Defined in Table 7).
This data is shown in Figure 23. Only fluxes at certain energies above 1200 MeV have been retained for brevity in this table; if needed, fill intervening fluxes with log-log interpolation between these retained energies.

Energy (MeV)	GEO	HEO	LEO	GPS
0.1	7.28E+07	1.46E+09	2.48E+06	9.62E+08
0.2	2.79E+07	1.01E+09	2.48E+06	5.92E+08
0.4	3.75E+06	4.35E+08	2.48E+06	2.18E+08
0.6	2.48E+06	1.87E+08	2.48E+06	7.62E+07
0.8	2.48E+06	1.02E+08	2.48E+06	2.75E+07
1	2.48E+06	6.67E+07	2.48E+06	1.05E+07
2	2.48E+06	3.69E+07	2.48E+06	2.48E+06
4	1.47E+06	1.23E+07	1.47E+06	1.47E+06
6	9.96E+05	4.80E+06	9.96E+05	9.96E+05
8	7.25E+05	2.07E+06	7.25E+05	7.25E+05
10	5.51E+05	1.20E+06	5.51E+05	5.51E+05
15	3.15E+05	3.25E+05	3.15E+05	3.15E+05
20	2.00E+05	2.00E+05	2.00E+05	2.00E+05
30	9.77E+04	9.77E+04	9.77E+04	9.77E+04
50	3.45E+04	3.45E+04	3.92E+04	3.45E+04
60	2.30E+04	2.66E+04	3.60E+04	2.30E+04
80	1.17E+04	2.10E+04	3.01E+04	1.17E+04
100	6.74E+03	1.68E+04	2.54E+04	6.74E+03
150	2.37E+03	9.49E+03	1.80E+04	2.37E+03
200	1.10E+03	5.10E+03	1.36E+04	1.10E+03
300	3.60E+02	1.52E+03	7.42E+03	3.60E+02
400	1.55E+02	6.35E+02	4.40E+03	1.55E+02
700	2.57E+01	8.64E+01	1.14E+03	2.57E+01
1200	4.72E+00	4.72E+00	3.54E+01	4.72E+00
2012.32	9.31E-01	9.31E-01	9.31E-01	9.31E-01
3002.77	2.65E-01	2.65E-01	2.65E-01	2.65E-01
4012.33	1.07E-01	1.07E-01	1.07E-01	1.07E-01
5987.19	3.03E-02	3.03E-02	3.03E-02	3.03E-02
8000.13	1.22E-02	1.22E-02	1.22E-02	1.22E-02
10115.7	5.84E-03	5.84E-03	5.84E-03	5.84E-03
20169.5	6.64E-04	6.64E-04	6.64E-04	6.64E-04
30096.9	1.86E-04	1.86E-04	1.86E-04	1.86E-04
40215.7	7.22E-05	7.22E-05	7.22E-05	7.22E-05
60009.7	1.74E-05	1.74E-05	1.74E-05	1.74E-05
80185.5	4.39E-06	4.39E-06	4.39E-06	4.39E-06
98629.3	1.94E-07	1.94E-07	1.94E-07	1.94E-07
100000	0.00E+00	0.00E+00	0.00E+00	0.00E+00

Table 23. LET Spectra at High Latitudes with Minimal Geomagnetic Shielding
LET is in the first column, the next 5 columns are from a solar quiet period for 5 shielding thicknesses, and the last 5 columns are during the CREME96 Worst Week with 5 shielding thicknesses. The fluxes are in particles/(m^2 sec sr). This data is taken from Figure 24.

LET (MeV cm2/mg)	Quiet 100 mils	Quiet 300 mils	Quiet 500 mils	Quiet 700 mils	Quiet 1000 mils	Worst Week 100 mils	Worst Week 300 mils	Worst Week 500 mils	Worst Week 700 mils	Worst Week 1000 mils
0.10103	16.004	14.466	13.445	12.605	11.557	117820	14509	5314.8	2683.5	1311.8
0.20027	6.9716	6.2838	5.7753	5.348	4.8228	23206	2684.3	974.6	490.47	239.27
0.30053	4.4994	4.0411	3.6901	3.3934	3.0313	7666.4	849.57	306.09	153.53	74.713
0.4016	3.0581	2.7284	2.475	2.2626	2.0059	3065.4	319.73	113.69	56.687	27.474
0.42067	2.922	2.6065	2.3639	2.1604	1.9147	2572.2	263.2	93.171	46.366	22.442
0.44064	2.7545	2.4543	2.2235	2.0302	1.7971	2113.2	210.43	74.007	36.722	17.739
0.46156	2.6193	2.3327	2.1122	1.9276	1.7052	1682.1	160.78	55.976	27.648	13.313
0.48348	2.5075	2.2329	2.0215	1.8444	1.6312	1262.2	112.05	38.253	18.724	8.9594
0.5006	2.4204	2.1545	1.9497	1.7779	1.5714	938.34	74.103	24.426	11.756	5.5578
0.50643	2.3948	2.1316	1.9289	1.7588	1.5543	824.52	60.591	19.489	9.2654	4.3409
0.60265	2.059	1.8321	1.6564	1.5088	1.3312	470.79	28.871	8.6366	3.9589	1.8111
0.70071	1.7786	1.5798	1.4253	1.2954	1.1397	351.55	22.028	6.6717	3.0918	1.4344
0.80534	1.5821	1.404	1.2649	1.1479	1.0075	266.5	17.083	5.2502	2.4653	1.1631
0.90436	1.4184	1.2565	1.1295	1.0227	0.89485	211.35	13.829	4.3128	2.0524	0.98446
1.0038	1.2842	1.1354	1.0183	0.91985	0.80216	170.39	11.398	3.6142	1.7453	0.85184
1.1014	1.1691	1.0302	0.92065	0.82859	0.71885	139.93	9.5845	3.0938	1.5167	0.75268
1.2085	0.82534	0.71528	0.63076	0.5612	0.48013	113.86	7.9992	2.62	1.2952	0.64515
1.3107	0.64283	0.55014	0.48024	0.42355	0.3585	94.074	6.7896	2.2551	1.1225	0.56005
1.4052	0.52531	0.44505	0.38531	0.3375	0.28332	78.731	5.8518	1.9698	0.98598	0.4921
1.5064	0.44023	0.36996	0.31825	0.27725	0.23128	63.694	4.9484	1.6954	0.85465	0.42704
2.013	0.22634	0.18571	0.15694	0.13476	0.11053	35.532	2.9405	1.0219	0.51033	0.24811
3.0208	0.090951	0.072887	0.060815	0.051811	0.042031	20.042	1.5491	0.50998	0.24279	0.112
4.0367	0.04719	0.037435	0.031072	0.026404	0.021349	12.821	0.90876	0.28748	0.13335	0.060086
5.0318	0.028391	0.022433	0.018562	0.015742	0.012707	8.7489	0.57394	0.17781	0.08151	0.036372

LET (MeV cm2/mg)	Quiet 100 mils	Quiet 300 mils	Quiet 500 mils	Quiet 700 mils	Quiet 1000 mils	Worst Week 100 mils	Worst Week 300 mils	Worst Week 500 mils	Worst Week 700 mils	Worst Week 1000 mils
6.0576	0.018382	0.014514	0.011982	0.010149	0.008181	6.1729	0.37959	0.1162	0.052953	0.023524
7.0433	0.012852	0.010153	0.008367	0.007079	0.005698	4.4648	0.26364	0.080516	0.036675	0.016297
8.0016	0.009485	0.0075	0.006171	0.005215	0.004191	3.3287	0.19129	0.05855	0.02672	0.0119
9.0903	0.007069	0.005584	0.004588	0.003875	0.003111	2.5596	0.14284	0.04367	0.019927	0.008877
10.09	0.005504	0.004343	0.003565	0.003007	0.002411	2.0144	0.11043	0.033837	0.015468	0.006903
13.023	0.002856	0.002244	0.001835	0.001544	0.001233	1.0621	0.056401	0.017471	0.008042	0.003612
16.046	0.001599	0.00125	0.00102	0.000856	0.000681	0.57773	0.030307	0.009548	0.004437	0.002009
20.001	0.0008	0.00062	0.000503	0.00042	0.000332	0.3025	0.015608	0.004931	0.002292	0.001037
21.195	0.000634	0.000491	0.000397	0.000332	0.000261	0.24495	0.012626	0.004	0.001861	0.000842
22.201	0.000522	0.000403	0.000326	0.000272	0.000214	0.20628	0.010596	0.003354	0.001559	0.000704
23.255	0.000417	0.000322	0.00026	0.000216	0.00017	0.17105	0.008748	0.002764	0.001282	0.000578
24.079	0.000343	0.000264	0.000213	0.000177	0.000139	0.14549	0.007415	0.002338	0.001083	0.000487
25.222	0.000251	0.000193	0.000156	0.000129	0.000101	0.11217	0.005685	0.001786	0.000825	0.00037
26.115	0.000183	0.00014	0.000113	9.32E-05	7.27E-05	0.086365	0.00435	0.001362	0.000627	0.000279
27.039	0.000118	9.06E-05	7.25E-05	5.98E-05	4.63E-05	0.058921	0.002944	0.000915	0.000419	0.000185
28.323	9.65E-06	7.56E-06	6.1E-06	5.05E-06	3.93E-06	0.003214	0.000168	5.23E-05	2.4E-05	1.06E-05
29.326	6.41E-06	4.91E-06	3.91E-06	3.21E-06	2.47E-06	0.001747	9.13E-05	2.83E-05	1.29E-05	5.67E-06
30.014	3.93E-06	2.99E-06	2.37E-06	1.94E-06	1.49E-06	0.001015	5.35E-05	1.66E-05	7.56E-06	3.33E-06
40.108	2.84E-07	1.94E-07	1.44E-07	1.14E-07	8.61E-08	2.25E-05	1.5E-06	4.68E-07	2.16E-07	9.64E-08
50.577	1.31E-07	8.73E-08	6.39E-08	5.02E-08	3.77E-08	9.29E-06	6.05E-07	1.87E-07	8.57E-08	3.8E-08
60.187	6.44E-08	4.21E-08	3.04E-08	2.37E-08	1.76E-08	3.66E-06	2.3E-07	7.01E-08	3.2E-08	1.41E-08
70.796	2.84E-08	1.83E-08	1.3E-08	1E-08	7.37E-09	1.77E-06	1.07E-07	3.19E-08	1.45E-08	6.34E-09
80.429	1.14E-08	7.28E-09	5.09E-09	3.88E-09	2.81E-09	8.92E-07	5.15E-08	1.51E-08	6.78E-09	2.93E-09
90.318	1.34E-09	8.8E-10	6.02E-10	4.52E-10	3.24E-10	1.5E-07	8.25E-09	2.34E-09	1.02E-09	4.28E-10
100.25	8.25E-11	6.08E-11	4.33E-11	3.4E-11	2.61E-11	3.71E-09	2.13E-10	6.13E-11	2.8E-11	1.29E-11
102.61	1.77E-11	1.32E-11	9.36E-12	7.34E-12	5.62E-12	7.95E-10	4.56E-11	1.31E-11	5.95E-12	2.72E-12

Table 24. Proton Energy Spectrum at High Latitudes with Minimal Geomagnetic Shielding
Energy is in the first column, the next 2 columns are from a solar quiet period for 100 and 300 mil shielding thicknesses, and the last 2 columns are during the CREME96 Worst Week with 100 and 300 mil shielding thicknesses. The fluxes are in protons/(m^2 sec sr MeV). Note they are differential fluxes. This data is taken from Figure 25.

Energy (MeV)	Quiet 100 mil	Quiet 300 mil	Worst Week 100 mil	Worst Week 300 mil
0.1	0.008032	0.0094006	16923	2163.3
0.30166	0.011159	0.013092	23610	3021
0.50269	0.013951	0.016378	29496	3779.2
0.70009	0.016568	0.019456	34969	4487.1
1.0023	0.020693	0.024311	43519	5599.7
3.0236	0.043174	0.050853	86605	11507
5.0385	0.062549	0.073897	116300	16239
7.017	0.080237	0.095029	135360	20099
10.046	0.10607	0.12578	149030	24699
30.305	0.28581	0.3181	82646	28537
50.501	0.48042	0.49669	34822	18204
70.332	0.65104	0.65752	16631	10763
100.69	0.86069	0.85452	6585.5	5028.4
303.75	1.3768	1.3661	216.28	203.69
506.17	1.3363	1.3251	35.092	33.766
704.94	1.1914	1.1809	9.3122	9.0579
1009.2	0.96014	0.95013	2.4534	2.3976
3002.8	0.22838	0.2259	0.040731	0.040039
5003.8	0.087048	0.086126	0.0059721	0.0058803
7065.6	0.041749	0.041304	0.0016316	0.0016071
10116	0.018403	0.018214	0.00042331	0.00041735
30097	0.001211	0.0011982	0.000007011	6.9143E-06
50153	0.00031568	0.00031237	1.0275E-06	1.0138E-06
70819	0.00012553	0.00012422	2.8071E-07	2.7711E-07
100000	0.000049537	0.000049024	7.6703E-08	7.5758E-08

AEROSPACE REPORT NO.
TOR-2022-00016

Best Practices for Generating Space Environment Specifications with Modern Tools

Approved Electronically by:

Robert D. Rutledge,
DIRECTOR - DEPARTMENT
SPACE SCIENCE
APPLICATIONS
LABORATORY
PHYSICAL SCIENCES
LABORATORIES
ENGINEERING &
TECHNOLOGY GROUP

David M. Cardoza,
ASSISTANT GENERAL
MANAGER
SPACE SYSTEMS
ARCHITECT DIVISION
LAUNCH & ARCHITECTURE
OPERATIONS
SPACE SYSTEMS GROUP

James P. Nokes, PRINCIPAL
DIRECTOR
PHYSICAL SCIENCES
LABORATORIES
ENGINEERING &
TECHNOLOGY GROUP

Cognizant Program Manager Approval:

Michael W. Vanik, PRINCIPAL DIRECTOR
IMAGERY PROGRAMS DIV
NATIONAL SYSTEMS GROUP

Aerospace Corporate Officer Approval:

Craig M. Heatwole, GENERAL MANAGER
NATIONAL SYSTEMS GROUP
OFFICE OF EVP

SY0921

AEROSPACE REPORT NO.
TOR-2022-00016

Best Practices for Generating Space Environment Specifications with Modern Tools

Content Concurrence Provided Electronically by:

Timothy B. Guild, SENIOR SCIENTIST
MAGNETOSPHERIC & HELIOSPHERIC SCIENCES
SPACE SCIENCES DEPARTMENT
ENGINEERING & TECHNOLOGY GROUP

Technical Peer Review Performed by:

T Paul P. O'Brien, SENIOR SCIENTIST
MAGNETOSPHERIC & HELIOSPHERIC SCIENCES
SPACE SCIENCES DEPARTMENT
ENGINEERING & TECHNOLOGY GROUP

Robert D. Rutledge, DIRECTOR - DEPARTMENT
SPACE SCIENCE APPLICATIONS LABORATORY
PHYSICAL SCIENCES LABORATORIES
ENGINEERING & TECHNOLOGY GROUP

Special Programs Security Approval Granted Electronically by:

Talia Y. Jordan, SECURITY SPECIALIST IV
EXPORT CONTROL-OTR
GOVERNMENT SECURITY
OFFICE OF THE CHIEF INFORMATION OFFICER

SY0921